

POLITECNICO DI TORINO

**Corso di Laurea Magistrale
in Ingegneria Energetica e Nucleare**

Tesi di Laurea Magistrale

**Model development for studying natural
circulation with the DYNASTY facility**



Relatori

Prof. Lelio Luzzi

Prof. Roberto Zanino

Candidato

Alessio Siviero 231788

A.A. 2017/2018

ABSTRACT

The goal of this thesis is to analyze and improve models for the study of the dynamic behavior of natural circulation loops with distributed heating. The reference system for this work is the DYNASTY facility which is a natural circulation loop whose experimental operation will be employed to validate the developed models. The need of modeling improvement arises from the fact that the models adopted in the design phase of DYNASTY are characterized by simplifying hypotheses (e.g., the use of empirical correlations in the friction factor and the heat transfer coefficient definition, the adoption of adiabatic pipes and of a uniform wall temperature cooler).

In particular, stability maps and 1D Object-Oriented (O-O) models have been investigated.

Despite their purposes being different (they respectively study the infinite and finite time horizon equilibrium), they are both founded on similar hypotheses and can be considered complementary.

Indeed, stability maps allow individuating, in the whole operating range of the system, the most interesting equilibrium states which can then be further analyzed through the use of dynamic models.

Modifications in the stability map output, due to variations in reference parameters and assumptions, entail variations in the asymptotic stability of the equilibrium prediction as well as provide insights on the 1D O-O model sensitivity. These are the reasons that led to the sensitivity analysis (this is a first-time study on a natural circulation loop) on DYNASTY stability map to be performed in the first part of the thesis. What happens when actual time-simulations are executed with improved 1D O-O models constitutes the focus of the second part of the thesis, where models more adherent to DYNASTY are developed from scratch, implemented and verified against the ones existing in literature and the actual capabilities of the new models are examined.

Results indicate that the prediction of the stability of the equilibrium strongly depends on the specific treatment of transition from laminar to turbulent regime. On the other hand, variations on the thermal inertia of the pipe do not seem to affect much the map shape. As far as the dynamic behavior is concerned, the new models are successfully verified against the existing ones; the new physics implemented are the obvious cause of the differences between the results of the two models.

It is also recognized how new models can open to modeling cases which were not achievable with the existing ones. Future works may still concentrate on performing a multi-variate sensitivity analysis on the stability map and on the benchmark and experimental validation of the O-O components developed in the present work.

INDEX

ABSTRACT	III
INDEX	V
List of tables	VII
List of figures.....	IX
1 Introduction.....	1
2 Description of the DYNASTY facility.....	5
2.1 Introduction	5
2.2 Technical features	6
2.3 The measurement and acquisition system.....	7
2.4 DYNASTY thermal carrier: molten salt	10
2.5 Concluding remarks	11
3 DYNASTY stability map and sensitivity analysis	13
3.1 Introduction	13
3.2 The stability maps	15
3.2.1 Governing equations	15
3.2.2 Friction factor and heat transfer correlations	18
3.2.3 Steady state	19
3.2.4 Modal analysis.....	23
3.2.5 The reference stability map for Dynasty	26
3.3 Sensitivity analysis.....	27
3.3.1 Stability map sensitivity to friction factor coefficient definition.....	28
3.3.2 Stability map sensitivity to heat transfer coefficient definition.....	33
3.3.3 Stability map sensitivity to temperature	35
3.3.4 Stability map sensitivity to uncertainty in sizes and local pressure losses	36
3.3.5 Quantitative sensitivity analysis	39
3.4 Concluding remarks	43
4 Improvements on the one-dimensional Object-Oriented models for DYNASTY.....	45

4.1	Introduction.....	45
4.2	DYNASTY pre-existing model.....	47
4.3	Improved components for DYNASTY	50
4.3.1	The PipeFEM2WithLosses component	51
4.3.2	The VentilatedPipe component.....	54
4.3.3	The VentilatedPipe_controller component.....	55
4.4	DYNASTY models comparison.....	58
4.4.1	Controller tuning	60
4.4.2	Simulation set-ups and results	60
4.5	Concluding remarks	72
5	Conclusions and further developments	75
	References.....	77

List of tables

Table 2.1. DYNASTY size specifics.	6
Table 2.2. DYNASTY design specifics.....	7
Table 2.3. DYNASTY power lines specifics.	7
Table 2.4. SALT1 thermal properties.....	10
Table 2.5. SALT2 thermal properties.....	10
Table 2.6. SALT3 thermal properties.....	10
Table 3.1. Correlations for the Nusselt number calculation and applicability ranges.....	20
Table 3.2. Adopted quantities for the computation of DYNASTY reference stability map.....	26
Table 3.3. Adopted parameters for the sensitivity analysis to <i>Retrans</i>	29
Table 3.4. Adopted parameters for the sensitivity analysis to the sigmoid steepness σ	29
Table 3.5. Adopted parameters for the sensitivity analysis to Pr_{trans}	33
Table 3.6. Adopted parameters for the sensitivity analysis to γ	33
Table 3.7. Analyzed cases for the sensitivity analysis to temperature.	35
Table 3.8. Adopted parameters for the sensitivity analysis to <i>Dpipe</i>	36
Table 3.9. Adopted parameters for the sensitivity analysis to τ	36
Table 3.10. Adopted values for the sensitivity analysis to <i>Leq</i>	37
Table 3.11. Synthesis of the developed sensitivity study.	40
Table 3.12. Sensitivity study results in term of FOM and sensitivity coefficients.....	40
Table 3.13. Maximum normalized sensitivity coefficients for the analyzed sensitivity cases.....	42
Table 4.1. Variation of the heat transfer coefficient for natural circulation on horizontal and vertical pipes.	54
Table 4.2. Power and temperature conditions considered for the simulations.....	61

List of figures

Figure 1.1. Schematic representation of the MSFR.....	2
Figure 1.2. Internal Heat Generation (left) and External Heat Flux (right) heating modes representation.	3
Figure 2.1. DYNASTY facility scheme and sizes.....	8
Figure 2.2. Location of the measuring devices. Red circles refer to thermocouples, the blue circle to the mass flow rate meter. The green circle identifies the centrifugal pump.....	9
Figure 2.3. DACS schematics	9
Figure 3.1. Schematic representation of a rectangular NCL.....	16
Figure 3.2. Equivalent electric circuit for the pipe wall with IHG.	18
Figure 3.3. Equivalent electric circuit for the pipe wall with EHF.....	18
Figure 3.4. Employed friction factor correlation.....	19
Figure 3.5. Nusselt number trends.....	20
Figure 3.6. DYNASTY reference stability map.....	27
Figure 3.7. Friction factor behavior with changing <i>Retrans</i>	29
Figure 3.8. Friction factor behavior with changing σ	30
Figure 3.9. Stability map with varying <i>Retrans</i>	30
Figure 3.10. Stability map with varying σ	31
Figure 3.11. Comparison between the reference and the modified friction factor correlations....	32
Figure 3.12. Comparison between the reference stability map and the map which employs the modified friction factor correlation.....	32
Figure 3.13. Stability map with varying γ	34
Figure 3.14. Stability map with varying Pr_{trans}	34
Figure 3.15. Stability map with varying reference temperature.....	36
Figure 3.16. Stability map with varying D_{pipe}	37
Figure 3.17. Stability map with varying τ	38
Figure 3.18. Stability map with varying Le_q	38
Figure 3.19. Maximum FOM variation for the analyzed sensitivity cases.....	42
Figure 4.1. External (bottom left) and expanded view of the ThermostatedPipe_2 component...	48
Figure 4.2. External (bottom left) and expanded view of the PipeFEM_2 component.	49
Figure 4.3. Pre-existing DYNASTY models employing Thermostated_2 and PipeFEM2 components.	50
Figure 4.4. External (bottom left) and expanded view of the PipeFEM2WithLosses component.	52
Figure 4.5. External (bottom left) and expanded view of the VentilatedPipe component.	55
Figure 4.6. External (bottom left) and expanded view of the VentilatedPipe_controller component	56

Figure 4.7. PI controller scheme.	57
Figure 4.8. PI controller with anti wind-up scheme.	58
Figure 4.9. DYNASTYmodel_1 Dymola scheme.	59
Figure 4.10. DYNASTYmodel_2 Dymola scheme.	59
Figure 4.11. Cooler wall mean temperature for different controller parameters.	60
Figure 4.12. Inlet cooler flow rate for the 500W - 180°C case.	61
Figure 4.13. Inlet cooler temperature for the 500W - 180°C case.	62
Figure 4.14. Outlet cooler temperature for the 500W - 180°C case.	62
Figure 4.15. Temperature difference on the cooler for the 500W - 180°C case.	62
Figure 4.16. Cooler wall mean temperature for the 500W - 180°C case.	63
Figure 4.17. Inlet cooler flow rate for the 500W - 230°C case.	63
Figure 4.18. Inlet cooler temperature for the 500W - 230°C case.	64
Figure 4.19. Outlet cooler temperature for the 500W - 230°C case.	64
Figure 4.20. Temperature difference on the cooler for the 500W - 230°C case.	64
Figure 4.21. Cooler wall mean temperature for the 500W - 230°C case.	65
Figure 4.22. Inlet cooler flow rate for the 750W - 180°C case.	65
Figure 4.23. Inlet cooler temperature for the 750W - 180°C case.	66
Figure 4.24. Outlet cooler temperature for the 750W - 180°C case.	66
Figure 4.25. Temperature difference on the cooler for the 750W - 180°C case.	66
Figure 4.26. Cooler wall mean temperature for the 750W - 180°C case.	67
Figure 4.27. Cooler wall heat transfer coefficient comparison for the 500W-180°C and 750W-180°C.	67
Figure 4.28. Inlet cooler flow rate for the 750W - 230°C case.	68
Figure 4.29. Inlet cooler temperature for the 750W - 230°C case.	68
Figure 4.30. Outlet cooler temperature for the 750W - 230°C case.	68
Figure 4.31. Temperature difference on the cooler for the 750W - 230°C case.	69
Figure 4.32. Cooler wall mean temperature for the 750W - 230°C case.	69
Figure 4.33. Cooler wall temperature at inlet and outlet of pipe, compared with the mean wall temperature.	70
Figure 4.34. Cooler wall spatial temperature distribution for different time instants.	70
Figure 4.35. Inlet and outlet bottom pipe fluid temperature comparison for old and new set-ups.	71
Figure 4.36. Inlet and outlet vertical heated pipe fluid temperature comparison for old and new set-ups.	72

1 Introduction

The Molten Salt Fast Reactor (MSFR) belongs to the set of six new advanced nuclear reactor designs (the so called “Generation IV”) that were chosen for further research and development, with the purpose of their deployment before 2030 (<https://www.gen-4.org/>, 2017).

The selected projects are seen as representatives of the future shape of nuclear energy and they all share advances in terms of sustainability, economics, safety, reliability and proliferation resistance with respect to the old generations (Serp et al., 2014).

The Molten Salt Fast Reactor, (schematically seen in Fig. 1.1 (<http://samofar.eu/>)) whose peculiarity is the thorium-uranium salt mixture adopted as fuel, can be thought of as made of two main zones: the core cavity, where most of the fission energy production occurs and the recirculation loops, which comprehend the heat exchangers and the pumping system.

Unlike the conventional reactors working nowadays, in a MSFR the fission energy is released in the salt mixture that circulates in the whole primary circuit, since no sharp separation exists between fuel and coolant. If the fission chain reaction is stopped, the heat is still produced by the decay of the fission products which are uniformly distributed in the fluid.

The value of such power is estimated to be about 0.1GW one second after shutdown and about 1 MW after one year (Merle-Lucotte et al., 2012). The salt must then be quickly cooled in order to avoid it heating up, damaging the core and starting an accidental scenario.

Indeed, the fluid temperature may rise in time posing a threat to the structural material integrity.

The SAMOFAR project (Safety Assessment of the MOlten salt FAst Reactor) was founded with the purpose of analyzing and assessing, with advanced modeling and experimental efforts, the safety measures of the MSFR, with a primary focus on the decay heat removal system (<http://samofar.eu/>).

In particular, a passive system employing natural circulation was chosen for the purpose of removing the decay heat from the reactor in case of reactor shut-down.

In general, natural circulation employs the working fluid capability of being lighter at higher temperature and heavier at lower temperature. When such fluid belongs in a thermal-hydraulic system which is subject to a temperature gradient, induced by the presence of, for example, a top heat sink and a bottom heat source, then the fluid may start circulating and remove heat from the hot region while releasing it to the cold one.

The onset of the natural circulation in a fluid is dictated by the balance between the buoyancy forces, which are strictly dependent on the temperature-driven density differences, and the viscous forces which come out as a result of the resistance to motion offered by the system (Bergman, 2011). When these two forces balance, a flow rate establishes and heat is removed from the hot region of the system.

Unlike usual thermal-hydraulic systems, in natural circulation the flow rate is not externally set by a mechanic component, but it is the result of the interconnection of all the flow quantities. If on the one hand this assures that the motion cannot be interrupted by a failure or breach of an active component, on the other hand the necessary conditions for the phenomenon to happen must be ensured.

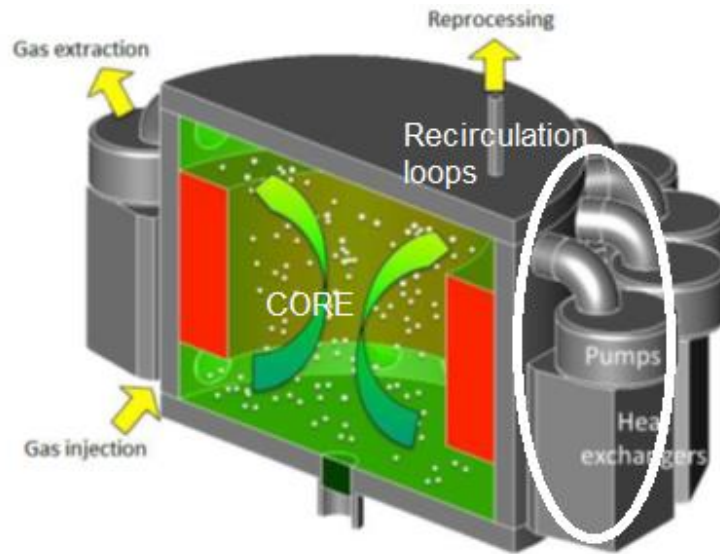


Figure 1.1. Schematic representation of the MSFR.

As far as the MSFR is concerned, the heat source is not confined anymore to a small region of the system; indeed, the decaying fission products are uniformly distributed in the salt mixture and therefore heat is being produced in the whole circuit. This type of heat production which is uniformly present in the totality of the system is hereby defined Internal Heat Generation (IHG). It is easy to imagine how the presence of the IHG can affect the temperature and density distributions eventually jeopardizing the forces that drive natural circulation. The driving and the resistance forces are constantly on a dynamic equilibrium which tightly depends on the working conditions. When a stable equilibrium state is reached, an infinitesimal perturbation (way smaller than the equilibrium value) on one of the state variables (such as temperature or flow rate) is not able to bring the system away from the equilibrium state: the system will be perturbed somehow, but in the end, even if on a very long time, it will come back to the equilibrium (Astrom, 2010). When the system is in an unstable equilibrium state, a perturbation on a flow variable is able to move the system to another equilibrium state; the system may also not reach an equilibrium state at all and start pulsating or oscillating (Vijayan P. K., 2002). In reality, a system is never able to reach an unstable equilibrium state since real systems are continuously affected by perturbations. For this reason, when a system is subject to certain working conditions and it reaches a steady state then the equilibrium of the natural circulation is said (inappropriately) to be stable: conversely, when the quantities do not reach a steady state then the equilibrium state is said to be unstable. Two different equilibrium stability definitions were given: one deals with the effect of a perturbation on an infinite time while the other relates to the possibility of reaching a stationary state in a finite time. These two definitions are reflected in the modeling choices adopted for the study of the dynamic behavior of natural circulation. Indeed, the asymptotic stability of the equilibrium of a system state can be approached through linear tools, as stability maps (Misale M. , 2014); on the other hand, if one wants to observe if the equilibrium is reached in a finite time then tools capable of simulating the finite time evolution of the system are needed - this is the case of Object-Oriented Models and Computational Fluid Dynamics (Luzzi et al., 2017).

Trying to immediately address the study of natural circulation dynamics on the MSFR would entail enormous efforts, since the phenomena are very complex, not sufficient matter is known about them (especially on the effects of IHG) and they are strongly space dependent (Bergman, 2011). For this reason, the study of this topic is initially faced by referring to simpler geometries in order to grasp the physical key-points of natural circulation dynamics in presence of distributed heating. Following a common practice in research, natural circulation dynamics are investigated through the use of

natural circulation loops (NCL). These are vertical thermal-hydraulic systems with a rectangular or toroidal shape constituted of connected pipes in which a fluid can flow. Some parts of the system are subject to heating or cooling in order to provide a heat source and a heat sink conditions.

However, if the aim is to get an insight also on the behavior of naturally circulating systems subject to distributed heating, then some alterations on the loops need to be considered: the fluid should be heated from the inside and the power should be supplied everywhere in the loop. It is quite complicated to practically obtain these conditions on an NLC. However, for a system whose pipes are characterized by a very high length-to-diameter ratio, the flow quantity distributions can be seen as one-dimensional and the study of the system state equilibrium (i.e., whether it is stable or unstable) in presence of IHG can be equivalently well reproduced by a system working with an all External Heat Flux (EHF) (Pini, 2017). As shown in Fig. 1.2 the EHF is provided by heating the pipe walls which in turn heat the fluid; on the other hand, when the IHG is present it is the fluid that heats up first, subsequently followed by the walls.

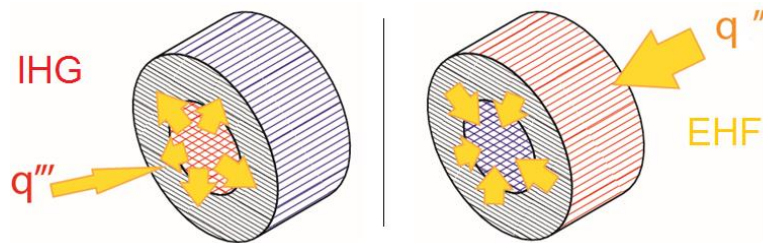


Figure 1.2. Internal Heat Generation (left) and External Heat Flux (right) heating modes representation.

This resolution brought to the design and construction of the DYNASTY (DYNamics of NATural circulation Systems inTERNally heated) facility, located in the Energy Labs of Politecnico di Milano. DYNASTY is a natural circulation loop, designed with the purpose of studying natural circulation dynamics in presence of distributed heating. The experimental data obtained by running the facility will offer the chance to validate the predictive models and thus obtain further insight on the phenomena.

Models capable of analyzing the infinite and finite time behavior of natural circulation loops in presence of distributed heating have been developed at Politecnico di Milano. Stability maps are the linear tool adopted for the study of the natural circulation equilibrium asymptotic behavior; the Object-Oriented language Modelica, implemented through the means of the Dymola software, is used, among other environments, to investigate the equilibrium of the system state on a finite time horizon.

Hence, the main goal of this thesis is to analyze how particular modeling choices, both in the linear and Object-Oriented environments, can modify the prediction about both the asymptotic and the finite time horizon equilibrium of the system.

The necessity of assessing and improving the outcome from both the modeling tools lies in the fact that they are deeply interconnected and complementary to each other. Both the models rely on one dimensional governing equations and approach the heat transfer and friction problems in the same way; additionally, they both carry with them the uncertainty related to the flow regime transition (the laminar to turbulent transition point is actually unknown for natural circulation in a loop). In the end, this allows a complementary use of the results, even though they are related to two different time frames. Indeed, since the stability map allows the visualization of the (asymptotic) equilibrium states for the whole operating range of the facility, it is easier to observe which are the equilibria that may need further investigation with more advanced tools, as O-O models. On top of that, considerations obtained from results of one model are very likely to apply to the other one too, due to the common background they share. Stability maps then serve also the role of preliminary tool to 1D time-

Introduction

dependent analysis, besides their role in assessing asymptotic stability. Moreover, the two approaches allow to observe the system equilibrium behavior on both asymptotic and finite time, offering a wider perspective on the natural circulation dynamics. It is then clear why both tools are adopted in this work.

As far as stability maps are concerned, they rely on the use of correlations for modeling the major pressure losses and the heat transfer phenomena; moreover, some of the parameters needed by the model are affected by uncertainties. Nonetheless, the effects of modifications on the founding assumptions and on the input parameters have never been investigated thoroughly. In the present work, a sensitivity analysis is performed to evaluate, both qualitatively and quantitatively, how uncertainties and limited knowledge of phenomena can alter the assessment of the asymptotic behavior of the equilibrium and if there are factors more responsible than others. It is clear that this study has also effects for the 1D O-O models, since it can highlight factors that are relevant in modifying the system evolution, for the reasons explained before. It is also true that performing a sensitivity analysis on a stability map is way less computationally expensive than doing it on a dynamic model.

For the study of the finite time horizon equilibrium, the existing available O-O models are not adequate for modeling DYNASTY since they rely on hypotheses which are not found in the real facility. During this thesis work new models were developed mostly from scratch so as to be able to model real conditions in a more proper way. Once again, it is also investigated if strong alterations in the prediction of the equilibrium of the system state on a finite time are brought by the new models with respect to the results achieved with the previous ones - in doing so, verification of the new components with the existing ones is achieved. The increased modeling capability offered by the new models is also highlighted with respect to those available in literature.

The reference loop adopted for all the following considerations made is DYNASTY, which is presented with a detailed description in Chapter 2. The general framework for the realization of the stability map of a natural circulation loop is presented in Chapter 3 and the reference stability map for DYNASTY is obtained; the sensitivity analysis is then shown and discussed. In Chapter 4 the Object-Oriented approach for the study of complex systems is introduced; the state of the art is then disclosed and the main limitations are made clear. The new improved components are presented and a comparison between the present work and the state of the art components is analyzed and discussed. In the end, a final chapter draws the conclusions of this work.

2 Description of the DYNASTY facility

***Abstract.** The study of natural circulation in presence of distributed heating is performed thanks to natural circulation loops (NCLs). Due to their simplified geometry NCLs can be used to obtain insight about the physics involved in natural circulation avoiding secondary effects appearing in complex geometries. NCLs represent the experimental support required for the development and validation of models. Among NCLs, the DYNASTY (Dynamics of NATural circulation for molten Salt internally heated) facility, designed and located at Politecnico di Milano, has the peculiar feature of distributed heat generation, allowing for simulation of the internal heat generation characterizing molten salt reactors. Moreover, it can be operated with either water or molten salt as working fluid. This chapter offers a detailed description of the DYNASTY facility along with information on the molten salt to be adopted during experiments.*

2.1 Introduction

Natural circulation dynamics is strongly dependent on the geometry and shape of the system (Bergman, 2011). Because of the complexity of the phenomena involved, natural circulation for single-phase fluids has been studied through the years by means of simplified geometries (Welander, 1967), (Creveling, 1975), (Vijayan P. K., 1995), (Misale M. , 2014), i.e., natural circulation loops. These loops are vertical thermal-hydraulic circuits constituted by the union of vertical and horizontal pipes. Both rectangular and toroidal set-ups are possible (Gorman et al., 1986). To create conditions for natural circulation to occur, one region of the circuit is heated while another one is cooled. The typically investigated configuration considers a heat source in the bottom part of the loop and a heat sink in the top part, with the other pipes being adiabatic (Vijayan P. K., 2002). Restricting the analysis to rectangular loops, four main categories of NCL can be individuated depending on the orientation of the heater (i.e., the part of the circuit being heated) and that of the cooler (i.e., the part of the circuit being cooled), (Vijayan P. K., 2001):

- VVHC: Vertical Heater, Horizontal Cooler;
- HHHHC: Horizontal Heater, Horizontal Cooler;
- HHVC: Horizontal Heater, Vertical Cooler;
- VVHC: Vertical Heater, Vertical Cooler.

The DYNASTY facility, located in the Energy Labs at Politecnico di Milano, is a rectangular NCL which can work in VVHC and HHHHC configurations, thanks to the possibility of providing distributed external heat flux (EHF) to all the pipes of the loop (except the top horizontal one, which is always the cooler). In particular, all three of the heater sections (the two vertical legs and the bottom horizontal one) can provide power simultaneously, so to provide an EHF. This flexibility in the distribution of the heat source is one of the main innovative features of DYNASTY compared to existing NCLs (Pini, 2017). DYNASTY schematic representation can be seen in Fig. 2.1. This chapter presents DYNASTY technical features, along with the characteristic of the salt selected as one of its possible working fluid, the other being water.

2.2 Technical features

DYNASTY is a vertical rectangular hydraulic circuit constituted of five main sections:

- Cooler;
- Hot leg;
- Cold leg;
- Forced convection branch;
- Natural convection branch.

DYNASTY size specifics are reported in Table 2.1. while a full representation of the facility with geometrical sizes is given in Fig 2.1.

Table 2.1. DYNASTY size specifics.

Facility height	6410±10 mm
Facility width	3370±10 mm
Facility depth	1140±10 mm
Loop height	3090±10 mm
Loop width	3100±10 mm
Nominal pipe internal diameter	38 mm
Nominal pipe thickness	2 mm
Nominal pipe roughness	0.03-0.06 mm
Insulation thickness	~70 mm
Tank volume	25 dm ³

In DYNASTY, the horizontal bottom part of the system branches in two legs that can be used for different experiment types. The topmost branch is equipped with a centrifugal pump which can be used to initialize the mass flow rate at the system start-up and can also be useful to conduct experiments in forced circulation. The lower branch is devised for natural circulation experiments and it houses a mass-flow meter. Each of the branches can be isolated from the rest of the loop using valves.

The horizontal pipe at the top of DYNASTY houses a finned pipe serving as cooler for the system. It can operate both in natural circulation, being exposed to air, or coupled to a fan which forces an air cross-flow whose velocity can be regulated.

Two tanks are installed in the facility: one at the top serves as expansion tank and as salt fusor, the other at the bottom allows for the salt drain.

The structural components are made of AISI 316 stainless steel; the pipes are assembled through flanges allowing future modification of the system. All the pipes, except the cooler, are insulated with rock wool; the insulation is then enclosed in a AISI 304 stainless steel thin foil. The main technical features of DYNASTY are summed up in Table 2.2. DYNASTY can be operated safely up to 350 °C, with temperature ranging between ambient and 100°C when operating with water and between 180 °C and 350 °C when operating with molten salt. The topmost tank is open to air to set the pressure at the top of the system to the pressure one.

As far as the heating system is concerned, fiberglass electrical resistances are wound around the whole circuit (except the cooler) and supply the EHF uniformly on the loop, except on the zones where the mass flow rate sensor and the pump are located. Each resistance strip can provide a maximum 836 W power.

Description of the DYNASTY facility

Table 2.2. DYNASTY design specifics.

Maximum thermal power (uniformly distributed) available for experiments (kW)	5.34
Minimum working temperature (°C)	250
Maximum working temperature (°C)	350
Maximum mass flow rate in natural circulation (kg/s)	0.35
Mass flow rate (m³/h)	10
Head provided by the pump (m)	5
Pump velocity (rpm)	1450

The power lines are divided into four groups so that different heating configurations are possible: localized heat flux (if only a specific line is heated), distributed heat flux (if the whole loop is heated) and also mixed configurations. Moreover, the power per branch can be partialized thanks to regulable transformers.

The two vertical power lines (“GV1” and “GV2”) are wound with three strips, while each of the two horizontal branches (“GO1” and “GO2”) is wrapped with two strips. The details regarding the power lines length and relative maximum power are reported in Table 2.3.

The minimum linear power in the loop is 543 W/m; since the total length of the heated loop is 9.88 m this means that the maximum power that can be supplied in order to have a uniform distribution is 5343 W. Otherwise, if uniform distribution is not required the maximum power value is 6688 W.

Table 2.3. DYNASTY power lines specifics.

Line	Number of strips	Line length (m)	Maximum power (W)	Maximum linear power (W/m)
GO1	2	3.08	1672	543
GO2	2	2.78	1672	601
GV1	3	3.38	2508	742
GV2	3	3.38	2508	742

Additional strips are installed on some components and are needed to allow operation of the plant with molten salt. One strip envelopes the upper tank and can provide 2.2 kW to melt the salt and keep it in molten form; another strip is necessary to keep the salt hot between the tank and the loop, providing 836 W.

2.3 The measurement and acquisition system

The DYNASTY data acquisition system registers temperatures and mass-flow rate. As aforementioned, the mass flow rate sensor (a Coriolis-effect mass-flow meter) is located on the natural circulation branch. Regarding the temperature sensors, J-type thermocouples are installed on the loop: five of them measure the fluid temperature while the remaining ones the pipe wall temperature. Their location on the facility is reported in Fig 2.2. Two of the fluid thermocouples are placed at the ends of the finned cooler, two are located at the bottom of each vertical leg while one is installed in the fusor tank to check the temperature of the molten salt.

Another thermocouple is positioned to measure the temperature in the junction pipe between the top tank and the circuit.

The signals acquired from the temperature and flow rate sensors are converted to digital form thanks to the Data Acquisition and Control System (DACS); the whole information is managed by

2.3 The measurement and acquisition system

MATLAB through a serial interface. The DACS consists of a microcontroller and of an electronic circuit board.

The electronic board collects and manages the signals coming from the sensors while the microcontroller converts the signals and transfers the data to MATLAB.

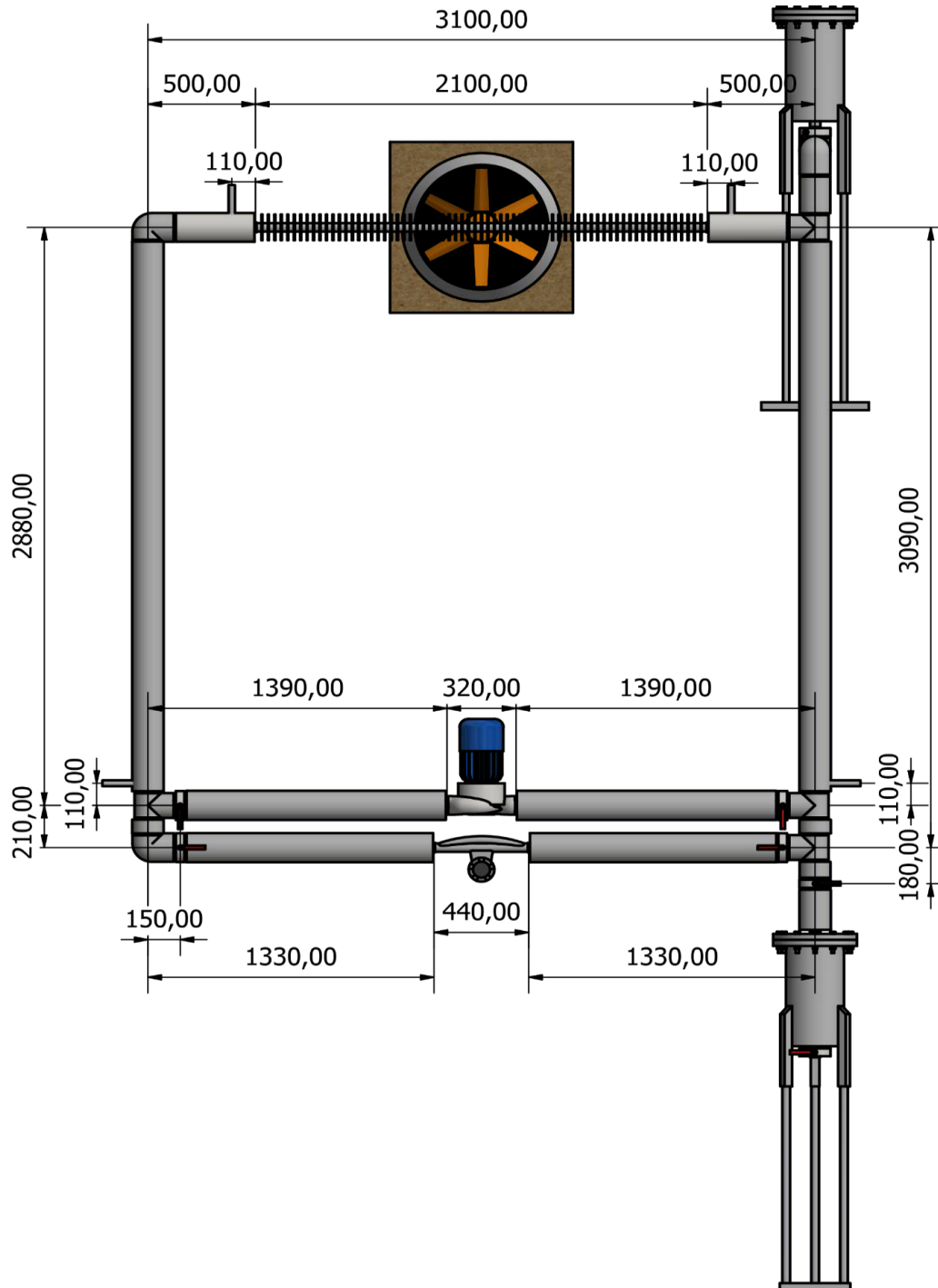


Figure 2.1. DYNASTY facility scheme and sizes.

Description of the DYNASTY facility

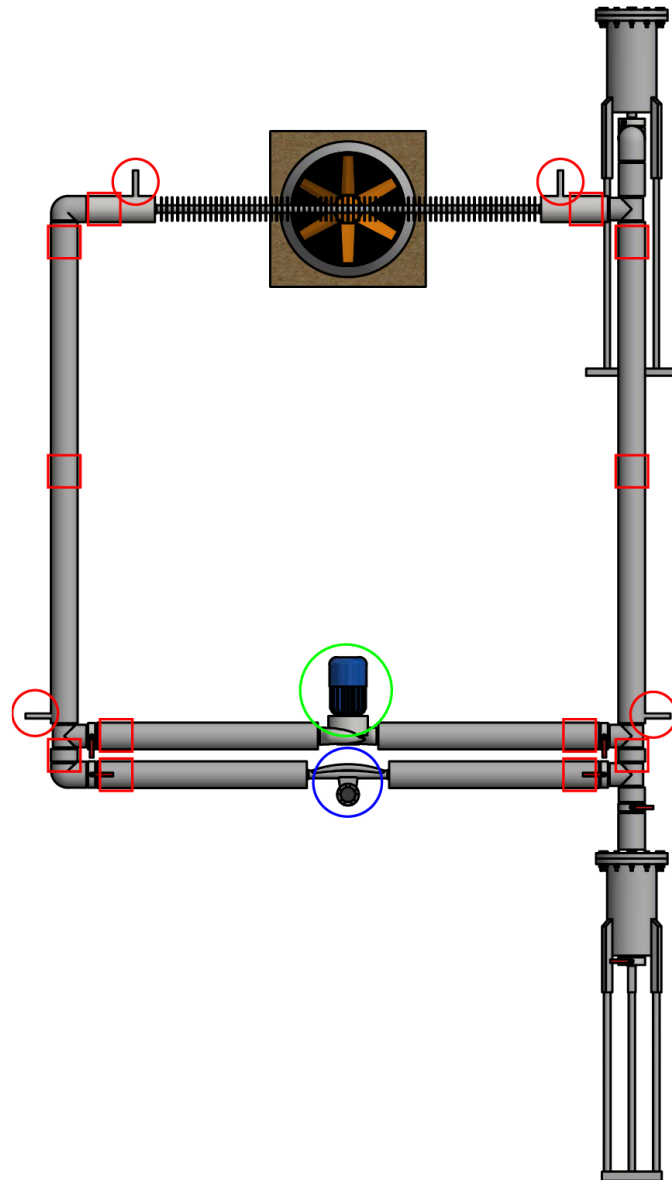


Figure 2.2. Location of the measuring devices. Red circles refer to thermocouples, the blue circle to the mass flow rate meter. The green circle identifies the centrifugal pump.

The DACS system will be integrated with control functionalities by adding a second circuit board and a second microcontroller. A representation of the whole DACS (with control functionalities) is reported in Fig 2.3 (Padovani, 2017).

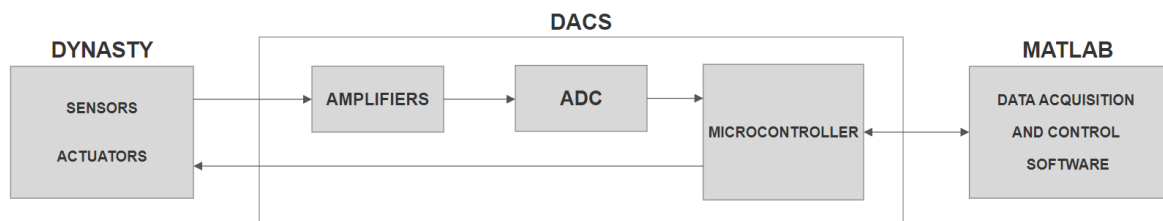


Figure 2.3. DACS schematics

2.4 DYNASTY thermal carrier: molten salt

DYNASTY can be run using either water or a molten salt. In particular, DYNASTY was designed to employ a specific molten salt as thermal carrier; this salt is a mixture of NaNO_2 (for the 40% in weight), of NaNO_3 (for the 7% in weight) and of KNO_3 (for the 53% in weight). The salt has a melting temperature of 142 °C and can be used up to 540 °C. It is chemically inert, non-flammable and shows no corrosion problems. From literature, three different set of correlations are available for the calculation of its thermal properties; the three set of correlations will be referred to as “SALT1”, “SALT2” and “SALT3” respectively and their expressions can be found in Table 2.4, Table 2.5, Table 2.6.

Table 2.4. SALT1 thermal properties

Property	Definition	Temperature		
		250°C	300°C	350°C
Thermal conductivity [$\text{Wm}^{-1}\text{K}^{-1}$]	Constant 0.48	0.48	0.48	0.48
Heat capacity [$\text{J kg}^{-1}\text{K}^{-1}$]	Constant 1560	1560	1560	1560
Density [kg m^{-3}]	$2279.799 - 0.7324 T(K)$	1896.75	1860.13	1823.51

Table 2.5. SALT2 thermal properties.

Property	Definition	Temperature		
		250°C	300°C	350°C
Thermal conductivity [$\text{Wm}^{-1}\text{K}^{-1}$]	$0.78 - 1.25 \cdot 10^{-3} T(K) + 1.6 \cdot 10^{-6} T(K)^2$	0.56	0.59	0.62
Heat capacity [$\text{J kg}^{-1}\text{K}^{-1}$]	Constant 1510	1510	1510	1510
Density [kg m^{-3}]	$2080 - 0.733 (T(K) - 273.15)$	1896.86	1860.21	1823.56

Table 2.6. SALT3 thermal properties.

Property	Definition	Temperature		
		250°C	300°C	350°C
Thermal conductivity [$\text{Wm}^{-1}\text{K}^{-1}$]	$7 \cdot 10^{-10} (T(K) - 273.15)^3 - 2 \cdot 10^{-6} (T(K) - 273.15)^2 + 0.0006 (T(K) - 273.15) + 0.3982$	0.43	0.42	0.39
Heat capacity [$\text{J kg}^{-1}\text{K}^{-1}$]	Constant 1500	1500	1500	1500
Density [kg m^{-3}]	$2293.6 - 0.7497 T(K)$	1901.51	1864.02	1826.54

It is possible to observe the decreasing trend of density with temperature and a constant (but different) value of specific heat capacity for all the three sets; conversely, for one set the thermal conductivity shows a constant value (this is the set-up referred as SALT1 and corresponds to Hitec in (Serrano-López, 2013)), for another the thermal conductivity increases with temperature (referred to as SALT2 (Boerema, 2012)) and for the last one it decreases with the increasing temperature (SALT3, defined in (Coastal Chemical Co., 2016)). The set of correlations adopted in the existing DYNASTY models

is SALT1; the influence of this choice on the results of the models presented in this work is examined in Chapter 2.

2.5 Concluding remarks

The DYNASTY facility is an improved version of a classical natural circulation loop. The implemented all External Heat Flux system allows investigating the natural circulation dynamics in presence of distributed heating, making DYNASTY a first-of-a-kind NCL capable of operating in this condition. Moreover, it has the flexibility to use both water and molten salt as work fluid, alternatively. On top of that, the facility can also work with localized heat flux (i.e., as a conventional NCL). In the followings, the DYNASTY facility is going to represent the reference system on which the modeling efforts are developed and assessed.

2.5 Concluding remarks

3 DYNASTY stability map and sensitivity analysis

***Abstract.** The stability map is a tool based on one dimensional linear modal analysis that is used to investigate the asymptotic stability of the system equilibrium. It shows, in graphical form, how the working region of the system divides in asymptotically stable and asymptotically unstable regions. The stability map has shown to be a reliable tool in describing the asymptotic behavior of the equilibrium states of a NCL in presence of internal heat generation. However, the construction of stability maps is based on several hypotheses, e.g., the adoption of correlations for the heat transfer and friction factor coefficient or the use of reference thermal properties, potentially hindering the generality of the results. This chapter presents a sensitivity analysis on the most relevant parameters used in the construction of stability maps referred to DYNASTY, focusing on both the modeling choices and the parameter uncertainties that may affect the map shape.*

3.1 Introduction

The stability map is a semi-analytical tool based on modal analysis which is used, for a generic thermal-hydraulic system, to discriminate asymptotically stable equilibrium states from unstable ones. Since free convection dynamics in NCLs has been extensively described with stability maps, a chronological review is reported in the following with the aim of focusing on developments and research linked to both NCLs and stability maps (see (Pini, 2017) for a complete overview). The review focuses mostly on rectangular circuits and includes results obtained experimentally or with time dependent tools; in those cases, the concept of “Lyapunov stability” (Lyapunov, 1892), which is linked to an infinite time frame, cannot be applied and the equilibrium state of the system is evaluated in terms of its steadiness on a finite time. The first theoretical analysis on NCLs regarded modeling activity focused on rectangular loops characterized by vertical pipes connected by short horizontal pipes (Welander, 1967). Point-like heat source and heat sink were located on the horizontal bottom and top part of the loop, respectively. According to this model, small amplitude oscillations in a natural circulation system grow due to the formation of hot and cold “wave packets”; these wave packets are amplified when passing through the heat source (“heater”) and damped when going through the heat sink (“cooler”). As a wave packet exits the heater it causes an increase in the buoyancy force, boosting the flow rate magnitude; conversely as the wave packet exits the cooler zone it has reached its minimum dimension implying also a minimum flow rate. Hence periodic growth and reduction of the wave packets happen; this oscillating behavior of the fluid flow was termed “Welander instability” and was retrieved also experimentally by Creveling while working on toroidal loops (Creveling, 1975).

3.1 Introduction

As far as rectangular NCLs are concerned, another theoretical study showed that the height-to-width ratio has a strong impact on the dynamic behavior of these systems with the most unstable configuration reached for a ratio equal to one (Chen, 1985).

Experiments (Vijayan, 1995) underlined the fact that rectangular loops with uniform larger diameters are more prone to instabilities, with flow reversal frequency increasing with increasing supplied power. Further experimental studies allowed to observe three different oscillatory modes: unidirectional pulsing, bidirectional pulsing, and chaotic switching between unidirectional and bidirectional pulsing (Vijayan 2001, 2002).

The effect of the heater and cooler orientations on the single-phase natural circulation in rectangular loops was also investigated (Vijayan, 2007). Through the adoption of linear tools, such as the stability maps, it was discovered that the HHHC configuration is the one entailing the smallest number of asymptotically stable equilibrium states while the VHVC is, in this sense, the most stable.

The stability map tool was also utilized to study the asymptotic behaviour of differently oriented rectangular NCLs considering a more comprehensive approach to the friction factor modeling (Swapnalee and Vijayan, 2011).

The studies cited up to this point accounted only for the fluid region of the natural circulation loops, neglecting the effects induced by the piping material. Among the first attempts to deal with this feature, a 2D numerical analysis was adopted to investigate the effect of the pipe thermal capacity on natural circulation dynamics (Misale et al., 2000).

A theoretical model was also later developed (Jiang and Shiji, 2002) for toroidal loops and it showed that oscillations in natural circulation flow occurring in pipes made with a higher thermal conductivity material are damped more quickly in time.

Confirming these theoretical results, experimental research (Misale et al., 2005) conducted with rectangular loops made in AISI-304 and Plexiglas showed that the thermal inertia of the pipes was involved in the determination of the steady (for the AISI-304 circuits) and oscillating (for the Plexiglas tubes) behavior of the loops in a specific operational condition.

A theoretical study (Rao et al., 2012) analyzed the effect of the wall thermal inertia in the heater and in the heat sink sections of a rectangular NCL through the use of both time-dependent tools and stability maps. It was noticed that the number of stable states in the map widens if the wall thermal properties are considered.

All the cited works only involved classical natural circulation loops, in the sense that the heating source was always localized in a finite region of the system. Beside confirming the role of the pipe thermal inertia in determining the stable or unstable behaviour of conventional natural circulation in rectangular NCLs, the work by Pini (Pini, 2017) analyzed free convection in NCLs in presence of distributed heating given from the exterior of the circuit, of internal heat generation in the fluid or of mixed conditions. Among the tools adopted, the stability maps served the purpose of studying the asymptotic dynamics of the systems analyzed. It was discovered that internal heat generation generally leads to a decrease in the stable region in the map and that, most importantly, for very high pipe length-to-diameter ratios the results obtained in case of distributed heating of the pipes closely coincide with those obtained with internal heat generation in the fluid (this result was also confirmed thanks to time-dependent models). Indeed, this latter consideration allows to study the dynamics of free convection in presence of internal heat generation through the use of experimental devices working with distributed heat sources, as it is the case for DYNASTY.

This literature review surely highlighted the multitude of factors that can affect the natural circulation dynamics of the flow in a NCL; it was also pointed out how the stability map is usually one of the tools adopted to infer information about the infinite time horizon behaviour of the system. On the other hand, the stability map relies on a certain number of simplifying assumptions and on the

choice of external parameters which may influence its output. After presenting the theoretical model and the stability map for DYNASTY, the remainder of this chapter is dedicated to a sensitivity study on the DYNASTY map in order to assess the relevance of these assumptions and parameters in the computation of the map.

3.2 The stability maps

The tool adopted to study the asymptotic behavior (i.e., understand if the system goes back to the original condition in an infinite time after a small perturbation is applied to it) of a NCL is the stability map. This is a representation of equilibrium stability in the state plane of a system, collecting stable and unstable equilibrium states as zones of the plane.

For a NCL an equilibrium state is uniquely defined by a pair of dimensionless numbers (Reynolds, Prandtl, Grashof or Stanton numbers are viable options; in the following Reynolds and Prandtl numbers are used for practical reasons). For any of the points in the plane defined by such pair it is possible to define if perturbations are damped or amplified, hence if the state will return to the starting equilibrium state in an infinite time.

A brief description of the main steps to obtain the stability map of a NCL system is provided in the following subsections. For more details, reference is made to (Pini, 2017).

3.2.1 Governing equations

The governing equations are written for a closed rectangular loop configuration with circular constant cross section, characterized by a single cooler (L_c long) and a single heater (L_h long). Both the fluid and the metallic pipe are taken into account. The length of the pipes connecting the cooler to the heater (i.e. the cold leg) is denoted as L_{cl} while that of the tubes connecting the heater to the cooler (i.e. the hot leg) as L_{hl} . The total length of the circuit is $L_t = L_h + L_c + L_{hl} + L_{cl}$. A schematic representation can be observed in Fig 3.1. In order to simplify the problem, the equations are written considering only one spatial dimension: the axial curvilinear coordinate s , whose origin is at the cooler entrance.

3.2 The stability maps

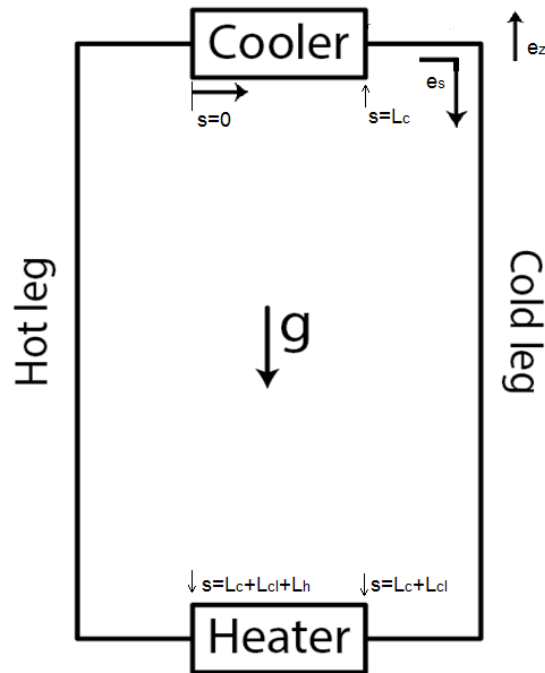


Figure 3.1. Schematic representation of a rectangular NCL.

In order to account for a huge number of cases, three types of heat source are present:

- q_l'' or LHF (external heat flux) which is used to model the localized heating due to an external heat flux (i.e., what was previously called the heat source);
- q_d'' or EHF (distributed heat flux) which serves as a distributed heat source acting on the whole system except the cooler;
- q''' or IHG (internal heat generation) which serves to model the volumetric heat source.

The IHG and the EHF are mutually exclusive, as they are meant to represent alternative ways of providing distributed heating, while either can coexist with the LHF. The following assumptions on the fluid side are made:

- The fluid flow is considered to be one-dimensional and, as aforementioned, the position inside the loop is given by the curvilinear coordinate “s”.
- The Boussinesq approximation is adopted and this entails a linear variation of the fluid density with the temperature when writing the gravitational term in the momentum equation.
- The cooler is modeled as a constant temperature wall.
- Heat conduction in the fluid is neglected and so is the dissipation term in the energy conservation equation.
- The fluid flow is considered incompressible and the same flow regime (laminar, transitional, turbulent) is assumed to exist in the whole loop.

For what concerns the solid regions, the pipe walls are discretized along the radial direction into two coaxial shells (the inner and outer wall) adopting a lumped parameter approach. The following assumptions are made:

- The wall thickness τ_w and the outer diameter D_{wo} of the pipe are constant throughout the loop.
- A specific heat capacity c_w is assigned to each shell while a conductive thermal resistance R_w is placed between the two shells.

- The wall thermo-physical properties are assumed constant.
- The axial conduction and the thermal dissipations are neglected.

The governing equations for the fluid are then:

$$\frac{\partial G}{\partial s} = 0 \text{ where } G = \rho_f^* U, \quad (3.1)$$

$$\frac{\partial G}{\partial t} + \frac{\partial}{\partial s} \frac{G^2}{\rho_f^*} = -\frac{\partial p}{\partial s} - \frac{1}{2} \lambda \frac{G^2}{\rho_f^* D_f} - g \rho_f \hat{e}_z \cdot \hat{e}_s(s), \quad (3.2)$$

$$\rho_f c_f \frac{\partial T_f}{\partial t} + G c_f \frac{\partial T_f}{\partial s} = -h(T_f - T_{w_i}) \frac{\tilde{S}_f}{\tilde{V}_f} + q''', \quad (3.3)$$

while for the walls they are:

$$\rho_w c_w \frac{\partial T_{w_i}}{\partial t} = h(T_f - T_{w_i}) \frac{\tilde{S}_{w_i}}{\tilde{V}_{w_i}} - \frac{T_{w_i} - T_{w_o}}{\tilde{V}_{w_i} \tilde{R}_w}, \quad (3.4)$$

$$\left\{ \begin{array}{l} T_{w_o} = T_c \text{ cooler} \\ \rho_w c_w \frac{\partial T_{w_o}}{\partial t} = \frac{T_{w_i} - T_{w_o}}{\tilde{V}_{w_o} \tilde{R}_w} + \frac{\tilde{S}_{w_o}}{\tilde{V}_{w_o}} (q_d'' + q_l'') \text{ heater} \\ \rho_w c_w \frac{\partial T_{w_o}}{\partial t} = \frac{T_{w_i} - T_{w_o}}{\tilde{V}_{w_o} \tilde{R}_w} + \frac{\tilde{S}_{w_o}}{\tilde{V}_{w_o}} q_d'' \text{ otherwise} \end{array} \right., \quad (3.5)$$

where

$$\begin{aligned} \tilde{V}_f &= \pi \left(\frac{D_f}{2} \right)^2 \tilde{s}, \tilde{S}_f = \pi D_f \tilde{s}, \\ \tilde{V}_{w_i} &= \pi \left[\left(\frac{D_{w_i}}{2} \right)^2 - \left(\frac{D_f}{2} \right)^2 \right] \tilde{s}, \tilde{S}_{w_i} = \pi D_{w_i} \tilde{s}, \\ \tilde{V}_{w_o} &= \pi \left[\left(\frac{D_{w_o}}{2} \right)^2 - \left(\frac{D_{w_i}}{2} \right)^2 \right] \tilde{s}, \tilde{S}_{w_o} = \pi D_{w_o} \tilde{s}, \\ \tilde{R}_w &= \frac{\ln \left(\frac{D_{w_o}}{D_f} \right)}{2\pi k_w \tilde{s}}. \end{aligned} \quad (3.6)$$

Eqs. (3.1-3.3) represent respectively the mass, momentum and energy balances for the fluid while Eqs.(3.4-3.5) are the energy balances for the inner and outer wall section. Eqs. (3.6) define quantities used in the previous equations. For Eqs. (3.1-3.6) G is the mass flux, ρ the density, U the velocity magnitude, p the pressure, λ the Darcy friction factor, D the diameter, g the gravity acceleration, c the heat capacity, T the temperature, h the heat transfer coefficient, k the thermal conductivity. The subscripts f and w stand for “fluid” and “wall”, respectively, while subscripts i and o for “inner” and “outer”; the superscript $*$ is attached to the quantities obtained at a reference positions taken as the cooler entrance ($s=0$). The unit vectors \hat{e}_s, \hat{e}_z indicate respectively the direction of the s coordinate and that of gravity (i.e., that of the z versor). The pipe wall equivalent electric circuits for the internal heat generation and external heat flux cases can be seen in Fig 3.2 and Fig 3.3.

The Darcy friction factor λ and the heat transfer coefficient are obtained by using correlations and Section 3.2.2 deals with the definition of such correlations.

3.2 The stability maps

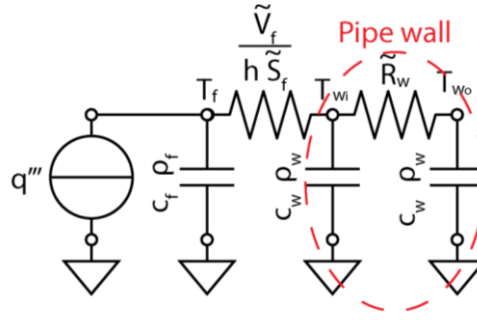


Figure 3.2. Equivalent electric circuit for the pipe wall with IHG.

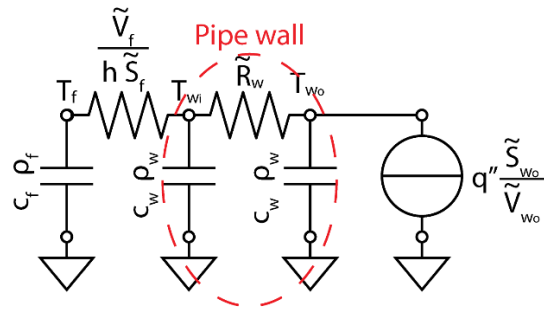


Figure 3.3. Equivalent electric circuit for the pipe wall with EHF.

3.2.2 Friction factor and heat transfer correlations

Natural circulation flow can cover laminar to turbulent regimes, depending on the given thermal power. In laminar flow the friction factor can then be calculated as $\lambda_{laminar} = \frac{64}{Re}$ (Re is the Reynolds number, $Re = \frac{\rho UD}{\mu_f}$ with μ_f the fluid dynamic viscosity) while for turbulent flow the friction factor correlation is $\lambda_{turbulent} = \frac{0.316}{Re^{0.25}}$ (De Nevers, 1970). The transition from laminar to turbulent occurs, for a straight infinite pipe, at about $Re \approx 2500$, while for a closed loop it has been observed at lower Re (≈ 340 , (Hallican and Viskanta, 1986)). In order to deal with this delicate zone a correlation of the type $f \doteq \frac{a}{Re^b}$ is used (Ruiz et al., 2015): it employs a sigmoid factor ψ_λ such that the friction factor can be ultimately written as λ (Eq. 3.7):

$$\lambda = \frac{a}{Re^b} = \frac{64 \psi_\lambda 0.316^{1-\psi_\lambda}}{Re^{\psi_\lambda + 0.25(1-\psi_\lambda)}}, \quad (3.7)$$

$$\text{with } \psi_\lambda(Re) = \left[1 + \exp\left(\frac{Re - 2530}{120}\right) \right]^{-1}.$$

The friction factor was built by fitting experimental steady-state data on fluid flow inside a straight infinite tube (Perry and Green, 2008). The proposed correlation obviously converges towards the laminar (and turbulent) friction factor as the Reynolds number goes to zero (and to infinity). It also allows to have a smooth transition from the laminar to the turbulent zone.

The full correlation is depicted in Fig. 3.4. A similar reasoning was adopted when treating the heat transfer correlations needed for the calculation of the Nusselt number ($Nu = \frac{hD_f}{k_f}$).

The latter can be computed as a function of both the Reynolds number and the Prandtl number ($Pr = \mu_f c_f / k_f$) hence the aim is to obtain a correlation which is able to span both dimensionless numbers range. As far as the Reynolds number is concerned, three ranges can be considered: for laminar flows ($Re \leq 2500$) the Hausen correlation is employed (Bergman et al., 2011), for $10^3 \leq Re \leq 10^5$ the Gnielinski correlation is adopted (Bergman et al., 2011), while for higher Reynolds number the Dittus-Boelter correlation is used (Bergman et al., 2011).

Since the three correlations deal with the variation with Re , another correlation is needed to cover also the lower Prandtl values range; hence Skupinski correlation was chosen for the purpose (Bergman et al., 2011). The Nusselt numbers computed using these correlations are combined using sigmoid factors. The total correlation is:

$$Nu = \left(Nu_H^{\psi_{Nu_1}} \left(Nu_S^{\psi_{Nu_3}} Nu_G^{1-\psi_{Nu_3}} \right)^{1-\psi_{Nu_1}} \right)^{\psi_{Nu_2}} \cdot \left(Nu_S^{\psi_{Nu_3}} Nu_D^{1-\psi_{Nu_3}} \right)^{1-\psi_{Nu_2}}, \quad (3.8)$$

with:

$$\begin{aligned} \psi_{Nu_1} &= \left(1 + \exp\left(\frac{Re - 2530}{20}\right) \right)^{-1}, \\ \psi_{Nu_2} &= \left(1 + \exp\left(\frac{Re - 10^5}{20}\right) \right)^{-1}, \\ \psi_{Nu_3} &= \left(1 + \exp\left(\frac{Pr - 0.6}{10^{-5}}\right) \right)^{-1}. \end{aligned} \quad (3.9)$$

In Eqs. (3.8 – 3.9) Nu_H, Nu_S, Nu_G, Nu_D represent respectively the Nusselt numbers calculated using Hausen, Skupinski, Gnielinski and Dittus-Boelter correlation while $\psi_{Nu_1}, \psi_{Nu_2}, \psi_{Nu_3}$ are the sigmoid factors for the transition from laminar to turbulent flow, from Gnielinski to Dittus-Boelter correlation and from a low to high Prandtl. The correlations adopted and their applicability range are shown in Table 3.1; their representation comes in Fig. 3.5 (Pini, 2017).

3.2.3 Steady state

The steady state temperature distribution can be obtained by imposing the derivative term in equations (3.3 – 3.5) equal to zero. The steady state quantities will be indicated with the subscript zero. For the sake of brevity only the fluid temperature distribution will be shown.

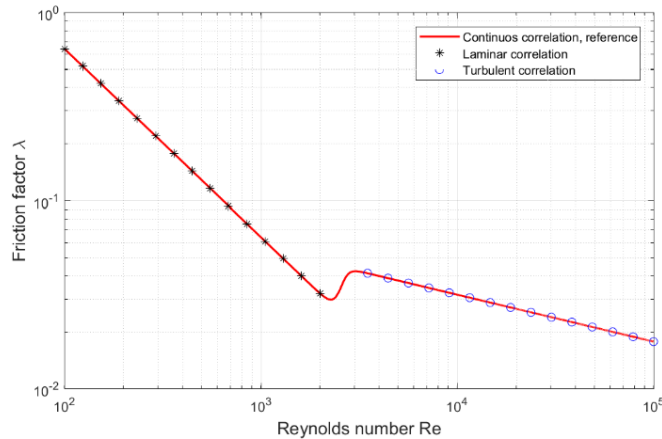


Figure 3.4. Employed friction factor correlation.

3.2 The stability maps

Table 3.1. Correlations for the Nusselt number calculation and applicability ranges.

Correlation name	Correlation formula	Reynolds range	Prandtl range
Skupinski et al.	$Nu = 4.82 + 0.0185(RePr)^{0.827}$	$3.6 \cdot 10^3 \leq Re \leq 9.05 \cdot 10^5$	$3 \cdot 10^{-3} \leq Pr \leq 5 \cdot 10^{-2}$
Hausen	$Nu = 3.66 + \frac{0.668 \frac{D_f}{L_t} Re Pr}{1 + 0.04 \left(\frac{D_f}{L_t} Re Pr \right)^{0.67}}$	Laminar	Uniform wall temperature
Gnielinski	$Nu = \frac{\frac{f}{8} (Re - 1000) Pr}{1 + 12.7 \left(\frac{f}{8} \right)^{0.5} (Pr^{0.67} - 1)}$ $f = (0.79 \ln Re - 1.64)^{-2}$	$3 \cdot 10^3 \leq Re \leq 5 \cdot 10^6$	$5 \cdot 10^{-1} \leq Pr \leq 2 \cdot 10^3$
Dittus-Boelter	$Nu = 0.023 Re^{0.8} Pr^{0.3}$	$Re \geq 10^4$	$6 \cdot 10^{-1} \leq Pr \leq 1.6 \cdot 10^2$ (Cooling)

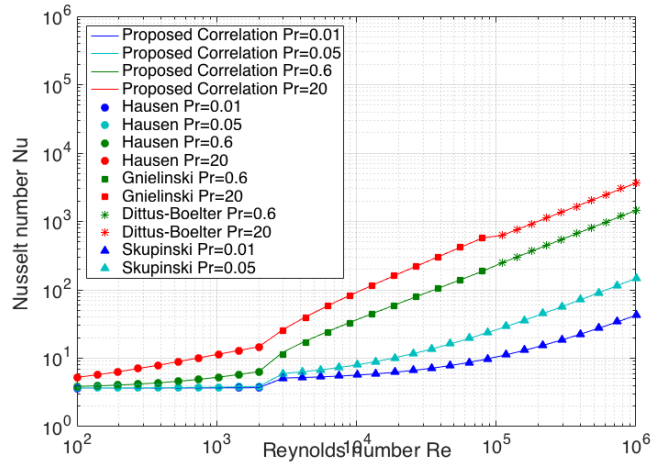


Figure 3.5. Nusselt number trends.

Eqs. (3.10-3.13) are respectively the steady state fluid temperature profiles for the cooler, the cold leg, the heater and the hot leg.

$$\begin{aligned}
 T_{f,0}(s) = & T_{f,0}(s = 0) \\
 & + \left(T_c + \frac{D_f}{4h_0} \left(1 + \frac{h_0 \left(D_f \ln \left(\frac{D_{w_0}}{D_f} \right) \right)}{2k_w} \right) q''' - T_{f,0}(s = 0) \right) \\
 & \cdot \left[1 - \exp \left(-\zeta \frac{s}{L_t} \right) \right], \quad (3.10)
 \end{aligned}$$

$$T_{f,0}(s) = T_{f,0}(s = L_c) + \frac{q'''}{G_0 c_f} (s - L_c) + \frac{q''_d}{G_0 c_f} \frac{4D_{w_0}}{D_f^2} (s - L_c), \quad (3.11)$$

$$T_{f,0}(s) = T_{f,0}(s = L_c) + \frac{q'''}{G_0 c_f} (s - L_c) + \frac{1}{G_0 c_f} \frac{4D_{w_o}}{D_f^2} [q_l''(s - L_c - L_{cl}) + q_d''(s - L_c)], \quad (3.12)$$

$$T_{f,0}(s) = T_{f,0}(s = L_c) + \frac{q'''}{G_0 c_f} (s - L_c) + \frac{1}{G_0 c_f} \frac{4D_{w_o}}{D_f^2} [q_l'' L_h + q_d''(s - L_c)], \quad (3.13)$$

with:

$$\zeta = \frac{St_{m,0}}{1 + h_0 \frac{D_f \ln\left(\frac{D_{w_o}}{D_f}\right)}{2k_w}}, \quad (3.14)$$

and $St_{m,0}$ in Eq. (3.14) being the modified Stanton number, defined as:

$$St_{m,0} = 4 \frac{L_t}{D_f} St_o = 4 \frac{L_t}{D_f} \frac{Nu_o}{Re_o Pr_o}. \quad (3.15)$$

Another equation is needed in order to close the problem and it is found by imposing that the temperature distribution (both for fluid and walls) at the cooler entrance is the same as that at the hot leg exit ($T_0(s = 0) = T_0(s = L_t)$). The resulting condition is then:

$$T_{f,0}(s = 0) = T_c + \frac{\frac{D_f}{4} \left(1 + h_0 \left(\frac{D_f \ln\left(\frac{D_{w_o}}{D_{w_i}}\right)}{2k_w} \right) \right)}{h_0} q'' + \frac{\frac{q_l''}{G_0 c_f} \frac{4D_{w_o}}{D_f^2} L_h + \frac{q'''}{G_0 c_f} (L_t - L_c) + \frac{q_d''}{G_0 c_f} \frac{4D_{w_o}}{D_f^2} (L_t - L_c)}{1 - \exp(-\zeta L_c \setminus L_t)}. \quad (3.16)$$

In Eq. (3.16) three fundamental terms arise, namely the fluid temperature difference in the cooler induced by the LHF ΔT_{LHF} , the fluid temperature difference caused by the IHG outside the cooler ΔT_{IHG} and the temperature jump produced by the EHF ΔT_{EHF} :

$$\Delta T_{LHF} = \frac{q_l''}{G_0 c_f} \frac{4D_{w_o}}{D_f^2} L_h, \quad (3.17)$$

$$\Delta T_{IHG} = \frac{q'''}{G_0 c_f} (L_t - L_c), \quad (3.18)$$

$$\Delta T_{EHF} = \frac{q_d''}{G_0 c_f} \frac{4D_{w_o}}{D_f^2} (L_t - L_c). \quad (3.19)$$

It is then possible to define the total temperature variation outside the cooler due to the presence of either the LHF and IHG ($\Delta T_{LHF+IHG}$) or the LHF and EHF ($\Delta T_{LHF+EHF}$) sources.

$$\Delta T_{LHF+IHG} = \Delta T_{LHF} + \Delta T_{IHG}, \quad (3.20)$$

3.2 The stability maps

$$\Delta T_{LHF+EHF} = \Delta T_{LHF} + \Delta T_{EHF}. \quad (3.21)$$

From the ratio between ΔT_{LHF} and the total temperature variation (either $\Delta T_{LHF+IHG}$ or $\Delta T_{LHF+EHF}$) the following parameters can be written:

$$\alpha_{LHF+IHG} = \frac{\Delta T_{LHF}}{\Delta T_{LHF+IHG}} \quad (3.22)$$

$$\alpha_{LHF+EHF} = \frac{\Delta T_{LHF}}{\Delta T_{LHF+EHF}} \quad (3.23)$$

Hereinafter, the symbols α and ΔT are used whenever the discrimination between the LHF+IHG or the LHF+EHF is not necessary. For $\alpha = 1$ only the localized heat source is present and it corresponds to the conventional natural circulation case. For $\alpha_{LHF+IHG} = 0$ only the IHG source is active in the system, similarly for $\alpha_{LHF+EHF} = 0$ only the EHF is functioning. In Eqs. (3.10-3.13), (3.16-3.19) one can notice that the steady state flow rate is employed; this quantity is obtained by solving the momentum conservation equation after having used Eq. (3.1) and integrating Eq. (3.2) over the entire loop. Doing so yields the following equation:

$$\frac{1}{2} \lambda_0 \frac{G_0^2}{\rho_f^*} \left(\frac{L_t + L_{eq}}{D_f} \right) = -g \oint \rho_{f,0}(s) \hat{e}_z \cdot \hat{e}_s(s) ds. \quad (3.24)$$

In Eq. (3.24) L_{eq} represents an equivalent length that takes into account the effect of localized pressure drops while $\rho_{f,0}(s)$ is the steady state density distribution inside the loop. The only accounted dependency for the density is the one on the temperature, through Boussinesq approximation (valid only if the fluid is far from saturation conditions):

$$\rho_f \approx \rho_f^* [1 - \beta_f (T_f - T_f^*)]. \quad (3.25)$$

In Eq. (3.25) β_f is the thermal expansion coefficient evaluated at the reference temperature T_f^* , taken as $T_{f,0}(s = 0)$. Hence, Eq. (3.24) becomes:

$$\frac{1}{2} \lambda_0 \frac{G_0^2}{\rho_f^*} \left(\frac{L_t + L_{eq}}{D_f} \right) = \rho_f^* g \beta_f \oint T_{f,0}(s) \cdot \hat{e}_z \cdot \hat{e}_s(s) ds \quad (3.26)$$

In Eq. (3.26) the temperature line integral depends on the loop geometry. For the case in which localized and distributed heating cause the temperature increment ΔT along the loop, it is possible to show (Ruiz et al., 2015) that such integral can be written as:

$$\begin{aligned} \oint T_{f,0}(s) \hat{e}_z \cdot \hat{e}_s(s) ds &= \Delta T_{LHF} \mathcal{L}_l + \Delta T_{IHG} \mathcal{L}_d \\ &= \Delta T_{LHF+IHG} (\alpha_{LHF+IHG} \mathcal{L}_l + \alpha_{LHF+IHG} \mathcal{L}_d), \end{aligned} \quad (3.27)$$

$$\begin{aligned} \oint T_{f,0}(s) \hat{e}_z \cdot \hat{e}_s(s) ds &= \Delta T_{LHF} \mathcal{L}_l + \Delta T_{EHF} \mathcal{L}_d \\ &= \Delta T_{LHF+EHF} (\alpha_{LHF+EHF} \mathcal{L}_l + \alpha_{LHF+EHF} \mathcal{L}_d). \end{aligned} \quad (3.28)$$

Eq. (3.27) holds when both LHF and IHG are present, while Eq. 3.28 holds when both LHF and EHF are the employed heating modes. \mathcal{L}_l represents the difference in height between the thermal barycenter of the heater and that of the cooler while \mathcal{L}_d is a weighted height of the loop which accounts for the heating effect for both IHG and EHF sources; these quantities can be analytically defined for a given direction of the steady state flow once the loop geometry is fully characterized. Having underlined that, Eq. (3.26) can be written in a general way as:

$$\frac{1}{2} \lambda_0 \frac{G_0^2}{\rho_f^*} \left(\frac{L_t + L_{eq}}{D_f} \right) = \rho_f^* g \beta_f \Delta T [\alpha \mathcal{L}_l + (1 - \alpha) \mathcal{L}_d]. \quad (3.29)$$

The parameter α which appears in the latter equation can take one of the forms shown in Eqs. (3.22-3.23) depending on whether the distributed heating is due to an external heat flux (EHF) or a volumetric source (IHG).

3.2.4 Modal analysis

The dynamic behavior of the NCL is studied making use of modal analysis which is valid for any circuit configuration. The system of equations is linearized around a steady-state condition meaning that the solution to the system of equations is seen as the sum of a stationary term, already obtained (Eqs. (3.10-3.13)) in terms of $G_0, T_{f0}, T_{w_i,0}, T_{w_o,0}$, and of a perturbation which is small in comparison to the stationary term but changing in time. The resolution of the system of equations then yields the evolution of the perturbation in time. In a more explicit way:

$$G(t) \simeq G_0 + \delta G(t) \text{ with } \delta G(t) \ll G_0 \forall t \in \mathbb{R}^+, \quad (3.30)$$

$$T_f(s, t) \simeq T_{f,0}(s) + \delta T_f(s, t) \text{ with } \delta T_f(s, t) \ll T_{f,0}(s) \\ \forall (s, t) \in [0, L_t] \times \mathbb{R}^+, \quad (3.31)$$

$$T_{w_i}(s, t) \simeq T_{w_i,0}(s) + \delta T_{w_i}(s, t) \text{ with } \delta T_{w_i}(s, t) \ll T_{w_i,0}(s) \\ \forall (s, t) \in [0, L_t] \times \mathbb{R}^+, \quad (3.32)$$

$$T_{w_o}(s, t) \simeq T_{w_o,0}(s) + \delta T_{w_o}(s, t) \text{ with } \delta T_{w_o}(s, t) \ll T_{w_o,0}(s) \\ \forall (s, t) \in [0, L_t] \times \mathbb{R}^+. \quad (3.33)$$

The perturbed variables (3.30-3.33) are inserted in the balance equations and a set of linear differential equations for the perturbed variables is obtained. During the linearization process the a and b parameters of the Darcy friction factor are kept constant, neglecting any dependence on $\delta G(t)$ (it brings some minor changes in λ only in the laminar-turbulent transition zone, (Ruiz et al.,2015)); conversely the heat transfer coefficient h is also linearized to take into account the effect that the mass flux perturbation (and therefore the Reynolds number) has on heat exchange in the cooler. If a correlation in the form of the Dittus-Boelter is expected for h , then it is possible to write:

$$h = \frac{k_f}{D_f} \varepsilon Re^B Pr^F = \frac{k_f}{D_f} \varepsilon \left[\frac{(G_0 + \delta G) D_f}{\mu_f} \right]^B Pr^F = h_0 \left(1 + \frac{\delta G}{G_0} \right)^B \quad (3.34)$$

Linearization of Eq. (3.34) gives a relation which links δh to δG :

$$\delta h = B \frac{h_0}{G_0} \delta G. \quad (3.35)$$

The term B allows considering a relation between the mass flux and heat exchange perturbation (Pini, 2017). To formally calculate B , it is possible to perform a Taylor expansion of h as a function of G :

$$h(G) \simeq h_0 + \left. \frac{\partial h}{\partial G} \right|_0 \delta G \quad (3.36)$$

Noting that:

$$\delta h = \left. \frac{\partial h}{\partial G} \right|_0 \delta G, \quad (3.37)$$

and comparing Eqs. (3.35) and (3.37) one can write:

$$B = \frac{G_0}{h_0} \left. \frac{\partial h}{\partial G} \right|_0 = \frac{Re_0}{Nu_0} \left. \frac{\partial Nu}{\partial Re} \right|_0 \quad (3.38)$$

Having done this consideration, it is possible to linearize the system of equations after substituting Eqs. (3.30-3.33) and Eq. (3.35) in the main balance equations, obtaining:

3.2 The stability maps

$$\frac{d\delta G}{dt} + \frac{1}{2}\lambda_0 \frac{2-b_0}{\rho_f^*} G_0 \delta G \frac{L_t + L_{eq}}{D_f} = \rho_f^* g \beta_f \phi \delta T_f(s, t) \hat{e}_z \cdot \hat{e}_s(s) ds, \quad (3.39)$$

$$\begin{aligned} & \rho_f c_f \frac{\partial \delta T_f}{\partial t} + G_0 c_f \frac{\partial \delta T_f}{\partial s} + \delta G c_f \frac{dT_{f,0}}{ds} = \\ & = -h_0 (\delta T_f - \delta T_{w_i}) \frac{\tilde{S}_f}{\tilde{V}_f} - \left. \frac{\partial h}{\partial G} \right|_0 \delta G (T_{f,0} - T_{w_i,0}) \frac{\tilde{S}_f}{\tilde{V}_f}, \end{aligned} \quad (3.40)$$

$$\begin{aligned} & \rho_w c_w \frac{\partial \delta T_{w_i}}{\partial t} = \\ & = -h_0 (\delta T_f - \delta T_{w_i}) \frac{\tilde{S}_{w_i}}{\tilde{V}_{w_i}} + \left. \frac{\partial h}{\partial G} \right|_0 \delta G (T_{f,0} - T_{w_i,0}) \frac{\tilde{S}_{w_i}}{\tilde{V}_{w_i}} - \frac{\delta T_{w_i} - \delta T_{w_o}}{\tilde{V}_{w_i} \bar{R}_w}, \end{aligned} \quad (3.41)$$

$$\left\{ \begin{array}{l} \delta T_{w_o} = 0 \text{ cooler} \\ \rho_w c_w \frac{\partial \delta T_{w_o}}{\partial t} = \frac{\delta T_{w_i} - \delta T_{w_o}}{\tilde{V}_{w_o} \bar{R}_w} \text{ otherwise} \end{array} \right. \quad (3.42)$$

Eqs. (3.39) and (3.40) represent the linear momentum and energy equations for the fluid, while Eqs. (3.41) and (3.42) represent the linear energy equation for the inner and outer walls. Each perturbation is written as an exponential of time, according to modal theory, in the form:

$$\delta \psi(s, t) = \tilde{\psi}(s) \exp(\omega \cdot t) \text{ with } \omega \in \mathbb{C}, \quad (3.43)$$

(where ψ can be one among G, T_f, T_{w_i}, T_{w_o}) and the following dimensionless quantities are defined:

$$\begin{aligned} \bar{\omega} &= \frac{\omega L_t \rho_f}{G_0}, \bar{G} = \frac{\tilde{G}}{G_0}, \bar{T}_{f, w_i, w_o} = \frac{\tilde{T}_{f, w_i, w_o}}{\Delta T}, \bar{s} = \frac{s}{L_t}, \bar{L}_i = \frac{L_i}{L_t} \\ \bar{\rho} &= \frac{\rho_f}{\rho_w}, \bar{c} = \frac{c_f}{c_w}, \bar{k} = \frac{k_f}{k_w}, \bar{V} = \frac{\tilde{V}_f}{\tilde{V}_w} (V_{w_i} \simeq V_{w_o} = V_w), \\ \bar{R}_w &= \frac{1}{2} \ln \left(1 + \frac{2\tau_w}{D_{w_i}} \right), \end{aligned} \quad (3.44)$$

so that the non-dimensional linear equations for the system are obtained:

$$\bar{\omega} \bar{G} + \frac{1}{2} \lambda_0 \frac{L_t + L_{eq}}{D_f} \left[(2 - b_0) \bar{G} - \frac{L_t}{\alpha \mathcal{L}_l + (1 - \alpha) \mathcal{L}_d} \phi \delta \bar{T}_f(\bar{s}) \hat{e}_z \cdot \hat{e}_s(\bar{s}) d\bar{s} \right] = 0, \quad (3.45)$$

$$\frac{d\bar{T}_f}{d\bar{s}} + \bar{\omega} \bar{T}_f + \frac{\bar{G}}{\Delta T} \frac{dT_{f,0}}{d\bar{s}} = -St_{m,0} (\bar{T}_f - \bar{T}_{w_i}) - BSt_{m,0} \bar{G} \frac{(T_{f,0} - T_{w_i,0})}{\Delta T}, \quad (3.46)$$

$$\frac{\bar{\omega}}{\bar{\rho} \bar{c}} \bar{T}_{w_i} = St_{m,0} (\bar{T}_f - \bar{T}_{w_i}) \bar{V} + BSt_{m,0} \bar{G} \frac{(T_{f,0} - T_{w_i,0})}{\Delta T} \bar{V} - St_{m,0} \frac{\bar{T}_{w_i} - \bar{T}_{w_o}}{Nu_0 \bar{k} \bar{R}_w} \bar{V}, \quad (3.47)$$

$$\left\{ \begin{array}{l} \bar{T}_{w_o} = 0 \text{ Cooler} \\ \frac{\bar{\omega}}{\bar{\rho} \bar{c}} \bar{T}_{w_o} = St_{m,0} \frac{\bar{T}_{w_i} - \bar{T}_{w_o}}{Nu_0 \bar{k} \bar{R}_w} \bar{V} \text{ Otherwise.} \end{array} \right. \quad (3.48)$$

The new set of Eqs. (3.45-3.48) represent the Laplace transform of the non-dimensional linear governing equations. This can be seen as an eigenvalue problem. Moreover, the real part of the

eigenvalue ω defines the change in magnitude of the perturbations in time, hence the stability condition is simply translated in the requirement that the real part of ω must be negative. $\Re(\omega) < 0$ allows the system equilibrium to be asymptotically stable since the mass flow and temperature perturbations decrease exponentially to zero in time. Overall, the system described by Eqs. (3.45-3.48) depends on dimensionless numbers (referred to steady-state conditions) and it can be solved once a couple is chosen. Since both Nu and St_m can be obtained as function of Re and Pr as:

$$Nu_0 = Nu_0(Re_0, Pr_0), \quad (3.49)$$

and

$$St_{m,0} = St_{m,0}(Nu_0(Re_0, Pr_0), Re_0, Pr_0). \quad (3.50)$$

Re and Pr result the more practical pair of dimensionless numbers to use. However, several coordinate changes can be applied to express solutions to Eqs. (3.45-3.48) using other non-dimensional couples. For instance, stability maps are often plotted in the $(St_{m,0}, Gr_{m,0})$ plane besides using the usual (Pr_0, Re_0) . The $St_{m,0}$ value can be easily calculated computing the Nusselt number for every (Pr_0, Re_0) using the empirical correlations shown in Table 3.1. The modified Grashof $Gr_{m,0}$ number can be defined writing Eq. 3.26 in an alternative way:

$$\frac{a_0}{2} Re_0^{3-b} \frac{L_t + L_{eq}}{D_f} = Gr_{m,0}, \quad (3.51)$$

with

$$Gr_{m,0} = \frac{\rho_{f,0}^2 g D_f^3}{\mu_{f,0}^2} \beta_f \Delta T_m \text{ and } \Delta T_m = \frac{G_0}{\mu_{f,0}} \Delta T (\alpha \Omega_l + (1 - \alpha) \Omega_d). \quad (3.52)$$

With these considerations, it is possible to solve the energy equations Eqs. (3.46-3.48) for all the sections of the systems, as a function of \bar{G} . The complete procedure is quite long and complex (Pini, 2017) and yields an analytical solution for the temperature field. Since the solved equations are linear, it is expected that the temperature perturbation \bar{T}_f depends linearly on the mass flux perturbation \bar{G} . It is then possible to substitute the retrieved solutions in the dimensionless momentum balance Eq. (3.45) to find the dispersion relation of the system. The line integral appearing in Eq. (3.45) can be written as follows:

$$\oint \bar{T}_f(\bar{s}, t) \hat{e}_z \cdot \hat{e}_s(\bar{s}) d\bar{s} = \int_{up} \bar{T}_f(\bar{s}) d\bar{s} - \int_{down} \bar{T}_f(\bar{s}) d\bar{s} = \bar{G} A(\bar{\omega}, Gr_{m,0}, St_{m,0}, \alpha, \bar{\rho}, \bar{c}, \bar{V}), \quad (3.53)$$

where A is a function that does not depend on the mass flux, \int_{up} stands for the line integral of the temperature perturbation on the side of the loop where the fluid is ascending and \int_{down} stands the same but for the descending fluid. When function A is substituted into Eq. (3.45) the dispersion relation of the system reads:

$$\bar{\omega} + \frac{1}{2} \lambda_0 \frac{L_t + L_{eq}}{D_f} \left[(2 - b_0) - \frac{L_t}{\alpha L_l + (1 - \alpha) L_d} A(\bar{\omega}, Gr_{m,0}, St_{m,0}, \alpha, \bar{\rho}, \bar{c}, \bar{V}) \right] = 0 \quad (3.54)$$

To sum up, the energy equations are solved so that the perturbed dimensionless temperature profiles can be obtained; hence, the integral in Eq. (3.53) can be calculated and expressed as a function of the perturbed dimensionless mass flux through the definition of A . The Eq. (3.53) integral in its new form can then be substituted back in the dimensionless momentum equation, causing elision of the perturbed mass flux and allowing to write the dispersion relation for $\bar{\omega}$. Such a relation depends on the steady-state modified Grashof and Stanton numbers $Gr_{m,0}, St_{m,0}$, the way heat is supplied to the system through α , the flow direction, the system geometry and the pipe wall characteristics. For given loop geometry, pipe properties and $Gr_{m,0}$, the dispersion equation can be solved with the constraint $\Re(\omega) = 0$ to find the corresponding $St_{m,0}$ number(s) which satisfies it: an equilibrium state

3.2 The stability maps

identified by the couple $Gr_{m,0}, St_{m,0}$, which corresponds to the transition between stable and unstable equilibria, is found. Repeating the process for a sufficiently wide range of Grashof numbers allows “mapping”, among all the equilibrium states of the system, only those which satisfy the Lypaunov stability requirement (Lyapunov, 1892), creating a geometrical locus that separates unstable and asymptotically stable system equilibria (i.e., a stability map). In the present work Eq. 3.54 is solved thanks to the Trust-Region-Dogleg algorithm of MATLAB (MATLAB, 2017).

3.2.5 The reference stability map for *Dynasty*

Obtaining the stability map of a rectangular natural circulation loop requires multiple steps which strictly depend on the peculiar geometry of the system. For instance, the weighted lengths \mathcal{L}_l and \mathcal{L}_d , which are necessary for retrieving the steady-state mass flux G_0 (Eq. (3.29)), require the resolution of the steady-state temperature line integrals (Eqs. 3.27-3.28) and therefore they are tightly tied to the loop geometrical configuration; similarly, the A function necessary to solve the dispersion relation is obtained after solving the perturbed temperature line integrals, hence it also depends on the circuit geometry. From now on, the reference geometry adopted will be that of DYNASTY as-built. In order to construct a stability map, also other parameters are required and the choice of such parameters influences the form of the map. In particular, the stability map presented here considers DYNASTY operating with molten salt. When computing the reference stability map for DYNASTY, the quantities in Table 3.2. are adopted. More specifically: the metal thermo-physical properties are calculated at 300°C, the salt properties are those for the SALT1 type, the L_{eq} parameter for the localized losses is taken as equal to 2.4 m after considering the specific DYNASTY loop, the transition from laminar to turbulent flow is considered to happen (Ruiz, 2015) at a Reynolds number equal to 2530 and power is provided in a distributed way. The latter consideration means that the α parameter met in Eq. (3.22) is being used and it is equal to 0.

Table 3.2. Adopted quantities for the computation of DYNASTY reference stability map.

Quantity	Value
Geometry of the loop	DYNASTY as-built sizes (see Fig. 1.1)
AISI 316 thermal properties (1): density (300°C)	8238 kg/m ³
AISI 316 thermal properties (2): specific heat capacity (300°C)	543.8 J/(kg · K)
AISI 316 thermal properties (3): thermal conductivity (300°C)	17.88 W/(m · K)
SALT1 thermal properties (1): density (300°C)	1860.13 kg/m ³
SALT 1 thermal properties (2): specific heat capacity (300°C)	1560 J/(kg · K)
SALT 1 thermal properties (3): thermal conductivity (300°C)	0.48 W/(m · K)
Heating mode	Distributed heating only, $\alpha = 0$
L_{eq}	2.4 m

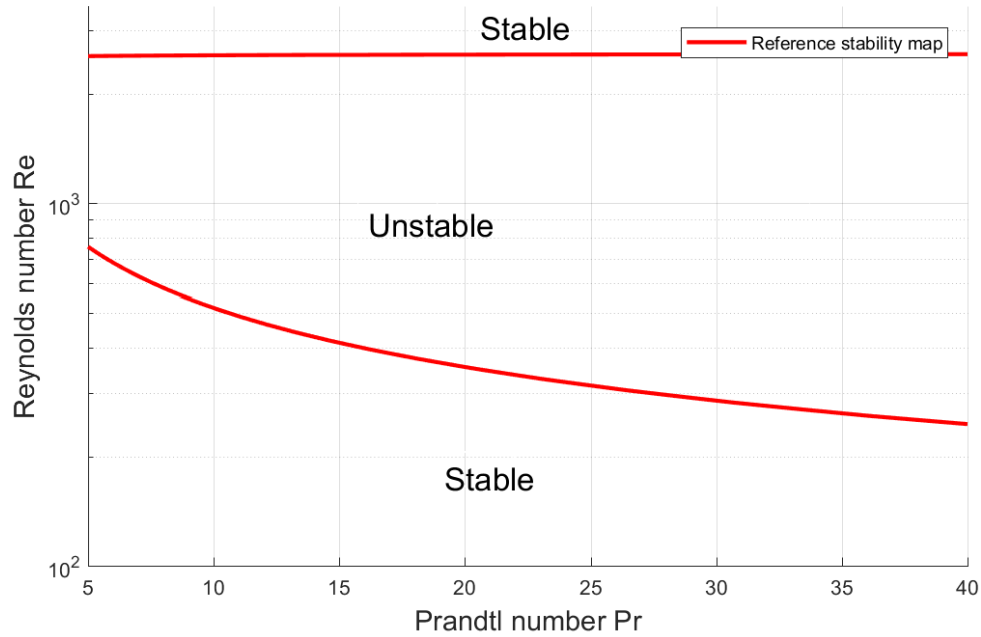


Figure 3.6. DYNASTY reference stability map.

The dimensionless number pair chosen for the representation (and for the sensitivity analysis) is the Prandtl - Reynolds one and the reference map obtained is shown in Fig. 3.6. The (Re, Pr) range used corresponds to values that can be reached by DYNASTY in operation, as the Prandtl number spans between approximately 7 and 30 and the Reynolds variates between about 100 and 3000, as expected from previous studies and simulations (Pini, 2017). For these intervals both stable and unstable behavior can be appreciated.

One can notice the asymptotically stable zones belonging to both turbulent and laminar flow states while instability seems linked to the flow regime transition zone; additionally, more equilibrium states are unstable with growing Prandtl number. The following sections will show how much a change in one of the parameters chosen for the map calculation can influence the shape of the reference map.

3.3 Sensitivity analysis

As stated before, a reference stability map is produced for DYNASTY: such a tool can be used to easily analyze the asymptotic behavior of the system on a wide range of equilibrium states and also give indication on the (Re, Pr) regions which need further investigation, for instance with the use of time-dependent models. However, the predictions of the stability maps are influenced by variations of parameters. The size of the facility, the diameter and thickness of the pipes, are affected by uncertainty and it is important to assess the influence of such uncertainty on the stability map. Additionally, the ratio of thermo-physical properties varies with temperature, while in the map model it is considered constant, thus the representative value is chosen by selecting arbitrary reference conditions. It is of interest to understand how the choice of these “representative” values can influence the map. Seeing the influence the various parameters have on the stability map will allow, once experimental data on DYNASTY is obtained, to select the most apt values for the parameters themselves, if they are subject to some uncertainty.

3.3 Sensitivity analysis

In this framework, a sensitivity analysis on the chosen parameters of the stability map is needed to evaluate the changes of the map, and therefore the changes in the prediction of the asymptotic stability of an equilibrium state, due to both uncertainty in parameters and modifications in the modeling choices adopted. Such a study should highlight both qualitatively and quantitatively the elements whose change mostly affect the map form. Going more in detail, a sensitivity analysis is necessary for the following reasons:

- The friction factor coefficient is calculated, for any flow regime, using a correlation that blends the two correlations available for the laminar and turbulent flow, as shown in Eq. (3.7). The definition of the joining equation introduces two parameters (the Re transition value and the steepness of the sigmoid transition) that may have an effect on the map.
- Analogously to the friction factor, also the heat transfer coefficient on the fluid side is computed through many correlations merged together to cover wide Prandtl and Reynolds number ranges as shown by Eq. (3.8). This introduces new quantities whose influence on the map needs evaluation.
- In the stability map definition, the pipe wall properties are introduced as dimensionless ratios where the metal property is divided by the corresponding salt property at a reference temperature. It is of interest to evaluate if a variation of the reference temperature, which implies a change in these ratios, causes also a variation in the map. The sensitivity of the map to the implemented salt properties correlations is also studied.
- The effect of the uncertainty in the size of the facility pipes (thickness and diameter) on the map is taken into account as well as that in the L_{eq} parameter.

The qualitative effects of the changes on the map are visually displayed by showing the modified map outputs compared to the reference case. On the quantitative side, a figure of merit (FOM) was selected in order to attach a relevant number to each case and compare it to that of the reference. The figure of merit was defined in the following way:

$$FOM = \frac{\text{area of the stable region in the map}}{\text{total area of the map}}.$$

Both areas are limited to the Prandtl - Reynolds DYNASTY operative range. The FOM obtained for the modified map is compared against the one for the reference map giving an actual numerical comparison between the two cases. The FOM value for the reference case is equal to 0.3587 meaning that the 35.87% of the map is occupied by asymptotically stable equilibrium states. It should be pointed out that the stability map in Fig. 3.6 is plotted on semi-log axis, hence the stable region appears larger. All the points listed before are examined in the following paragraphs and eventually an overall quantitative view of the analysis is given through the introduction of sensitivity coefficients.

3.3.1 Stability map sensitivity to friction factor coefficient definition

Natural circulation results from the dynamic equilibrium of buoyancy and friction forces; it is then expected that changing the way the friction factor is calculated in the model influences the results of the model. For the computation of the reference stability map, the friction factor is calculated resorting to two different correlations, one for the laminar zone and one for the turbulent one, joined together using a sigmoid, as shown in Eq. (3.7). With such a function, two parameters are introduced, namely the transition Reynolds number Re_{trans} and the steepness σ , which are intrinsic to the sigmoid definition. Eq (3.55) presents the sigmoid function with the highlighted terms:

$$\psi_{\lambda}(Re) = \left[1 + \exp\left((Re - Re_{trans})\sigma\right) \right]^{-1}. \quad (3.55)$$

From literature (Ruiz et al., 2015), in the reference stability map Re_{trans} and σ were chosen to be 2530 and 120^{-1} respectively, but a change in these parameters may influence deeply the stability map. A sensitivity analysis is then performed using the values shown in Table 3.3 and Table 3.4.

It is possible to notice from Fig. 3.7 and Fig. 3.8 that a variation in Re_{trans} (keeping σ constant) implies a variation in the transition point in the friction factor correlation while a change in σ (with constant Re_{trans}) causes a change in the steepness of the transition (the two correlations merge more smoothly as σ decreases).

Table 3.3. Adopted parameters for the sensitivity analysis to Re_{trans} .

Case	σ	Re_{trans}
Tr1	120^{-1}	1500
Tr2 (reference)		2000
Tr3		2530
Tr4		3000
Tr5		3500

Table 3.4. Adopted parameters for the sensitivity analysis to the sigmoid steepness σ .

Case	Re_{trans}	σ
St1	2530	480^{-1}
St2 (reference)		240^{-1}
St3		120^{-1}
St4		80^{-1}
St5		68^{-1}

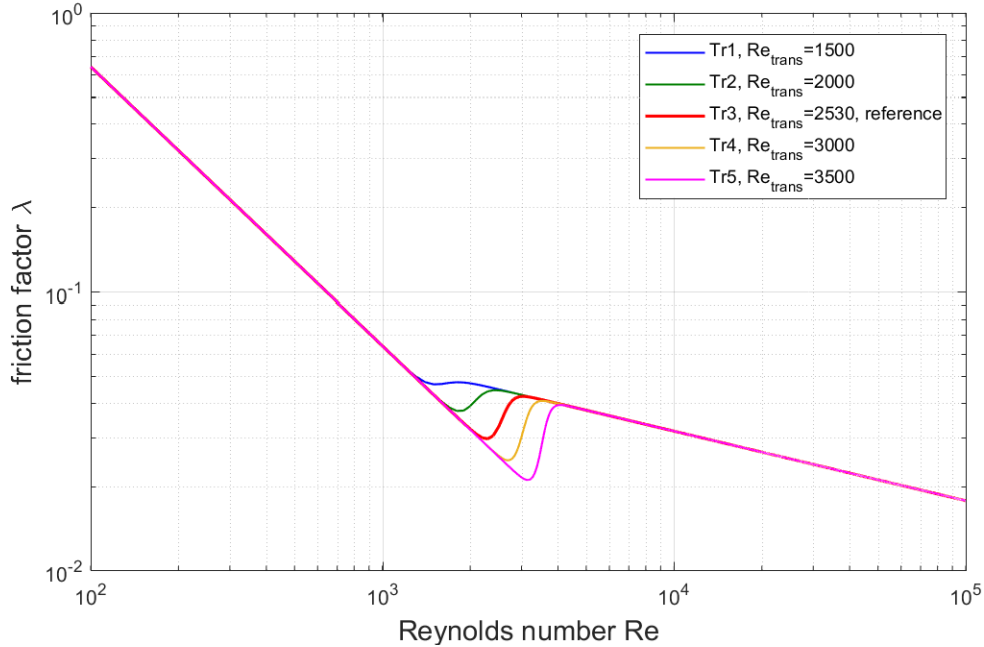


Figure 3.7. Friction factor behavior with changing Re_{trans} .

Fig. 3.9 shows that a variation in the transition Reynolds number highly impacts the stability map since the higher border of the map moves exactly with Re_{trans} ; on the other hand, the lower border, covering the laminar zone, is not impacted by the change. It is also possible to notice how the considered Reynolds range in the figure is larger than the reference case to allow visualization of the alterations induced by higher Re_{trans} .

3.3 Sensitivity analysis

Such a wide span of Re_{trans} was considered since the actual transition Reynolds number from laminar to turbulent regime is not well known as far as natural circulation flow is concerned. Overall it is observed that an increase in Re_{trans} causes a greater number of equilibrium states to be considered unstable. The highest FOM variation is seen for a transition Reynolds numbers equal to 1500, with an observed 85% change with respect to the reference value.

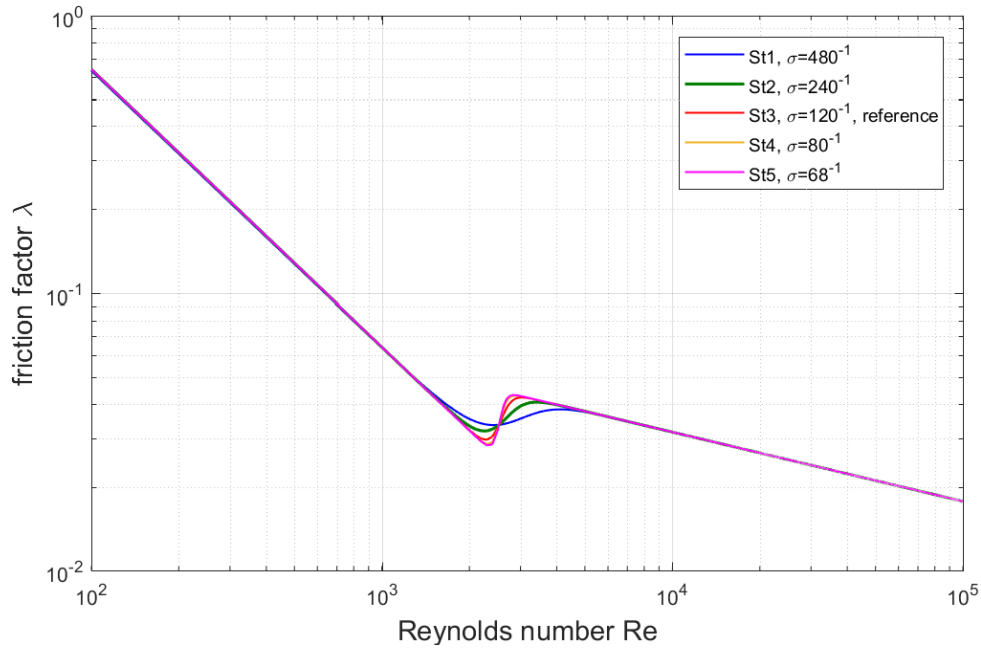


Figure 3.8. Friction factor behavior with changing σ .

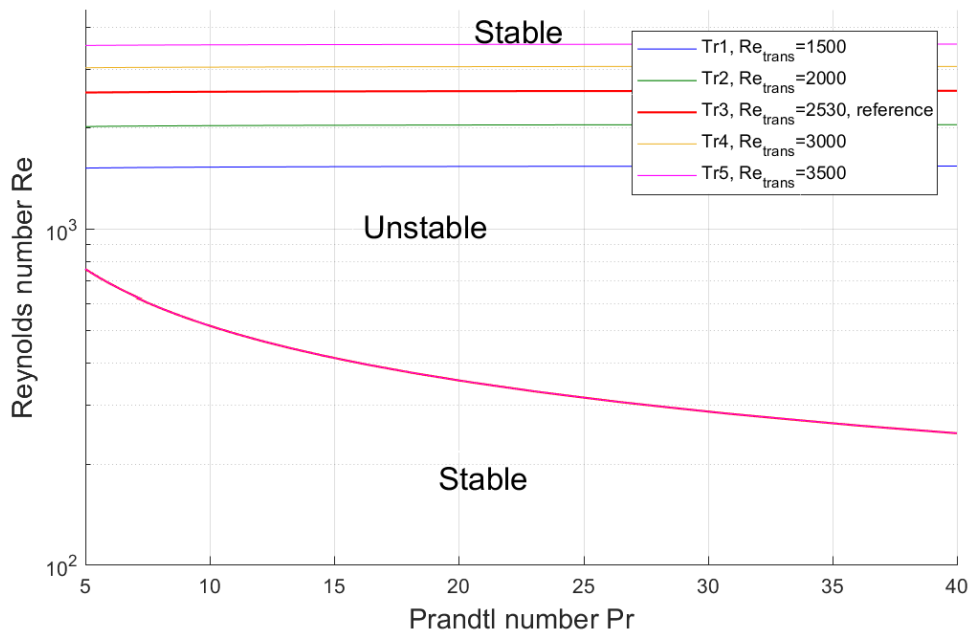


Figure 3.9. Stability map with varying Re_{trans} .

Such a trend is not observed when modifying the steepness value σ , as seen in Fig. 3.10; it appears that decreasing this quantity leads to a shrink of the stable region but quite limitedly with respect to

the reference case. A maximum 2% change (in comparison to the reference value) in the FOM value is registered, corresponding to the $\sigma = 1000^{-1}$ case (from Fig. 3.8, this effect can be ascribed to the change in the laminar region for such value of σ).

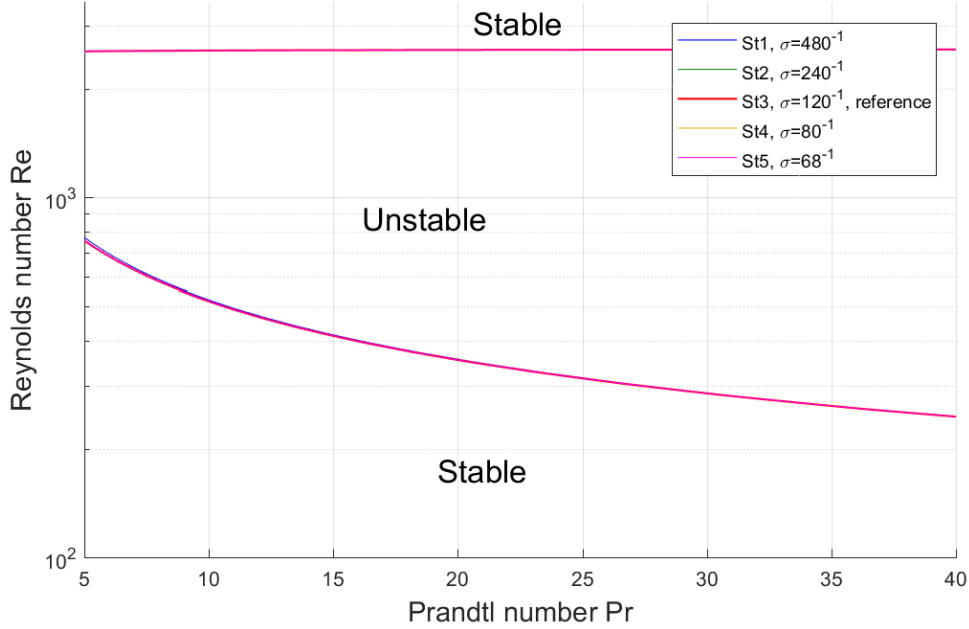


Figure 3.10. Stability map with varying σ .

Another way to join the correlations for the laminar and turbulent zone has been presented in literature (Swapnalee and Vijayan, 2011). In particular, a correlation for the transition zone is also available while the friction factor in the laminar and turbulent zone is calculated using the correlations seen previously. The friction factor coefficient can be computed as:

$$\lambda = \begin{cases} \frac{64}{Re}, & Re \leq 898 \\ \frac{1.2063}{Re^{0.416}}, & 898 < Re \leq 3196, \\ \frac{0.316}{Re^{0.253}}, & Re > 3196 \end{cases} \quad (3.56)$$

and a comparison between the two correlations can be observed in Fig. 3.11.

The difference between the two ways of computing the friction factor also reflects in the stability map. Fig. 3.12 shows a comparison between the reference map and the map computed using the latter correlation and it is quite evident the qualitative difference.

The “new” map is characterized by a stable-to-unstable border occurring at a higher Reynolds number with respect to the reference case, since the transition to the turbulent zone is now happening at a larger Reynolds number value; dissimilarities are also present in the transition regime due to the different modeling of the friction factor in that zone.

3.3 Sensitivity analysis

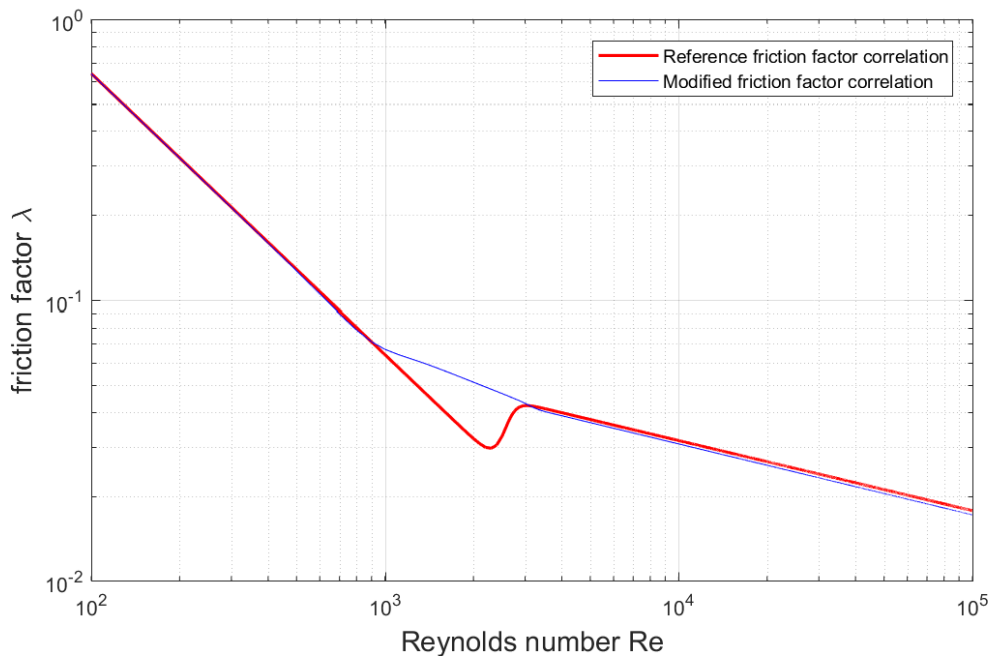


Figure 3.11. Comparison between the reference and the modified friction factor correlations.

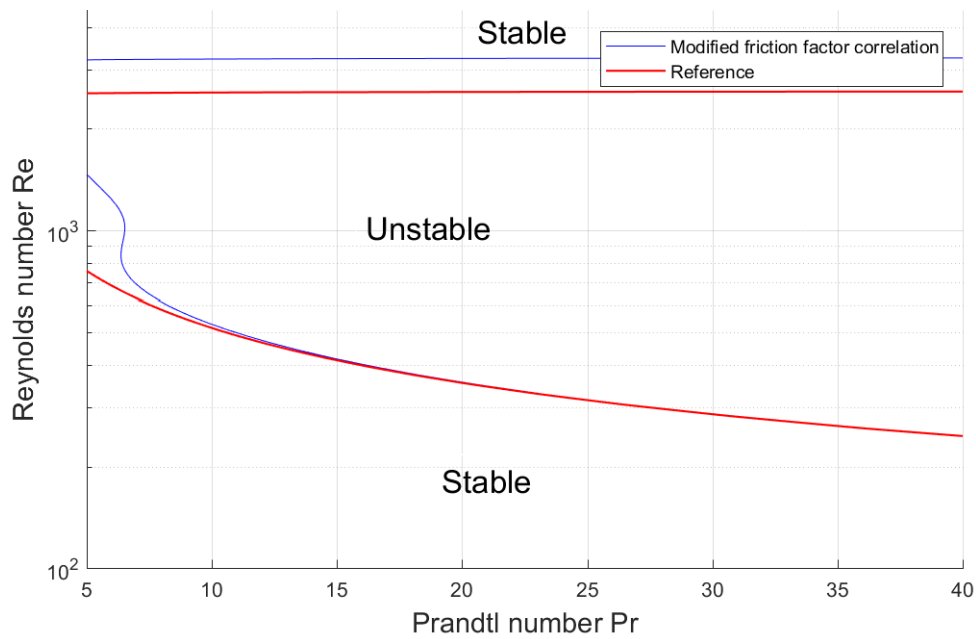


Figure 3.12. Comparison between the reference stability map and the map which employs the modified friction factor correlation.

Overall the number of asymptotically stable equilibrium states diminishes with the use of the three-zones correlations, underlining the huge impact that the friction factor definition has on the stability map shape. This can be confirmed by the FOM value (0.1757) which is about 50% lesser than the reference one (0.3586).

3.3.2 Stability map sensitivity to heat transfer coefficient definition

Following an approach analogous to that for the friction factor, also the heat transfer coefficient has been modeled using different correlations covering for a wide range of Reynolds and Prandtl numbers; these correlations were then merged thanks to the use of sigmoid functions (i.e., Eq. (3.9)). This causes the introduction of new parameters, namely the transition Prandtl numbers Pr_{trans} and the sigmoid steepness γ which are chosen as equal to respectively 0.6 and 0.05 in the reference case. The adopted sigmoid functions appear as follow:

$$\begin{aligned}\psi_{Nu_1} &= \left(1 + \exp((Re - Re_{trans})\gamma)\right)^{-1} \\ \psi_{Nu_2} &= \left(1 + \exp((Re - 10^5)\gamma)\right)^{-1} \\ \psi_{Nu_3} &= \left(1 + \exp\left(\frac{Pr - Pr_{trans}}{10^{-5}}\right)\right)^{-1}.\end{aligned}\tag{3.57}$$

A sensitivity study is performed on these parameters according to the values found in Table 3.5 and Table 3.6 considering a maximum 50% and 67% variation interval for Pr_{trans} and γ respectively in comparison to their reference value.

Table 3.5. Adopted parameters for the sensitivity analysis to Pr_{trans} .

Case	γ	Pr_{trans}
Pr1	0.05	0.2
Pr2		0.4
Pr3 (reference)		0.6
Pr4		0.8
Pr5		1

Table 3.6. Adopted parameters for the sensitivity analysis to γ .

Case	Pr_{trans}	γ
G1	0.6	0.025
G2		0.0375
G3 (reference)		0.05
G4		0.0625
G5		0.075

The results are shown in Fig. 3.13 and Fig 3.14. In this case the map results show no difference at all with the reference one in case of the Pr_{trans} change, since the transition value is actually never reached in the DYNASTY range, and only slight but negligible variation in the high Reynolds, high Prandtl zone for the γ case.

3.3 Sensitivity analysis

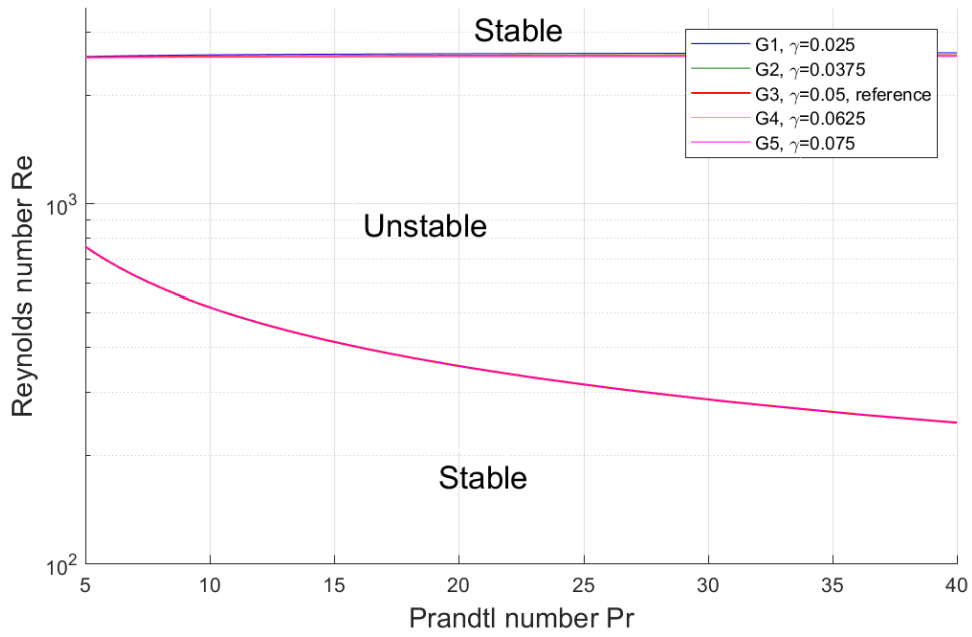


Figure 3.13. Stability map with varying γ .

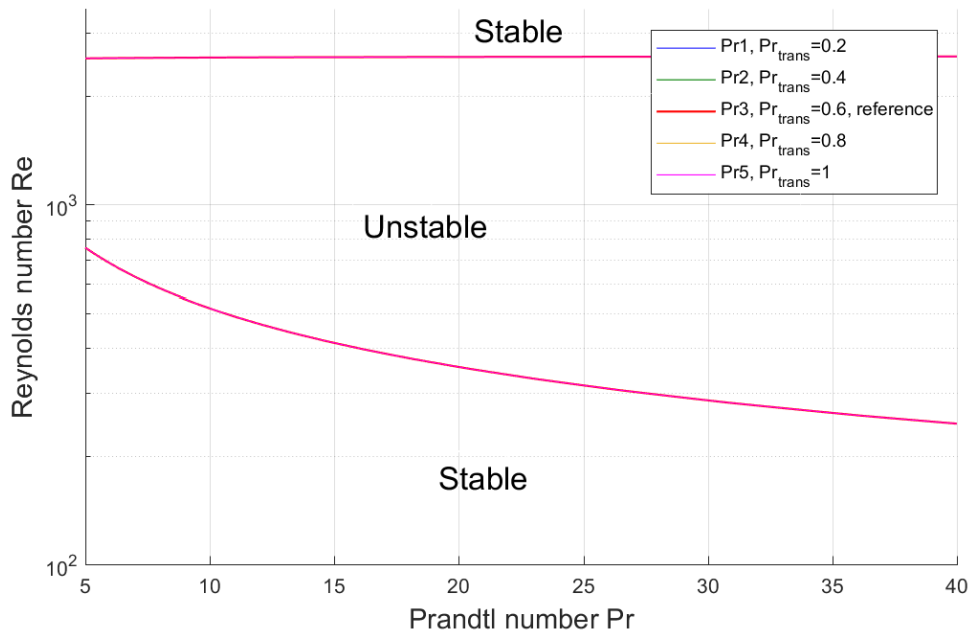


Figure 3.14. Stability map with varying Pr_{trans} .

On a quantitative side, the FOM value remains unchanged with respect to the reference value when varying the Pr_{trans} and has a maximum 2.8% change when modifying γ (for $\gamma = 0.025$).

3.3.3 Stability map sensitivity to temperature

In the definition of the stability map some of the system parameters are divided by reference values before being introduced in the model, as shown by Eqs. (3.44). Among these dimensionless parameters, the metal thermal properties (i.e., density, heat capacity and thermal conductivity) are divided by the salt corresponding thermal properties, all calculated at the reference temperature of 300 °C. Being both the salt and the metal properties dependent on the temperature, it has to be assessed how a change in the reference temperature affects the stability map form, due to the alterations in the metal and salt characteristics. This dependence on temperature conditions the stability map only in the definition of the ratios since changes in other properties are accounted by the dimensionless numbers that define the steady state. On top of that, a sensitivity on these quantities is needed since three sets of correlations are present in the literature for the salt adopted (as shown in Section 2.4).

The sensitivity study was performed with the following method: having chosen a set of correlations for the salt properties, a temperature at which the properties (for both salt and metal) are calculated is chosen, then the stability map is calculated using the dimensionless ratios found for that temperature. The operation is repeated for the whole desired temperature values (250 °C - 300°C - 350 °C i.e., DYNASTY design range) and for all the salt correlations considered. In this way all the metal-to-salt properties are modified at the same time and this allows to perform the stability map computation with reasonable values for all the properties. The values adopted for the sensitivity analysis are reported in Table 3.7 for the salt and the AISI 316 metal.

Table 3.7. Analyzed cases for the sensitivity analysis to temperature.

Case	Salt correlation	Temperature (°C)	ρ_{salt} ($\frac{kg}{m^3}$)	Cp_{salt} ($\frac{J}{kg \cdot K}$)	k_{salt} ($\frac{W}{m \cdot K}$)	ρ_{metal} ($\frac{kg}{m^3}$)	Cp_{metal} ($\frac{J}{kg \cdot K}$)	k_{metal} ($\frac{W}{m \cdot K}$)
T11	SALT1	250	1896.75	1560	0.48	8238	532.32	17.11
T12	SALT1	300	1860.13	1560	0.48	8238	543.52	17.88
T13	SALT1	350	1823.51	1560	0.48	8238	553.01	18.65
T21	SALT2	250	1896.86	1510	0.56	8238	532.32	17.11
T22	SALT2	300	1860.21	1510	0.59	8238	543.52	17.88
T23	SALT2	350	1823.56	1510	0.62	8238	553.01	18.65
T31	SALT3	250	1901.51	1500	0.43	8238	532.32	17.11
T32	SALT3	300	1864.02	1500	0.42	8238	543.52	17.88
T33	SALT3	350	1826.54	1500	0.39	8238	553.01	18.65

What can be noticed from Fig. 3.15 is that a variation in the considered temperature has only a very slight influence on the stability map form which results basically unchanged after the modifications. The highest FOM variation with respect to the reference case is of about 0.2%.

3.3 Sensitivity analysis

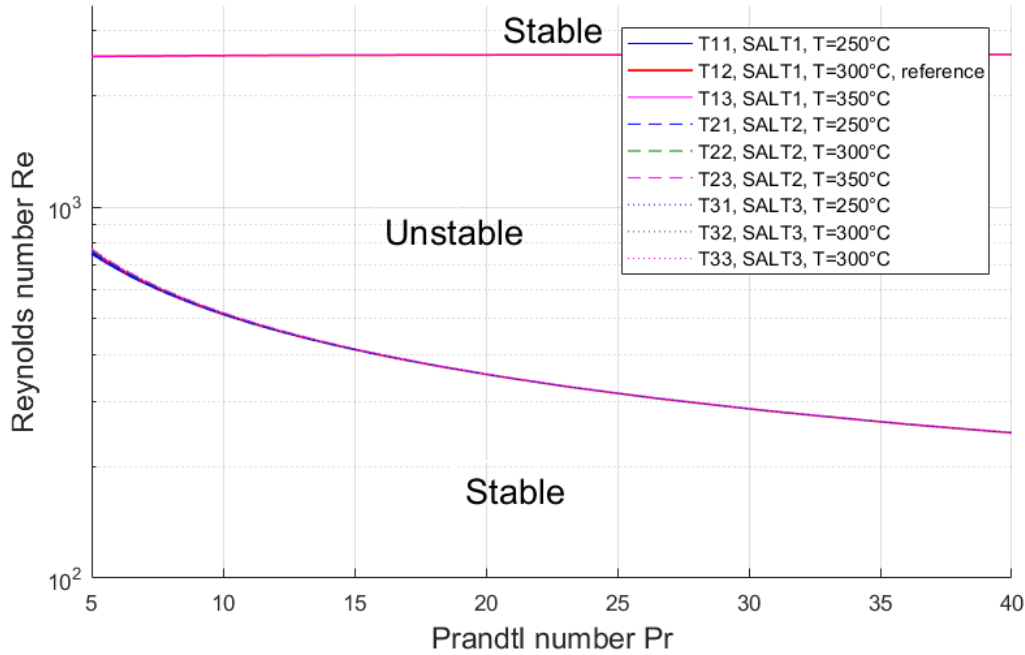


Figure 3.15. Stability map with varying reference temperature.

3.3.4 Stability map sensitivity to uncertainty in sizes and local pressure losses

Parameters such as the length and the thickness of a component are always known with a certain degree of uncertainty. In order to assess the effects that size tolerances on DYNASTY pipes may have on the stability map, a sensitivity analysis was performed modifying the thickness τ and inner diameter D_{pipe} values of the tubes according to the values in Table 3.8 and Table 3.9.

Table 3.8. Adopted parameters for the sensitivity analysis to D_{pipe} .

Case	τ (mm)	D_{pipe} (mm)
Di1	2	36.1
Di2		37.05
Di3 (reference)		38
Di4		38.95
Di5		39.9

A variation in the inner diameter D_{pipe} or in the thickness τ obviously implies a variation in the outer diameter D_o being it equal to $D_o = D_{pipe} + 2\tau$. The results of such changes are shown in Fig. 3.16 and Fig. 3.17.

Table 3.9. Adopted parameters for the sensitivity analysis to τ

Case	D_{pipe} (mm)	τ (mm)
Th1	38	1.8
Th2		1.9
Th3 (reference)		2
Th4		2.1
Th5		2.2

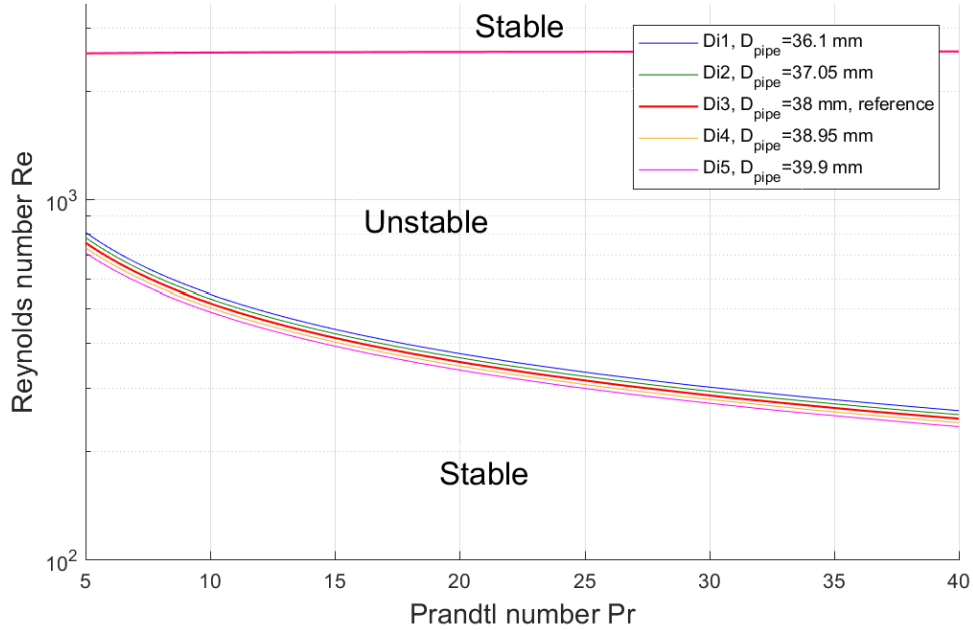


Figure 3.16. Stability map with varying D_{pipe} .

As far as the diameter change is concerned, a maximum 5% variation of the reference value was considered. It is possible to observe from Fig. 3.16 that an increase in the diameter causes an increase in the number of unstable equilibrium states, especially in the laminar region of the flow. This behavior could be due to the fact that an increase in the flow diameter makes the pipe thermal inertia stabilizing effect, as known from (Pini, 2017), less relevant since the fluid to metal mass ratio has increased. Conversely, an increase in the pipe thickness (up to 10% the nominal value) leads to an enlargement in the number, even if slight, of stable equilibrium states in the laminar zone probably due to a lower fluid-to-metal mass ratio, as it can be noticed in Fig. 3.17. The greatest evaluated FOM variations with respect to the reference map are respectively 0.35% and 1.9% for thickness and diameter change.

Uncertainties and lack of knowledge can affect also the choice of the L_{eq} parameter estimated from previous works to be equal to 2.4 m. A maximum 15 % variation on the reference value was then considered and a sensitivity analysis was performed using the values in Table 3.10.

Table 3.10. Adopted values for the sensitivity analysis to L_{eq} .

Case	L_{eq} (m)
L1	2.04
L2	2.16
L3 (reference)	2.4
L4	2.64
L5	2.76

3.3 Sensitivity analysis

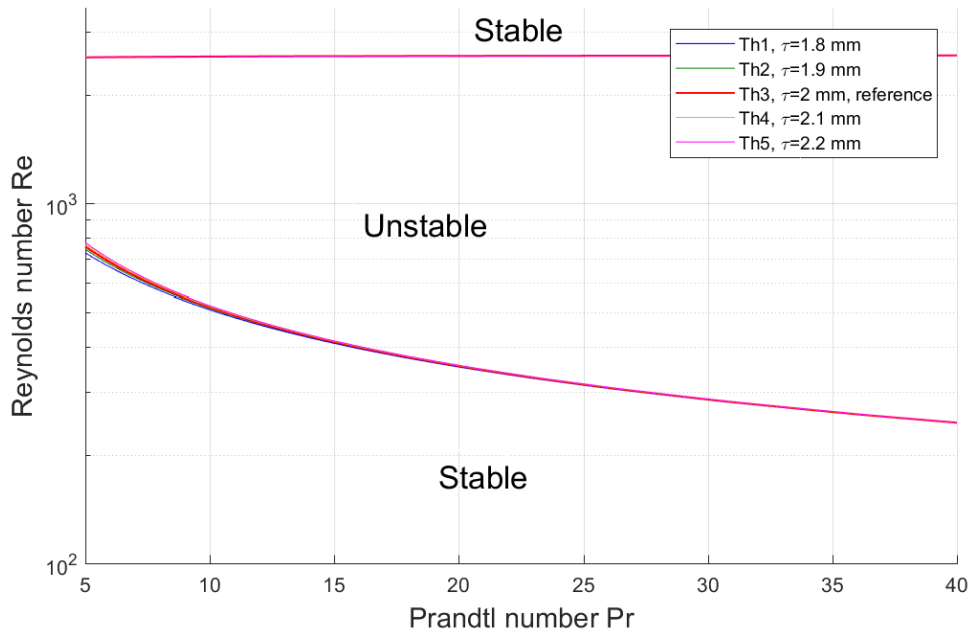


Figure 3.17. Stability map with varying τ .

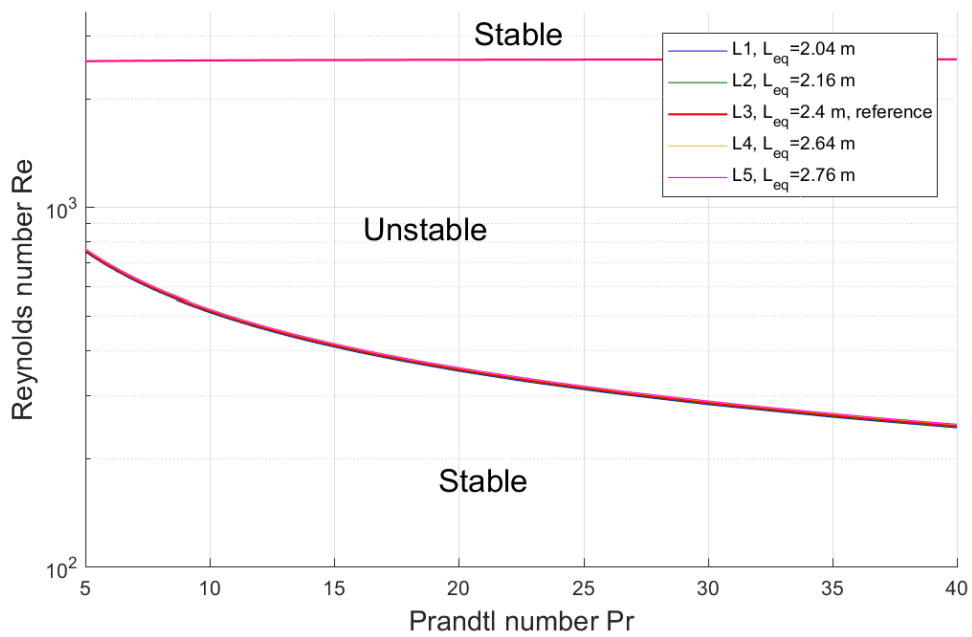


Figure 3.18. Stability map with varying L_{eq} .

The result shown in Fig. 3.18 highlights how the map is only limitedly affected by such changes, with modifications only in the laminar zone and the highest FOM variation with respect to the reference value being equal to 0.33%.

3.3.5 Quantitative sensitivity analysis

In this section a more quantitative look at the results obtained with the sensitivity analysis is given, highlighting with detail the changes with respect to the reference map using sensitivity coefficients. Given a function depending on many inputs $f(x_1, x_2, \dots, x_n) = y$, the sensitivity coefficient c_i of the function f to the i_{th} parameter can be obtained by differentiating the function with respect to that specific input:

$$c_i = \frac{\partial f(x_1, x_2, \dots, x_n)}{\partial x_i} = \frac{\partial y}{\partial x_i} \quad (3.58)$$

In the case under examination, the function to be differentiated is the FOM defined before: it is indeed a quantity that depends on many inputs, being the “stable” area of the stability map strictly related to the definition of these inputs. The “one-at-a-time” approach, which makes use of the coefficients defined in Eq. (3.58), consists in varying only one input variable at a time, while keeping the others fixed at their reference value. Such a technique was adopted for all the input parameter variations involved, except for the temperature change.

The temperature itself does not directly enter the model whereas the salt and metal thermal conductivity, heat capacity and density are inputs to the model, and since they depend on temperature they need to be altered simultaneously. Indeed, altering only one property per time would cause the model to be run with properties calculated at different temperatures and this would not be acceptable. Actually, the sensitivity coefficients usually computed are normalized in order to scale the changes of both function and inputs to that of their nominal values (y_{nom} and $x_{i,nom}$ respectively):

$$c_i^N = \frac{x_{i,nom}}{y_{nom}} \cdot \frac{\partial y}{\partial x_i} \quad (3.59)$$

A discrete version of Eqs. (3.58-3.59) is used in this work, since the FOM variation can only be recorded at discrete input changes (Par_i stands for parameter, while Par_{ref} is the reference input parameter):

$$c_i = \left| \frac{\Delta y}{\Delta x_i} \right| = \left| \frac{y_i - y_{i,nom}}{x_i - x_{i,nom}} \right| \equiv \left| \frac{FOM_i - FOM_{i,nom}}{Par_i - Par_{ref}} \right| \quad (3.60)$$

$$c_i^N = \left| \frac{x_{i,nom}}{y_{i,nom}} \cdot c_i \right| = \left| \frac{Par_{i,nom}}{FOM_{i,nom}} \cdot c_i \right| \quad (3.61)$$

The absolute values of the said coefficients are adopted since the magnitude of these numbers is the major interest.

Table 3.11 shows a synthesis of the whole sensitivity study developed in this work, underlining the input parameters changed and the respective nominal values adopted in the stability map.

The intervals for Re_{trans} and σ are quite wide: indeed, for natural circulation Re_{trans} is quite uncertain (number oscillating between 1000 and 2000 have already been observed (Hallican and Viskanta, 1986) and used (Ruiz et al., 2015)), while for σ a huge variation was considered since its effect was never deeply investigated. Analogously, this was done for the heat transfer parameters Pr_{trans} and γ . As for the case regarding the temperature change, the parameter variation observed is the ratio between the metal and salt thermal diffusivity (α_M and α_S respectively) since it condenses all the information relative to the quantities which were varied during those simulations; the variation chosen spans the DYNASTY operative range (250-350°C). The pipe and diameter thickness variation range were chosen according to the maximum tolerance allowed to industry steel manufacturers (EN ISO 1127) while the variation on L_{eq} was chosen after checking the alteration on the minor losses coefficients due to the allowed variation in diameter (Hydraulic Institute, 1979).

3.3 Sensitivity analysis

Table 3.11. Synthesis of the developed sensitivity study.

Sensitivity to:	Varied Parameter	Nominal value of the varied parameter	% variation range of the parameter
Friction factor definition (1)	Re_{trans}	2530	-40% to 40%
Friction factor definition (2)	σ	120^{-1}	-75% to +75%
Friction factor definition (3)	Friction factor correlation	Eq. (2.7)	/
Heat transfer coefficient definition (1)	Pr_{trans}	0.6	-66% to +66%
Heat transfer coefficient definition (2)	γ	0.05	-50% to +50 %
Temperature	$\frac{\alpha_M}{\alpha_S}$	24.13	-25% to +18%
Size (1)	D_{pipe}	38 mm	-5% to +5%
Size (2)	τ	2 mm	-10% to +10%
Local pressure losses coefficient	L_{eq}	2.4 m	-15% to +15%

In Table 3.12 the sensitivity coefficients (normalized and non-normalized), with the relative parameter variations with respect to the reference value, are presented for all the cases analyzed.

Table 3.12. Sensitivity study results in term of FOM and sensitivity coefficients.

Case	Input parameter value	% parameter change	FOM	% FOM change	c_i	c_i^N
Sensitivity to friction factor definition (1) - Re_{trans}						
Tr1	1500	-40.72	0.664	85.05	0.0003	2.089
Tr2	2000	-20.95	0.515	43.51	0.0003	2.077
Tr3 (reference)	2530	0.000	0.359	0.00	/	/
Tr4	3000	18.58	0.221	-38.36	0.0003	2.065
Tr5	3500	38.34	0.084	-76.67	0.0003	2.000
Sensitivity to friction factor definition (2) - σ						
St1	0.002	-75.00	0.3593	0.167	0.096	0.0022
St2	0.004	-50.00	0.3586	-0.019	0.016	0.0004
St3 (reference)	0.008	0.000	0.3587	0.000	/	/
St4	0.013	50.00	0.3588	0.037	0.032	0.0007
St5	0.015	76.47	0.3589	0.056	0.031	0.0007
Sensitivity to heat transfer coefficient definition (1) - Pr_{trans}						
Pr1	0.20	-66.67	0.3587	0.00	0.00	0.00
Pr2	0.40	-33.33	0.3587	0.00	0.00	0.00
Pr3 (reference)	0.60	0.00	0.3587	0.00	/	/
Pr4	0.80	33.33	0.3587	0.00	0.00	0.00
Pr5	1.00	66.67	0.3587	0.00	0.00	0.00

DYNASTY stability map and sensitivity analysis

Case	Input parameter value	% parameter change	FOM	% FOM change	c_i	c_i^N
Sensitivity to heat transfer coefficient definition (2) - γ						
G1	0.025	-50	0.3484	-2.862	0.411	0.057
G2	0.038	-25	0.3555	-0.874	0.251	0.035
G3 (reference)	0.050	0	0.3587	0.000	/	/
G4	0.063	25	0.3614	0.762	0.219	0.030
G5	0.075	50	0.3637	1.413	0.203	0.028
Sensitivity to temperature - T						
HITEC1, T=250°C	24.049	-0.343	0.3583	-0.0929	0.0040	0.2712
HITEC1, T=300°C	24.131	0.000	0.3587	0.0000	/	/
HITEC1, T=350°C	24.256	0.518	0.3590	0.0929	0.0027	0.1793
HITEC2, T=250°C	19.813	-17.893	0.3586	-0.0186	0.0000	0.0010
HITEC2, T=300°C	19.031	-21.137	0.3589	0.0743	0.0001	0.0035
HITEC2, T=350°C	18.109	-24.958	0.3593	0.1859	0.0001	0.0074
HITEC3, T=250°C	25.631	6.213	0.3586	-0.0186	0.0000	0.0030
HITEC3, T=300°C	26.758	10.885	0.3590	0.0929	0.0001	0.0085
HITEC3, T=350°C	28.518	18.180	0.3595	0.2230	0.0002	0.0123
Sensitivity to size (1) - D_{in}						
Di1	0.036	-5	0.3655	1.896	3.579	0.379
Di2	0.037	-2.5	0.3619	0.892	3.368	0.357
Di3 (reference)	0.038	0	0.3587	0.000	/	/
Di4	0.039	2.5	0.3559	-0.781	2.947	0.312
Di5	0.040	5	0.3529	-1.617	3.053	0.323
Sensitivity to size (2) - τ						
Th1	0.0018	-10	0.3574	-0.353	6.333	0.035
Th2	0.0019	-5	0.3582	-0.130	4.667	0.026
Th3 (reference)	0.002	0	0.3587	0.000	/	/
Th4	0.0021	5	0.3591	0.130	4.667	0.026
Th5	0.0022	10	0.3597	0.297	5.333	0.030
Sensitivity to local pressure loss coefficient - L_{eq}						
L1	2.04	-15	0.3575	-0.316	0.0031	0.021
L2	2.16	-10	0.3580	-0.186	0.0028	0.019
L3 (reference)	2.4	0	0.3587	0.000	/	/
L4	2.64	10	0.3595	0.242	0.0036	0.024
L5	2.76	15	0.3599	0.335	0.0033	0.022

In Table 3.13 the maximum absolute values of the normalized sensitivity coefficients are shown and what was already known from the previous qualitative analysis on the figures of merit is confirmed: the map is strongly sensitive to a change in the transition Reynolds number.

3.3 Sensitivity analysis

Table 3.13. Maximum normalized sensitivity coefficients for the analyzed sensitivity cases.

Re_{trans}	D_{pipe}	Temperature	γ	τ	L_{eq}	σ	Pr_{trans}
2.089	0.379	0.2712	0.057	0.035	0.024	0.022	0

The other parameter which has a relevant influence is the diameter tolerance. The maximum sensitivity coefficient to temperature changes has the third highest value but this is mostly due to the choice of the parameter α_M/α_S which slightly changes with temperature for SALT1; since the FOM also varies limitedly, then c_i^N acquires a high value. It can be noticed that Table 3.12 doesn't mention any sensitivity coefficient relative to the introduction of a different friction factor correlation (Eq. 3.56); a calculation of such a coefficient was not possible for this case since an adequate parameter to which the FOM change could be related could not be identified.

At this point, as a consequence of the “one-at-a-time” approach, the highest FOM variation ΔFOM_{max} in the model can be obtained by summing the maximum FOM variations (in absolute value) for all the cases:

$$\Delta FOM_{max} = \sum_i^n \Delta FOM_{max,i} = \sum_i^n \max |(FOM_i) - FOM_{ref}| \quad (3.62)$$

where FOM_i stands for the vector containing the FOMs calculated for the i-th sensitivity study; “n” is the number of sensitivity studies performed and is equal to nine.

The ΔFOM_{max} quantity can then be used to normalize the $\max |(FOM_i) - FOM_{ref}|$ values in order to visualize how much each maximum FOM variation weighs in the total value. The result of this operation can be observed in Fig 3.19. It is possible to notice how this type of normalization procedure allowed to include also the FOM variation due to the change in the friction factor correlation; it is then revealed that this change is one of those contributing most to the alteration of ΔFOM_{max} . The change in the transition Reynolds number has still the highest contribution, followed by the modified correlation; these two cases actually cover more than the 97% of the maximum FOM variation that can be possibly registered by our model, implying that the other parameter alterations matter very little to a change of shape of the stability map.

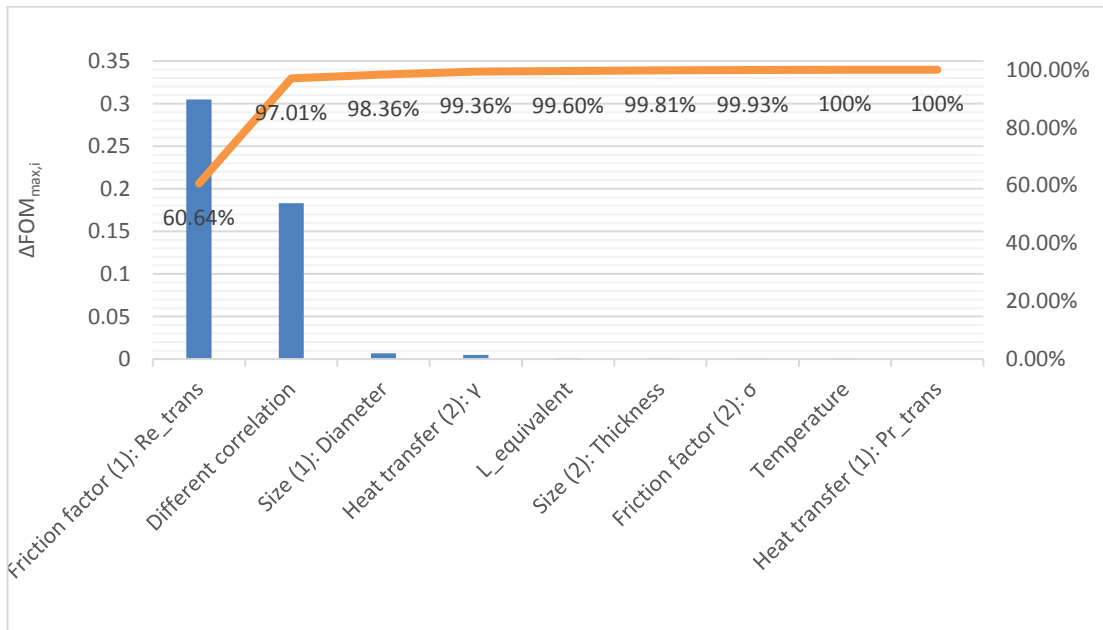


Figure 3.19. Maximum FOM variation for the analyzed sensitivity cases.

3.4 Concluding remarks

The stability map approach was adopted to model the asymptotic behavior of DYNASTY, leading to the construction of a reference stability map, covering the range of Reynolds and Prandtl numbers of interest for DYNASTY. This map shows two main stable regions: one for Reynolds number higher than the transition Reynolds number value and one for lower Reynolds number, in the laminar region of the flow. A sensitivity analysis was performed in order to assess the robustness of the tool to the change of certain parameters which are fed as inputs to the model; it was run varying the involved quantities “one at a time” within a prescribed reasonable range. The effects of these variations are shown both graphically and quantitatively via the use of a numerical figure of merit, which is defined as the ratio between the area of the map occupied by stable states and the total area of the map.

The sensitivity analysis performed according to the chosen figure of merit indicates that the equilibrium stability prediction given by the map is strongly depending on the friction factor definition: indeed, the highest observed changes happen when a different transition Reynolds is considered in the friction factor correlation or when a different correlation is considered (the two said changes cover more than about 97% of the maximum possible FOM variation).

On the other hand, the dependence of the map on other parameter changes seems to be very limited; in particular, it is to be underlined that even though stability maps quite change when the pipe thermal inertia is not considered (Pini, 2017), a variation of the pipe thermal inertia (which involves a variation in thermal properties or in the pipe size) causes only negligible changes in the map shape. Hence, it is suggested that, for the DYNASTY stability map, the “hydraulic” problem connected to the definition of the major pressure losses is more relevant in defining the map shape than the “thermal” one (linked to the definition of the pipe properties) and this is probably due to the fact that DYNASTY operative Reynolds range has been individuated in the typical flow transition region.

Overall, it is believed that the knowledge of a more precise correlation would decrease the highest degree of uncertainty of the stability map.

3.4 Concluding remarks

4 Improvements on the one-dimensional Object-Oriented models for DYNASTY

***Abstract.** The need to account for nonlinearities and to follow the time evolution of the velocity, temperature and pressure fields of the fluid in natural circulation loops requires the adoption of different types of models besides stability maps. Models relying on a 1D object oriented (O-O) approach have already shown the capability of reproducing with precision experimental trends and have been used to model the dynamic behavior of DYNASTY.*

The O-O approach is implemented resorting to Modelica, a language that is based on a-causal modeling, systems hierarchy and reusability of components. Dymola is the selected software chosen for the simulations of the systems developed with Modelica. Previous versions of DYNASTY models showed a certain degree of inadequacy in modeling the behavior of the natural circulation loop (e.g., the use of adiabatic pipes even when heat losses to the external are present and the use of a uniform wall temperature cooler to model a pipe immersed in an air cross-flow). Hence, this chapter is dedicated to the development of new components, enhancement of the existing ones, with the goal of obtaining a more accurate description of DYNASTY dynamics. The main purpose is to quantify the improvement brought by the introduction of new components in the prediction of the system behavior on a finite time horizon.

4.1 Introduction

The study of the behavior of a physical system usually implies the execution of experiments paired with the development of mathematical models representing the system. Indeed, if on the one hand experiments are the most reliable way of obtaining information from a certain physical apparatus, on the other hand they may be excessively costly, dangerous or inadequate in representing all the characteristic time scales. Conversely, physically-based simulations performed through a mathematical model do not entail the aforementioned issues. On the other hand, modeling a physical phenomenon in mathematical terms often involves the adoption of simplifications and assumptions.

Systems are often modelled using a causal approach. Knowing a-priori the input and the desired output quantities, the laws describing the physics are implemented so that the output variables (or, more precisely, the “state” variables) are function of the input ones.

This modeling approach presents several limitations. First, the equations describing the processes have to be obtained from constituting equations and conservation laws and reworked to satisfy the wanted causality. Second, the information flow direction is rigidly decided at the beginning and it is usually quite demanding to modify it, even for easy tasks as monitoring another variable.

During the last few years, another way of modeling, namely the a-causal modeling approach, has become more and more relevant (Fritzon, 2011). Following this approach, the governing equations for each component of the system are written in declarative form, without the need to define a-priori the input and output variables. The causality links (i.e., the ordered series of computational steps needed for the simulation) are only established when the equations are solved, depending on the

4.1 Introduction

applied boundary conditions. In this way, a more flexible and efficient data flow is achieved (Fritzson, 2011). Thanks to the a-causal modeling, the focus remains on the physical components of the system. Indeed, each component is modeled separately and independently from the others and eventually they are connected to form the desired physical system. This implies that components are then re-usable for other models. The mathematical formulation required by a-causal models are differential algebraic equations (DAE). This calls for the need of a simulator capable of analyzing big DAE systems.

The a-causal definition of model equations is one of the main characteristics of the object-oriented (O-O) modeling (Fritzson, 2015), which is a technique already largely used for the simulation of complex systems (Kossel et al., 2006). Its main features can be summarized with reference to Modelica, a language developed in 1997 with the purpose of modeling generical systems through the means of DAE in an O-O environment. The main characteristics of Modelica are (Fritzson, 2015):

- Declarative a-causal modeling. Every single component is described by a certain set of DAE written in a declarative form, in the sense that no reworking is done to highlight the inputs and outputs to the components. The system is made up of many connected elementary components and causality is established by the compiler.
- Code readability. The equations representing the system are directly embedded in components which are immediately recognizable as parts of the whole system, whose topology is then maintained. Indeed, the connections shown in the model represent actual physical connections, resulting in an increased readability of the code.
- Connectivity. All the components in a model are linked through the use of connectors: they are interfaces equipped with inlets and outlets which serve the function (through ad-hoc equations) of supplying communication between the state variables of different components.
- Inheritance, hierarchical structure and re-usability. Components can be structured in a hierarchical way, where a base part is modified by adding further equations or specifics in order to meet the wanted characteristics. All these features encourage the further use of these components in different models and their organization in specific libraries.

The simulation of systems built with the Modelica language needs a specific software. Dymola (DYNAMIC MODELing Laboratory - (DYMOLA, 2018)) has been chosen in this work to fulfill the purpose; it offers a simulation environment in which symbolic and numeric manipulation of the model equations are performed so to produce highly efficient simulation code (Fritzson, 2015).

The remainder of this chapter is dedicated to the development of “new” components written using Modelica in order to improve existing models of DYNASTY, since the ones already existing in literature lack some of the peculiar characteristics of the facility (Pini, 2017).

A sure way of improvement of current O-O models is by removal of the assumptions they rely on. This translates, for DYNASTY, in removing the simplifications that characterized the previously developed models, namely the cooler treated as a thermostated pipe and the other pipes having no heat losses to the exterior. In this chapter, different versions of these new components are developed according to different modeling choices and necessities. The main improvements introduced regard the possibility of considering heat losses to the external from the pipes (i.e., the pipe is no more considered adiabatic and the presence of insulation is taken into account) and the use of a component which models the cooler as-it-is in reality (i.e., a pipe cooled by an air cross flow). The main interest will be, when analyzing the time behavior of the system, to evaluate if after a finite time a steady state can be reached. The remainder of the chapter gives an overview the state of the art models; the

new components are then presented as well as results and considerations on the simulation comparison between the new and the previous models.

4.2 DYNASTY pre-existing model

The pre-existing DYNASTY O-O model was built using components belonging to the ThermoPowerIHG library (Pini, 2017) which was in turn developed as an extension of the ThermoPower library (Casella and Leva, 2006; ThermoPower, 2016). As previously said, the two main components of interest are *ThermostatedPipe_2* and *PipeFEM_2*. The *ThermostatedPipe_2* component, as shown in Fig 4.1, is made up of different subcomponents, namely *CustomFlowIDFEM*, *MetalTubeFEM*, *iHGIDFEM* and *tempSource*, which are interfaced through the use of connectors. The *customFlowIDFEM* is used to solve the one-dimensional mass, momentum and energy equations which are discretized through the use of the Finite Elements (FE) methods. The FE method was preferred over the Finite Volume (FV) one since during numerical tests it was noticed that the boundary condition treatment characterizing the FE discretization was able to handle the mass flow rate inversion in a more reliable way than the FV counterpart (Pini, 2017). Some basic modeling assumptions were made in the development of the *CustomFlowIDFEM* (Pini, 2017), (Casella, 2006)):

- The fluid state is always one-phase (subcooled liquid in our case).
- Uniform velocity is assumed on the cross section of the pipe (leading to a 1D model).
- The friction factor is calculated using the modified correlation shown in Eq. (3.7).
- The model is based on dynamic mass, momentum and energy balances.
- The longitudinal heat diffusion term is neglected.
- The energy balance equation is written assuming a uniform pressure distribution; the pressure drop is lumped either at the inlet or the outlet.
- The fluid flow can exchange thermal power through the lateral surface, which is represented by a wall connector. Internal heat generation can be provided too.

Hence, the equations that are implemented in the component are the following Eqs. (4.1 - 4.3).

Mass conservation:

$$\frac{\partial w}{\partial x} = 0, \quad (4.1)$$

Momentum conservation:

$$\frac{L}{A} \frac{dw}{dt} + (p_o - p_i) + \rho g(z_o - z_i) + \frac{C_f}{2} \frac{\omega \cdot L}{\rho \cdot A^3} |w|w = 0, \quad (4.2)$$

Energy conservation:

$$\frac{\partial(\rho \cdot A \cdot e)}{\partial t} + \frac{\partial(w \cdot h)}{\partial x} = \omega \cdot \phi + \dot{Q} \cdot A. \quad (4.3)$$

These equations are reworked and discretized with the FE method in order to obtain a system of equations having one flow rate, one pressure and N specific enthalpies as state variables, where “N” is the number of discretization nodes of the component. As for the notation used, w corresponds to the flow rate, L to the length of the pipe, A to the pipe cross-section, p to the pressure, ρ to the fluid density, z to the elevation, C_f to the Fanning friction factor, e to the internal energy, ϕ to the heat flux exchanged through the lateral boundaries, \dot{Q} to the internal heat generation (this term can be switched on or off) and ω is the pipe circumference. The \dot{Q} term is provided thanks to the *iHGIDFEM* component. The friction factor and heat transfer coefficient (which is hidden in ϕ) are

4.2 DYNASTY pre-existing model

retrieved using the same correlations adopted in Chapter 3. The subscripts “o” and “i” refer to outlet and inlet respectively.

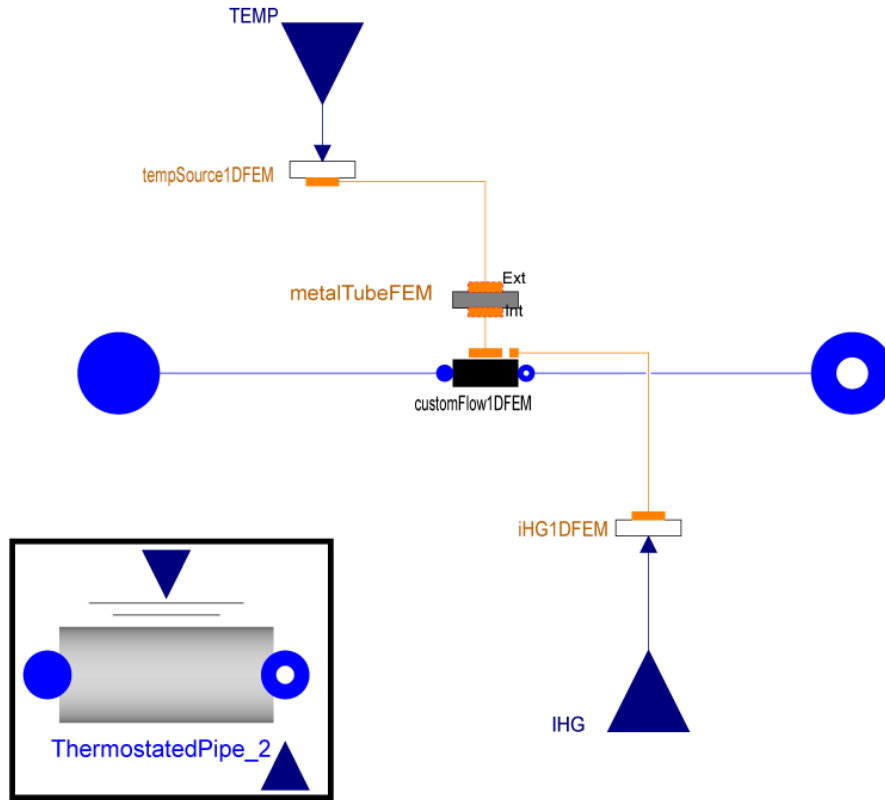


Figure 4.1. External (bottom left) and expanded view of the ThermostatedPipe_2 component.

The *metalTubeFEM* component serves the purpose of modeling the pipe containing the fluid and it accounts for its thermal inertia. The equations implemented for every node are the following Eqs. (4.4 - 4.6).

Pipe energy conservation:

$$\rho_m c_m A_m \frac{dT_m}{dt} = 2\pi \cdot r_{in} \cdot \phi_{in} + 2\pi \cdot r_{ext} \cdot \phi_{out} , \quad (4.4)$$

flux on the inner side ϕ_{in} :

$$\phi_{in} = \frac{k_m}{r_{in} \cdot \log\left(\frac{r_{in} + r_{ext}}{2r_{in}}\right)} \cdot (T_{in} - T_m) , \quad (4.5)$$

flux on the outer side ϕ_{out} :

$$\phi_{out} = \frac{k_m}{r_{ext} \cdot \log\left(\frac{2r_{ext}}{r_{in} + r_{ext}}\right)} \cdot (T_{ext} - T_m) . \quad (4.6)$$

In the previous equations r_{in} and r_{ext} refer to the inner and outer pipe radii, the “m” subscript refers to “metal”, while ρ is the density, c the thermal capacity, A the metal cross section ($\pi(r_{ext}^2 - r_{in}^2)$); T_{in} refers to the temperature on the inner surface of the pipe (i.e., the fluid side) while T_{ext} refers to the temperature on the outer surface of the pipe. The latter quantity is specified in the model thanks

to the connection with the *tempSource* component, which defines, for every discretization node, the temperature value of the external side of the wall.

The *PipeFEM_2* component shows a very similar structure to that of the *ThermostatedPipe_2*, as depicted in Fig 4.2. The main difference stands in the different source component: *tempSource* component is substituted by *heatSource1DFEM* which imposes a heat flux, rather than a temperature, to the tube external surface. It is to be noted that the *PipeFEM_2* is equipped to model both the external heat flux cases as well as the internal heat generation one.

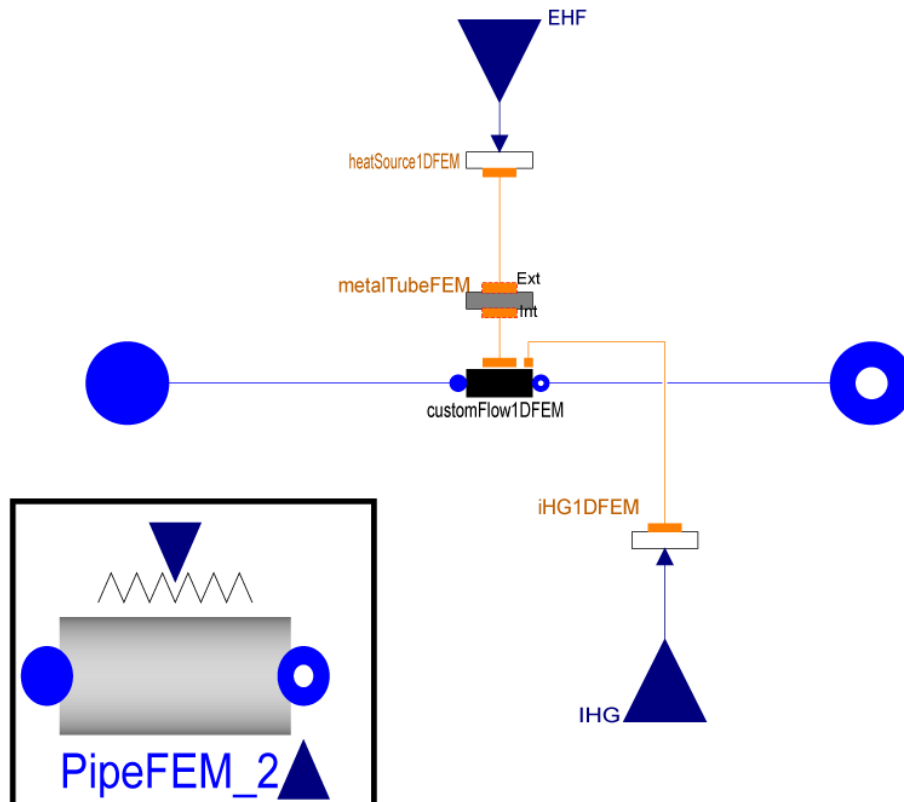


Figure 4.2. External (bottom left) and expanded view of the *PipeFEM_2* component.

However, as it was seen for loops with high length to diameter ratio (Pini, 2017), since the adoption of the distributed heat flux induces basically the same dynamics in the natural circulation flow as caused by the internal heat generation, the work presented here focuses on distributed heat flux source, since it is the closest condition to the experiments. A model of DYNASTY using mainly the *PipeFEM_2* and *ThermoStatedPipe_2* components has been built and is shown in Fig. 4.3. Other components appear in the model of the loop, namely the *PressDrop* component to model the localized pressure losses at the pipe bendings, the *sinkPressure* to model the expansion tank and the *flowSplit* which models the T-junction that connects the tank to the loop. These latter components all belong to the ThermoPower library. It has been shown (Cammi et al., 2016) that a good agreement could be found between the results obtained in terms of stability map and time dependent simulations obtained with this Dymola model.

As a closing remark, the Dymola model shown in Fig. 4.3 has already been validated against experimental data (Luzzi et al., 2017) on the L2 facility in Genova; among the peculiarities of this plant the heat is removed from the cooler thanks to a cryostat, which is actually very well represented, from a model point of view, by the *ThermoStatedPipe_2*; moreover, the fluid (water) is run at low

4.3 Improved components for DYNASTY

temperatures and thus the other pipe sections can be successfully modeled by the *PipeFEM_2* component, since losses to the exterior are quite limited.

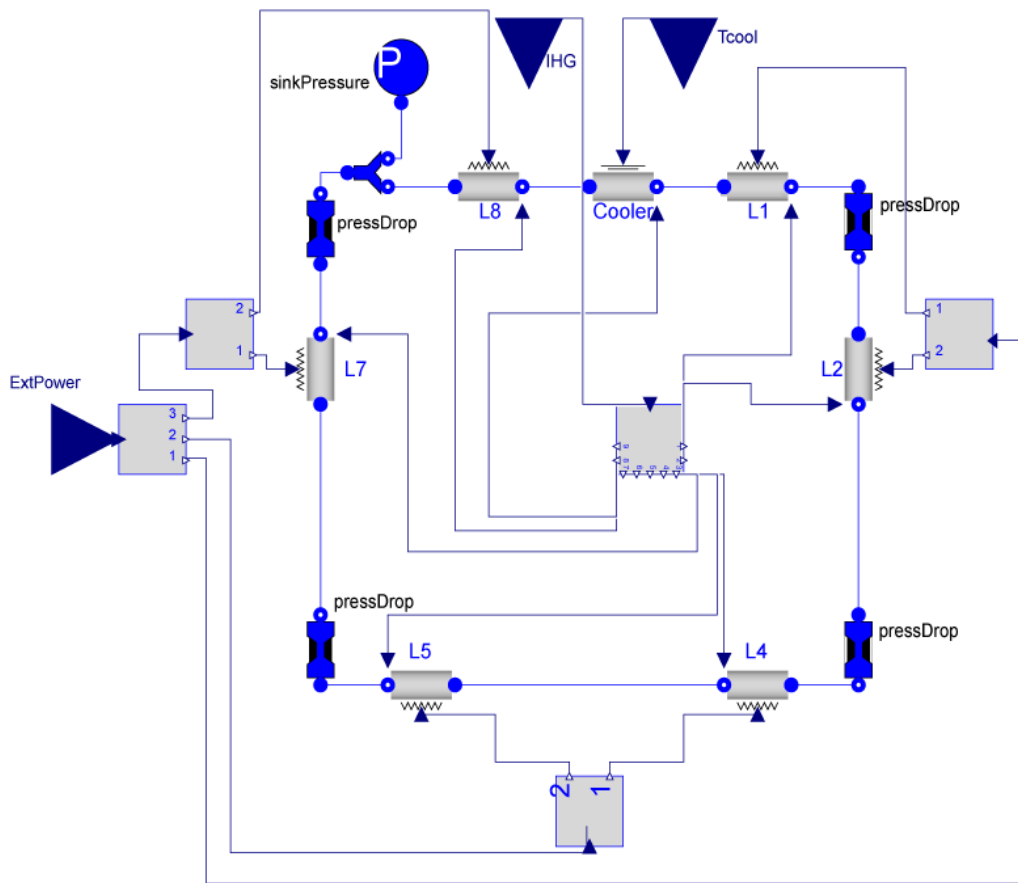


Figure 4.3. Pre-existing DYNASTY models employing *Thermostated_2* and *PipeFEM2* components.

4.3 Improved components for DYNASTY

The scope of this section is to offer valid alternatives to the pre-existing DYNASTY pipe components; this is deemed necessary because of the limitations the previously developed models entail.

PipeFEM_2 allows to model the behavior of the fluid in the pipe and accounts for the presence of the pipes and the external heating. On the other hand, the pipe is treated as if it was adiabatic when it is not true. Indeed, natural circulation is a very complicated phenomenon and it was made clear in paragraph 2.1 that a huge number of factors may influence its dynamics; in particular, it has been seen that the pipe thermal inertia can affect the stable or unstable behavior of the flow and therefore it comes naturally to think that also the insulator thermal inertia can affect the flow dynamics, also because the system can lose heat to the exterior. Therefore, a new component (*PIPEFEM2WithLosses*) was developed with the purpose of modeling the presence of the insulator and the heat exchange towards the exterior.

ThermostatedPipe2 models the behavior of a pipe whose surface is kept at uniform constant temperature. This was done to allow comparison between models built in different environments (and applying the same simplifications) but is not corresponding to the actual cooling mechanism of DYNASTY. The cooling action is provided by a fan which imposes an air cross flow on the cooler

surface, which is finned. When the fan action is not regulated by a controller a constant flow rate hits the pipe which is then far from having a uniform wall temperature. Conversely, with the adoption of a controller, the air flow rate on the pipe can be regulated and a comparison between the two types of models (only “previous” and only “improved” pipe components) can be performed by varying the air velocity to obtain a defined cooler wall mean temperature. Hence, the new component *VentilatedPipe* was realized in order to realistically model the cooler behavior. Different versions of this element are proposed so to be able to model various cases (changing air flow rate, constant air flow rate, cooling action by natural circulation on the cooler surface).

Overall, a model built with new components can offer positive incomes, namely:

- A more accurate representation of the natural circulation dynamics since the physics implemented are closer to the experimental reality. The modeling capability widens as more cases, not necessarily related to the model benchmark, can be simulated.
- The present work and previous models can be compared to see, at the same given external power and cooler wall temperature, how the time behavior of the naturally circulating flow is differently modeled. In particular, one is interested in the equilibrium of the natural circulation on the finite time horizon and if the addition of the new components is able to modify it.
- The development of a controlled cooling action can give some hints on the development of a real controller on the fan.

4.3.1 *The PipeFEM2WithLosses component*

The *PipeFEM2WithLosses* component can be seen in Fig. 4.4; it is built connecting different components, namely *CustomFlow1DFEM*, *SolidTubeFEM*, *MetalTubeFEM*, *iHG1DFEM*, *DoubleHeatSource1DFEM* and *HtcRadConvSource*. The way the fluid-dynamics equations are treated inside the pipe has not changed since *CustomFlow1DFEM* is used again to model the fluid behaviour; the *metalTube* component used to model the AISI 316 pipe has been substituted by *SolidTubeFEM* which solves again a set of equations similar to Eqs. (4.4 - 4.6) but this time considering temperature changing properties for the AISI 316 metal (Bergman, 2011) that constitutes the pipe walls. For the *PipeFem2WithLosses* the external power source is now connected to the *DoubleHeatSource1DFEM* component. The equation implemented in this object states that the externally given power must be partitioned between the pipe wall and the insulation material according to an energy balance. The said component is connected both to *SolidTubeFEM*, representing the pipe walls, and to *MetalTubeFEM* which is used to model the heat conduction through the insulation walls. Once again *iHG1DFEM* serves the purpose of considering the presence of internal heat generation. The last component to be considered is the *HtcRadConvSource*, which is needed in order to account for the heat exchange on the surface of the AISI 304 foil which envelopes the rock wool insulation.

4.3 Improved components for DYNASTY

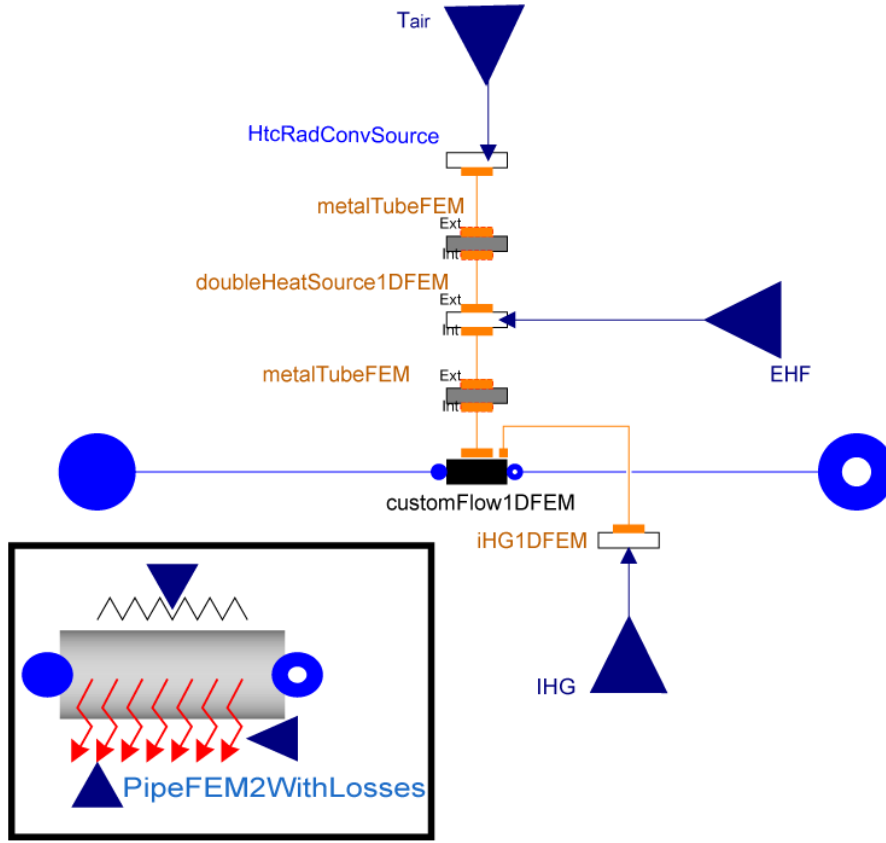


Figure 4.4. External (bottom left) and expanded view of the PipeFEM2WithLosses component.

The logic behind the modeling choices adopted for the realization of the *HtcRadConvSource* subcomponent are made clear in the following. As already explained in Chapter 2, all DYNASTY pipes are insulated thanks to a thick layer of rock wool which is then enclosed by a AISI 304 very thin layer. It can be shown that the thermal resistance to conduction of this foil is very little and totally negligible when compared to that of the rock wool; thus, heat conduction inside this sheet is neglected. As far as the heat exchange on the foil surface is concerned, both radiative and convective heat exchange are taken into account; radiative heat transfer is considered by making use of the “small surface - large isothermal enclosure” approximation (Bergman, 2011) while convective heat transfer is modeled through the use of a heat transfer coefficient. The heat flux at every node of the foil surface φ_i is then calculated as:

$$\varphi_i = \sigma \cdot \epsilon \cdot (T_{wall,i}^4 - T_{sur}^4) + h_{conv} \cdot (T_{wall,i} - T_{sur}), \quad (4.7)$$

where σ is the Stefan-Boltzmann constant ($5.67 \cdot 10^{-8} \text{ W/m}^2 \cdot \text{K}^4$), ϵ the wall emissivity, $T_{wall,i}$ is the i -th node wall temperature, T_{sur} is the surroundings temperature (i.e., the air temperature) and h_{conv} is the convection coefficient. The simplest version of *PipeFem2WithLosses* implements a constant reasonable value of the heat transfer coefficient h_{conv} ; it will be seen in the following that this approximation is not so rough. A more accurate model necessitates the use of correlations.

The convection mechanism happening on the pipe surface is natural circulation; this phenomenon is highly dependent on pipe orientation and indeed two different types of correlations for the Nusselt number are needed: one for horizontal pipes and the other for vertical pipes. As far as horizontal

cylinders are concerned, a correlation for the average Nusselt number over the entire circumference of an isothermal cylinder \overline{Nu}_D was proposed by Churchill and Chu (Churchill and Chu, 1975):

$$\overline{Nu}_D = \left\{ 0.60 + \frac{0.387Ra_D^{\frac{1}{6}}}{\left(1 + \left(\frac{0.559}{Pr}\right)^{\frac{9}{16}}\right)^{\frac{8}{27}}} \right\}^2, Ra_D \leq 10^{12}. \quad (4.8)$$

The Ra_D quantity is the Rayleigh number referred to the tube diameter:

$$Ra_D = \frac{g \cdot \beta \cdot (T_{wall} - T_{sur}) \cdot D^3}{\alpha \cdot \nu}, \quad (4.9)$$

where g is the gravity acceleration, β stands for the air volumetric expansion coefficient, T_{wall} is the surface temperature, T_{sur} refers to the surrounding air temperature, D is the pipe diameter, α the thermal diffusivity, ν the kinematic viscosity and Pr the Prandtl number. All the properties are calculated at the film temperature $T_{film} = \frac{T_{wall} + T_{sur}}{2}$.

The version of *PipeFem2WithLosses* that implements the Eq. (4.8) correlation is named *PipeFem2WithLosses_horizontal*.

For the vertical cylinders, another correlation proposed by Churchill and Chu (Churchill and Chu, 1975) is adopted, namely:

$$\overline{Nu}_L = \left\{ 0.825 + \frac{0.387Ra_L^{\frac{1}{6}}}{\left(1 + \left(\frac{0.492}{Pr}\right)^{\frac{9}{16}}\right)^{\frac{8}{27}}} \right\}^2, 10^4 \leq Ra_L \leq 10^{13}. \quad (4.10)$$

With Ra_L is the Rayleigh number referred to the pipe length L :

$$Ra_L = \frac{g \cdot \beta \cdot (T_{wall} - T_{sur}) \cdot L^3}{\alpha \cdot \nu}$$

The correlation shown in Eq. 4.10 was actually developed for vertical isothermal L long plates; nonetheless it can be also applied to vertical isothermal long cylinders once the condition that $\frac{D}{L} \geq \frac{35}{Gr_L^{0.25}}$ is satisfied (considering air properties calculated at a film temperature of 150°C and real pipe sizes, the inequality yields approximately 0.058 > 0.054). The Gr_L quantity stands for the Grashof number referred to the length L : $Gr_L = Ra_L / Pr$.

The version of *PipeFem2WithLosses* that implements Eq. (3.10) correlation is named *PipeFem2WithLosses_vertical*.

Since the correlations adopted refer to isothermal pipes, which is not the case, a mean wall temperature is calculated and only one heat transfer coefficient is computed for the whole pipe.

From Table 4.1 it can be appreciated that for both correlations even a high jump in temperature causes only a limited change in the heat transfer coefficient; hence, even if the pipe is not working at constant temperature condition the approximation adopted is acceptable.

The values found are calculated with respect to DYNASTY real pipe size, temperature-dependent air properties and 23 °C air temperature.

4.3 Improved components for DYNASTY

Table 4.1. Variation of the heat transfer coefficient for natural circulation on horizontal and vertical pipes.

Wall temperature (°C)	50	100	150	200	250	300
Heat transfer coefficient Eq. 3.8 $\left(\frac{W}{m^2 \cdot K}\right)$	4.85	6.55	7.53	8.51	8.85	9.39
Heat transfer coefficient Eq. 3.10 $\left(\frac{W}{m^2 \cdot K}\right)$	4.27	5.86	6.78	7.68	7.98	8.48

4.3.2 The *VentilatedPipe* component

A basic version of the *VentilatedPipe* can be seen in Fig. 4.5 ; it is the connection of different subcomponents, namely *CustomFlowIDFEM*, *SolidTubeFEM*, *iHGIDFEM*, *HeatTransferCoefficientSource*. The *SolidTubeFEM* substitutes the *metalTubeFEM* and is responsible for solving the conduction equation in the metal wall accounting for temperature depending properties; the *CustomFlowIDFEM* solves the governing equations of fluid-dynamics while *HeatTransferCoefficientSource* implements the heat transfer coefficient on the cooler surface. Heat transfer on the external cooler wall can happen either due to natural circulation, or due to forced convection. For the former case Eq. (4.8) can still be used to calculate the Nusselt number, while for the latter case the Zhukauskas correlation (Bergman, 2011) for a pipe immersed in a cross flow can be employed:

$$\overline{Nu}_D = 0.3 + \frac{0.62 \cdot Re_D^{\frac{1}{2}} \cdot Pr^{\frac{1}{3}}}{\left(1 + \left(\frac{0.4}{Pr}\right)^{\frac{2}{3}}\right)^{\frac{1}{4}}} \cdot \left[1 + \left(\frac{Re_D}{282000}\right)^{\frac{5}{8}}\right]^{\frac{4}{5}} \quad Re_D \cdot Pr \geq 0.2, \quad (4.11)$$

where \overline{Nu}_D and Re_D are the Nusselt and Reynolds number referred to the pipe external diameter, Pr is the Prandtl number; properties are calculated at the cross flow temperature.

An approximation is being made when using Zhukauskas correlation: the cooler pipe is being treated as if it was smooth while it is actually finned. This was done since no correlation has been found for a single finned pipe immersed in a air cross-flow.

The heat flux at the i -th pipe surface node φ_i is then calculated as:

$$\varphi_i = \sigma \cdot \epsilon \cdot (T_{wall,i}^4 - T_{sur}^4) + h_{conv,i} \cdot (T_{wall,i} - T_{sur}) \quad (4.12)$$

to take into account radiative exchange too; the notation is analogous to that for Eq. (4.7) except for the convection coefficient $h_{conv,i}$ which is now calculated for every node.

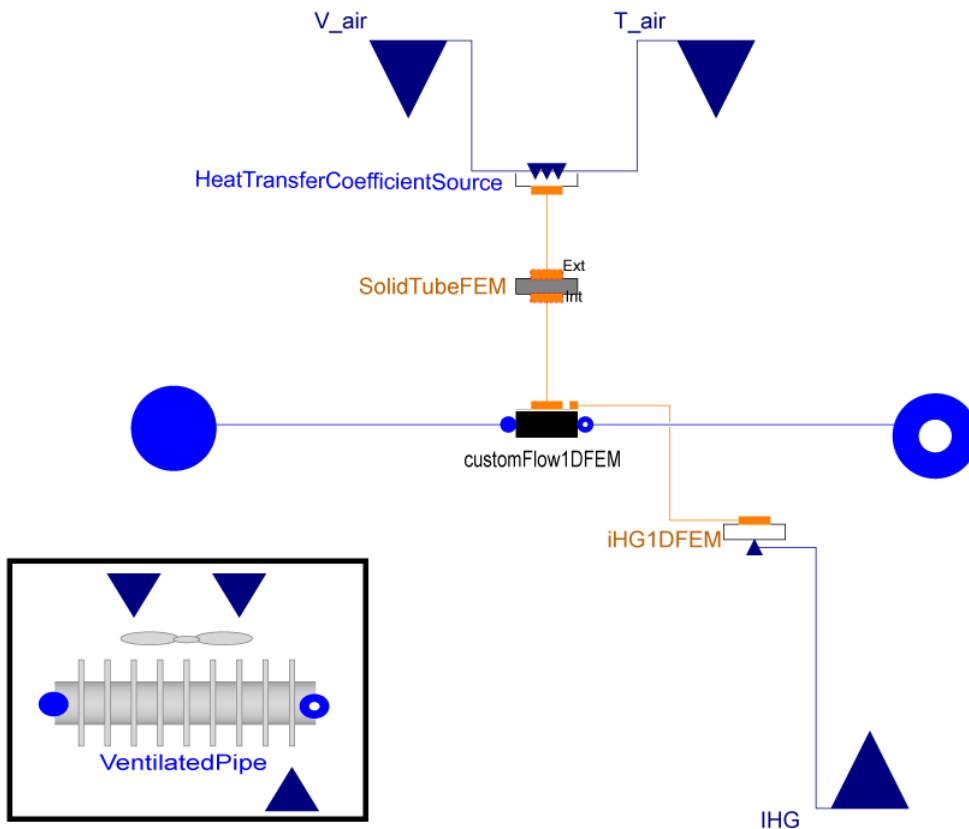


Figure 4.5. External (bottom left) and expanded view of the VentilatedPipe component.

The *VentilatedPipe* designed using the Eq.(4.8) correlation can be implemented in order to model those experimental cases in which DYNASTY is operated with the cooler operating with air in natural circulation. Conversely, the *VentilatedPipe* designed using the Eq. (4.11) correlation is able to model the heat transfer at the cooler surface in presence of a fixed (or, at least, externally controlled) flow rate; this condition can be useful during experimental assessment when a fixed imposed flow rate case is being imposed.

4.3.3 The *VentilatedPipe_controller* component

Control systems are the means by which certain variables of the system of interest are indirectly changed through the direct modification of a controllable variable. In the case of DYNASTY, the implementation of an actual control system allows to variate the air flow rate and therefore the heat removed from the cooler section. The final purpose of controlling the velocity of the air cross flow is to have a mean cooler wall temperature as possibly constant in time. Firstly, this allows understanding what are the differences (especially in terms of finite time horizon equilibrium) brought by the introduction of a controlled ventilated cooler with respect to a case where a thermostated cooler is considered. To have a complete analogy between a model using a thermostated cooler and one using a ventilated pipe, there would be the necessity to modify the air velocity so to allow the thermal uniformity on the ventilated pipe surface (it should be brought to the same temperature of the thermostated cooler wall).

4.3 Improved components for DYNASTY

Obviously, this condition cannot be achieved in reality and therefore a more realizable situation is chosen, namely the equality between the cooler wall mean temperature and the reference wall temperature of the thermostated cooler.

In second place, the controller implementation on the DYNASTY model can give insight and suggestions on what the problems connected to the realization of the real controller for the fan flow rate can be. Finally, such a device could provide the link necessary for the experimental validation of both old and new models.

The *VentilatedPipe_controller* component is shown in Fig. 4.6. Its structure is very similar to that of the *VentilatedPipe* component, with the exception of a new component, “PI” which models a proportional integral controller.

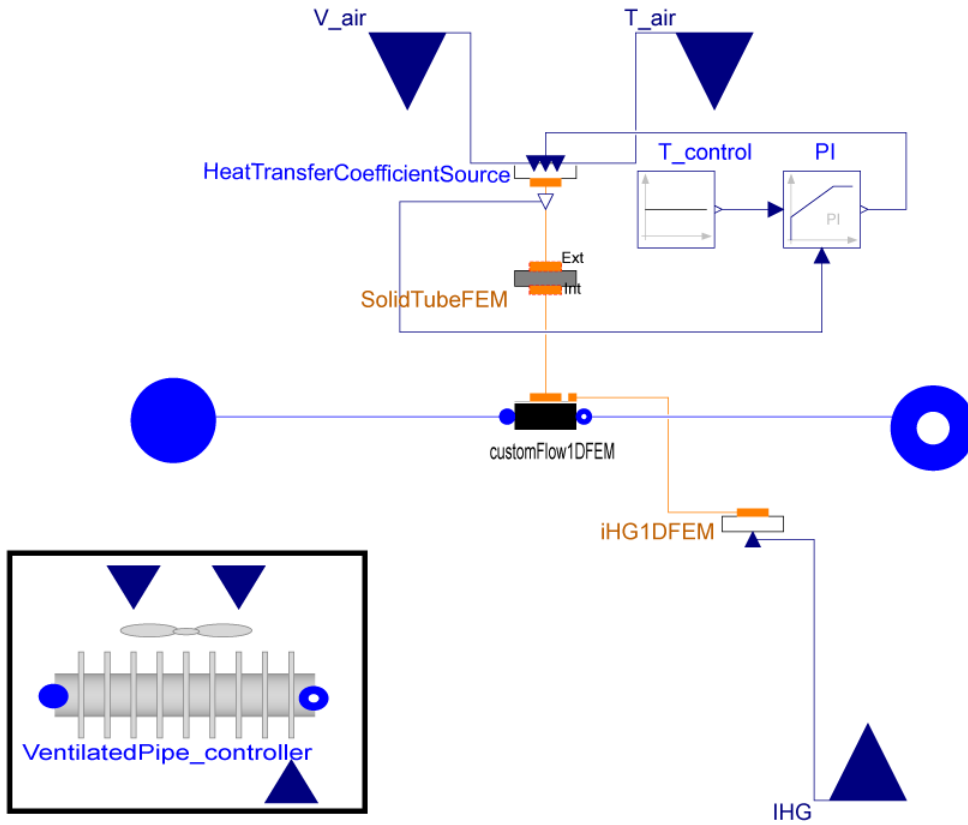


Figure 4.6. External (bottom left) and expanded view of the *VentilatedPipe_controller* component

The control logic implemented is hereby briefly introduced. As aforementioned, inserting a controller in the *Ventilated Pipe* component allows to variate the fan air flow rate on the cooler following the variation of a relevant parameter; this parameter is chosen to be the mean cooler wall temperature \bar{T}_{wall} calculated as:

$$\bar{T}_{wall} = \frac{1}{N} \sum_{i=1}^N T_{wall,i} , \quad (4.13)$$

where N is the total number of discretization nodes and $T_{wall,i}$ is the wall temperature at the i -th node. The controller acts such that for every time instant \bar{T}_{wall} is calculated and so is the error (e) with respect to the desired cooler wall temperature (to make the comparison with the models using *ThermostatePipe_2* possible); the error is acquired by the controller that modifies the air velocity

v_{air} to reduce the error between \bar{T}_{wall} and the desired temperature. The control logic implemented is that of a *Proportional Integral* controller:

$$v_{air} = k_p \cdot \left(e(t) + \frac{1}{T_i} \int_0^t e(\tau) \cdot d\tau \right), \quad (4.14)$$

and it is schematized in Fig. 4.7; k_p is the proportional gain, while T_i is the integral gain constant. The error e is given by the subtraction of the controllable variable y (\bar{T}_{wall} for this case) and the reference value r (the reference cooler wall temperature). On one line of the diagram, the error is multiplied by k_p to obtain the proportional contribution; on the other line the error is multiplied by the integral gain $k_i = k_p/T_i$ and integrated. The sum of the two terms constitutes the input u (i.e., the wanted air velocity) to the plant P and the plant will give back the control variable y as answer. The error e is then once again calculated using the updated y variable.

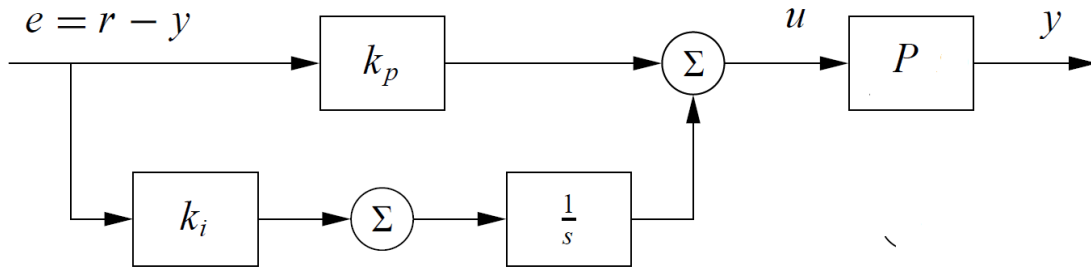


Figure 4.7. PI controller scheme.

More in detail, the $k_p \cdot e(t)$ term produces an output which is proportional to the error thanks to the gain k_p ; such a term reduces the steady state error but does not completely eliminate it (Astrom, 2010). This can be fixed by adding the integral term $\frac{1}{T_i} \int_0^t e(\tau) \cdot d\tau$ which totally removes the steady state error in the output (though eventually producing overshoot of the present value with respect to the set point, due to the accumulated error).

Actually, a slightly more sophisticated version of the shown controller has been implemented to avoid the integrator wind-up issue. Indeed, when the control variable (the fan flow rate in this case) reaches the actuator limits (i.e., the maximum flow rate admitted by the fan), the actuator remains stuck at its limit independently of the process output, leading to a build-up of the integral term. The integral term and the controller output may then become very large and it may take a long time before the integrator and the controller output come inside the saturation range; this situation leads to large transients. This problem can be avoided if the input to the integrator term consists not only of the error but also of a “reset” value based on the input saturation. As shown in Fig. 4.8 the actuator output u is taken and an error e_s is formed as the difference between the controller and the actuator outputs (i.e., $e_s = u - v$); this signal is fed to the integrator through the gain k_t . The higher k_t the shorter the reset time. The value of k_t is usually taken as a fraction of $1/T_i$ (Astrom, 2010).

The choice of the k_p and T_i parameters is a more delicate issue and will be discussed in Section 4.1.4.

4.4 DYNASTY model comparison

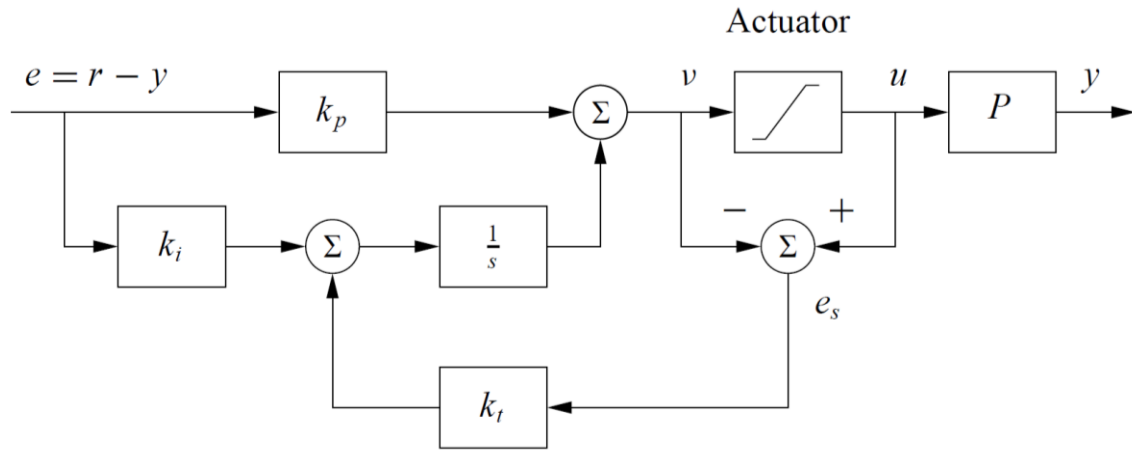


Figure 4.8. PI controller with anti wind-up scheme.

4.4 DYNASTY model comparison

This section is devoted to the comparison between the DYNASTY model obtained with only previously developed pipe components and the one obtained with the “new” pipe components. As already stated, this comparison has the main purpose of highlighting the differences in the simulation results from models that more closely reproduce reality with respect to those models which are built using the previous pipe components. The comparison is performed between two Dymola models:

- *DYNASTYmodel_1*, shown in Fig. 4.9, which adopts the *ThermoStatedPipe_2* and the *PipeFEM_2* to model the pipes of the facility;
- *DYNASTYmodel_2*, shown in Fig. 4.10, which uses the new components *VentilatedPipe_controller* and *PipeFem2WithLosses* (in the constant heat transfer coefficient version).

Both models are built using a total number of 4 pipes, three of which model the horizontal bottom leg and the two vertical legs and the fourth, horizontal top leg, models the cooler. One can also notice the *pressDrop* components which are used to model the lumped pressure losses, the T-junction which connects the facility to the top tank, modeled by the *sinkPressure* component. These setups are a simplified version of the real DYNASTY plant (the bottom horizontal leg is actually made of two joined pipes rather than one and the cooler does not completely occupy the top horizontal leg). These choices were made in order to reduce simulation times and avoid initialization problems. Obviously, the simulations with the two models need to be performed using the same geometrical and fluid parameters, external power level and initial conditions so to assure the simulation conditions to be analogous and the results comparable. The adoption of the controller in the “DYNASTYmodel_2” allows to perform the simulations with the requirement that the wall mean temperature equals the cooler wall reference value chosen for the model comparison. The choice of the controller parameters is discussed in the following Section, while the results immediately afterwards.

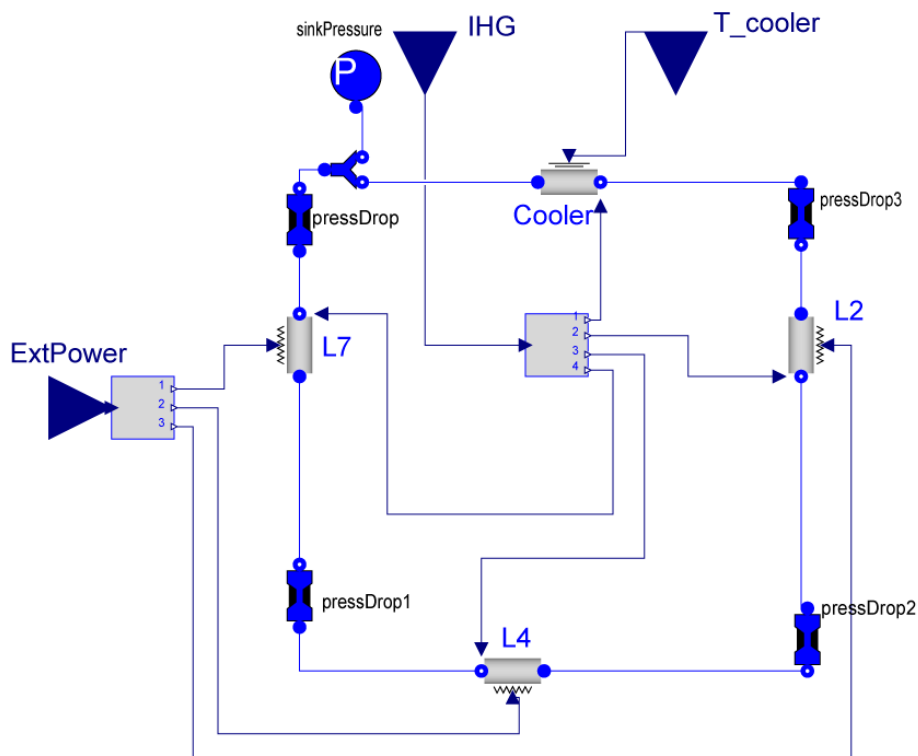


Figure 4.9. DYNASTYmodel_1 Dymola scheme.

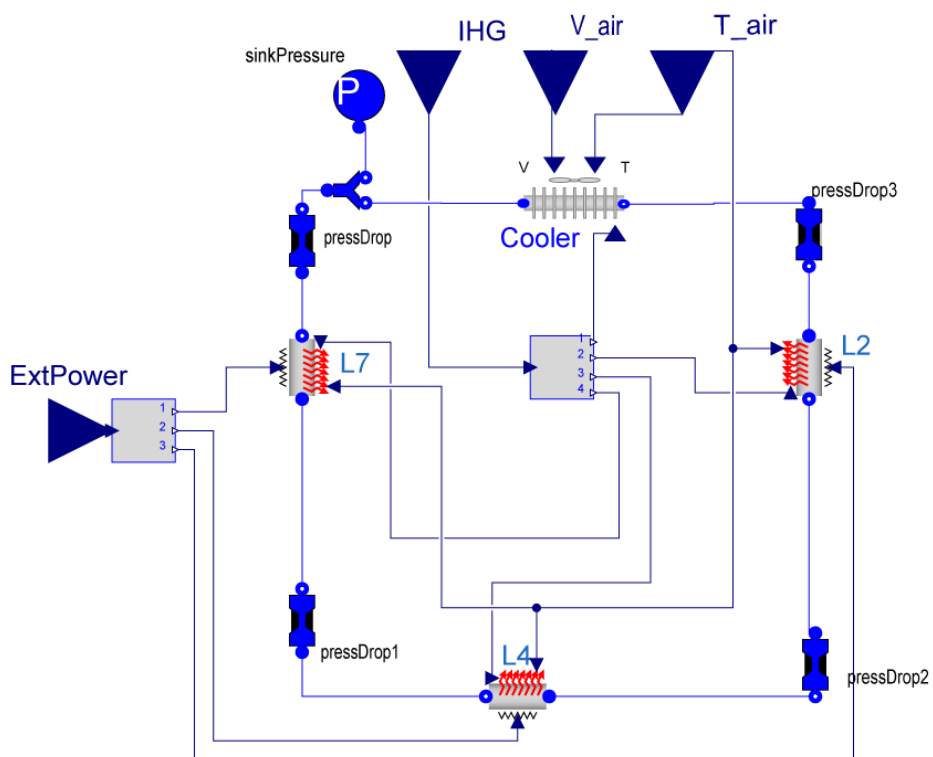


Figure 4.10. DYNASTYmodel_2 Dymola scheme.

4.4 DYNASTY model comparison

4.4.1 Controller tuning

By “controller tuning” is meant the set of operations that involves the adjustment of the controller parameters to obtain a desired behavior of the control variable. In this case (i.e., the tuning of the controller of the fan velocity in *DYNASTYmodel_2*), only two parameters are being adjusted, namely the proportional gain k_p and integral gain constant T_i , while the desired trend of the controlled variable \bar{T}_{wall} would be to reach the reference cooler temperature in the quickest time and with the least oscillations and overshoot. When reference is made to systems employing pneumatic components, empirical methods (such as the Ziegler-Nichols method (Astrom, 2010)) for retrieving k_p and T_i have proved successful, but this is not the case. On the other hand, controllers which are implemented onto space-state systems can be tuned thanks to computational routines like the PID tuner on MATLAB (MATLAB, 2017). Unfortunately, the application of such a tool is not suggested in this case, since it would require a coupling between two different environments (MATLAB and DYMOLA) and, most importantly, it would need many unnecessary runs of the model.

In the end, it was chosen to manually calibrate the controller following usual guidelines (Astrom, 2010). More in detail an initial guess is given for the k_p and T_i values, then k_p is enlarged until the closed-loop response cannot be improved anymore; the integral gain constant T_i is then modified and the one offering the fastest steady state achievement and lowest overshoot is preferred. The controller tuning was performed for the “DYNASTYmodel_2” having chosen a 500 W external power (supplied only to the L2 pipe) and a 180°C cooler wall temperature; the salt (SALT1) and the wall were initialized at a 250°C temperature, so to be able to observe stronger excursions in the temperature values.

The \bar{T}_{wall} trends observed during the tuning are shown in Fig 4.11. The whole procedure led to the choice of $k_p=0.1$ and $T_i = 35$.

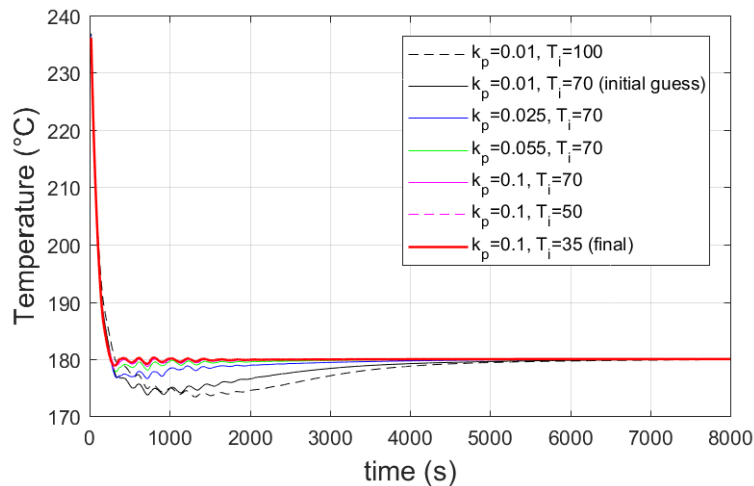


Figure 4.11. Cooler wall mean temperature for different controller parameters.

4.4.2 Simulation set-ups and results

The main parameters adopted for the simulations are shown in Table 4.2. Two different power levels and cooler wall temperatures are investigated, for a total of four cases. As a first approach, in the performed simulations the external power was only given to the L2 vertical pipe, therefore a

“conventional” natural circulation loop is being simulated. According to research (Vijayan, 2007) this is the configuration which is most likely to bring to a “stable” output or, more correctly, to a steady state on a finite time. If this confirms to be true (the transients lead to stationary point) such an analysis will bring an insight in what are the modifications caused by the introduction of the new components both on the steady state values obtained and on the transient part of the simulation.

Table 4.2. Power and temperature conditions considered for the simulations.

Power (W)	Cooler wall temperature (°C)	Initialization fluid and wall temperature (°C)
500	180	250
500	230	300
750	180	250
750	230	300

On the other hand, supplying power to only one pipe does not allow to have a comparison with the reference stability map (which, instead, takes into account the presence of the distributed heating). The fluid adopted for the simulations is the one previously called SALT1; the local pressure losses coefficients were picked as equal to 0.3 for every bend. The flow rate, inlet and outlet cooler fluid temperature, the temperature difference on the cooler fluid and the cooler wall mean temperature are the displayed quantities and will be compared for the two models analyzed. As far as the results are concerned, the trends obtained with *DYNASTYmodel_1* will be labeled as “SOTA” (State Of The Art) and often referred to “previous”, while those obtained with *DYNASTYmodel_1* as “present work”.

External power: 500 W - Cooler wall temperature: 180°C

From Fig 4.12 it is possible to observe that lower values of the steady state flow rate are predicted by the new setup simulations, with oscillations lasting longer for the new set-up. Lower values in comparison to those given by the old set-up are also reached by the steady state inlet and outlet cooler fluid temperatures (Fig 4.13 e 4.14); again, oscillations last longer in the new set-up results. Despite the temperatures reached being lower the obtained temperature difference on the cooler is basically the same for the two models (Fig 4.15). However, the transient part of the inlet and outlet temperatures in the new set-up shows a higher value than that of the SOTA set-up. Figure 4.16 shows that after few time-steps the cooler wall mean temperature of the new case become the same as the imposed temperature of the old case.

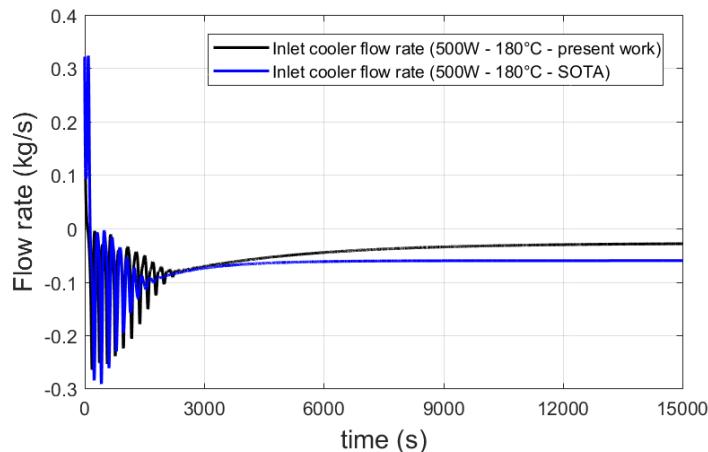


Figure 4.12. Inlet cooler flow rate for the 500W - 180°C case.

4.4 DYNASTY model comparison

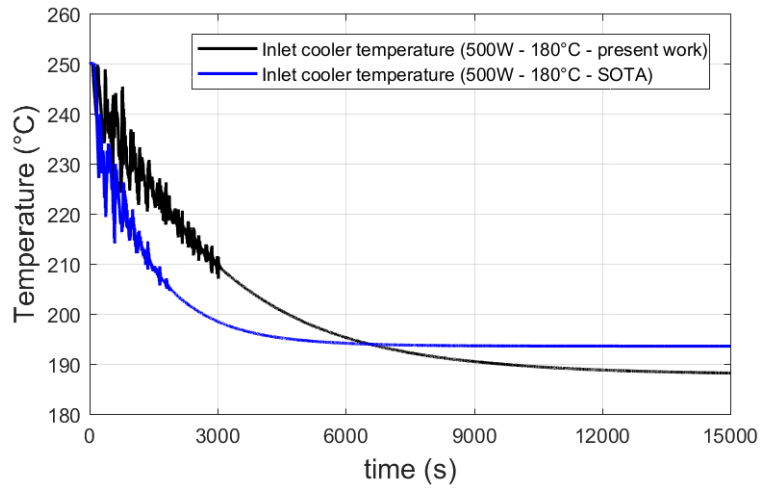


Figure 4.13. Inlet cooler temperature for the 500W - 180°C case.

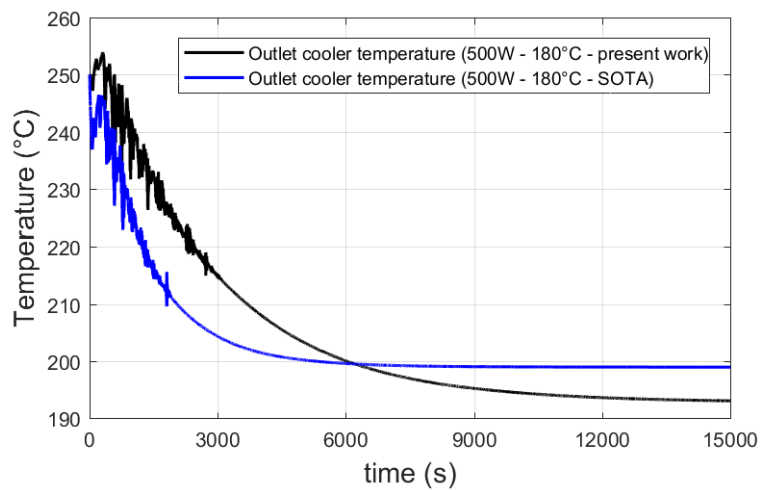


Figure 4.14. Outlet cooler temperature for the 500W - 180°C case.

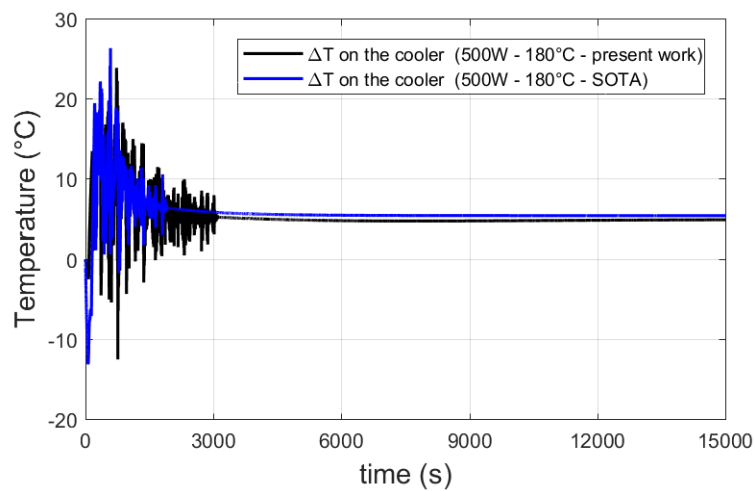


Figure 4.15. Temperature difference on the cooler for the 500W - 180°C case.

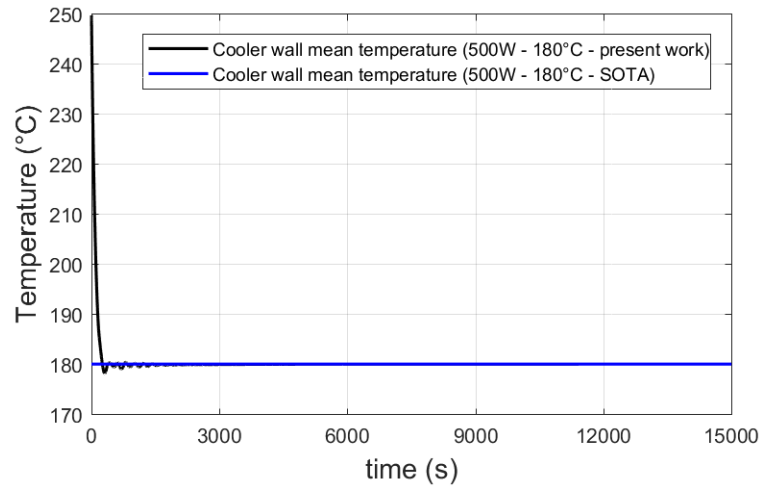


Figure 4.16. Cooler wall mean temperature for the 500W - 180°C case.

External power: 500 W - Cooler wall temperature: 230°C

The same characteristics highlighted for the 500W - 180 °C case can be retrieved here: lower values of flow rate (Fig. 4.17), inlet and outlet fluid temperatures (Fig 4.18 and Fig. 4.19) for the new set-up with respect to the old one and almost coincident temperature differences for the two cases (Fig 4.20). Even in this case oscillations last longer in the new set up case. The cooler wall mean temperature shows a spike in the first 500 seconds due to the presence of flow rate inversions in the same time interval; anyway, the reference value is reached in the first 2000 seconds (Fig. 4.21).

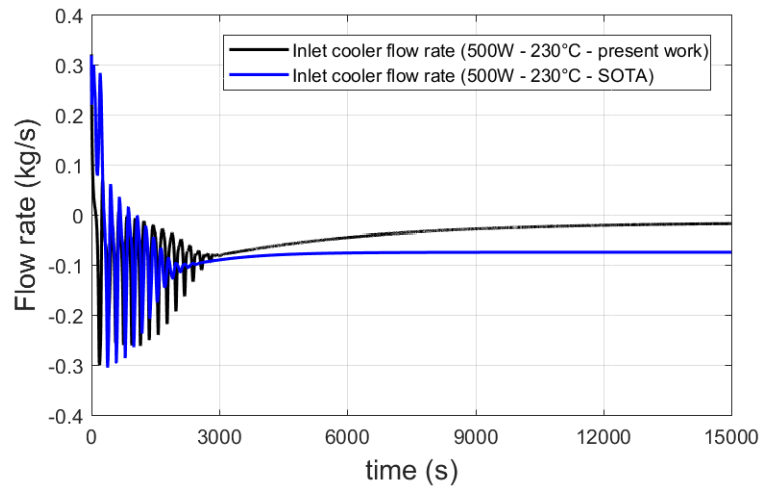


Figure 4.17. Inlet cooler flow rate for the 500W - 230°C case.

4.4 DYNASTY model comparison

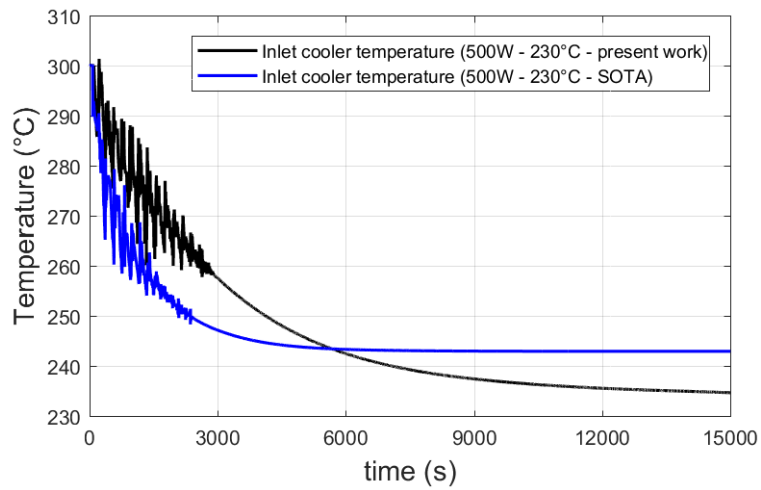


Figure 4.18. Inlet cooler temperature for the 500W - 230°C case.

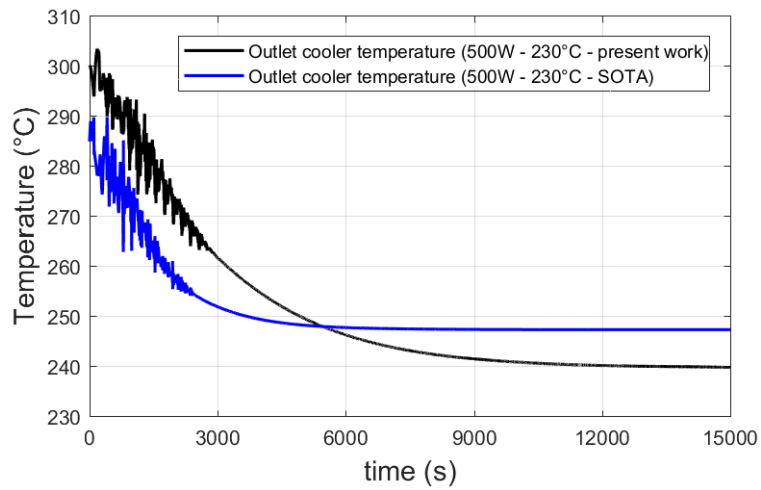


Figure 4.19. Outlet cooler temperature for the 500W - 230°C case.

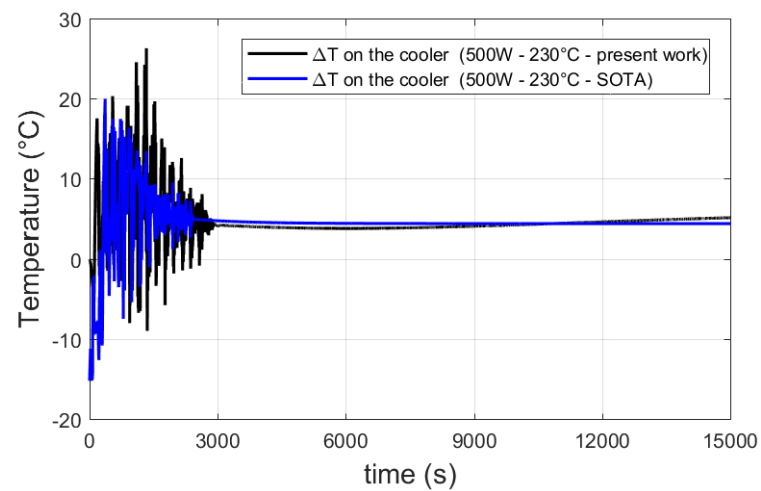


Figure 4.20. Temperature difference on the cooler for the 500W - 230°C case.

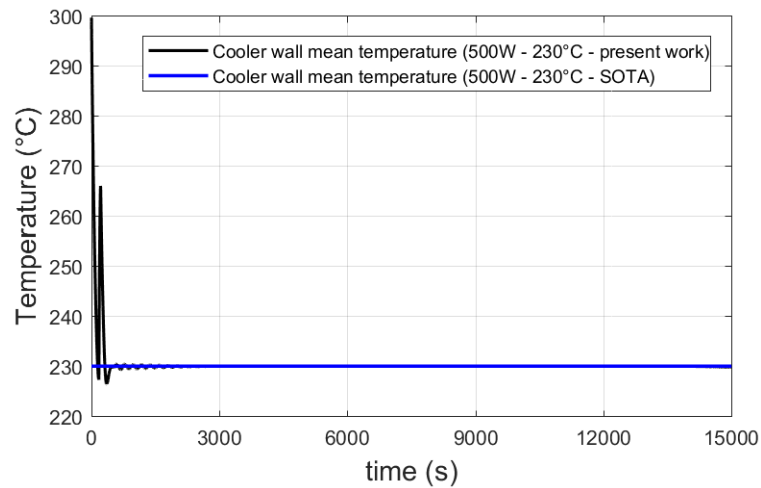


Figure 4.21. Cooler wall mean temperature for the 500W - 230°C case.

External power: 750 W - Cooler wall temperature: 180°C

The results of this case are in line with the previously described ones. However, it is possible to notice here that the final steady state values for both flow rate and temperatures are very similar between the new and SOTA setups, especially for the temperature (Fig. 4.23 and Fig 4.24). This was not the case for the (500W, 180°C) simulation and this is probably due to the fact that the increase in the externally given power (from 500W to 750W, always at 180°C) asks for the fan (through the controller action) to work at higher velocity, causing an increase in the heat transfer coefficient at the external wall of the cooler tube (Fig 4.27 shows an average value of the coefficient on the whole length), making the working conditions, and therefore the results, more similar for the new and old setups. Actually, the imposed temperature condition is equivalent to setting an infinite heat-transfer coefficient, so increasing the heat transfer coefficient (Fig 4.27) in the new setup brings the system closer to the imposed temperature case.

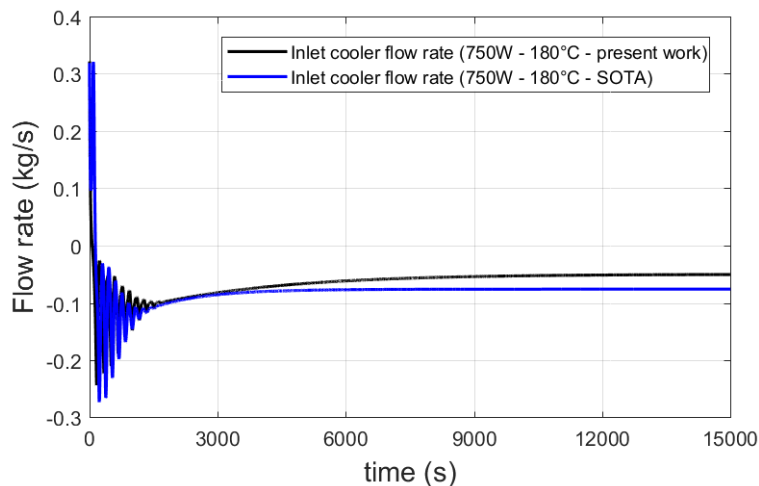


Figure 4.22. Inlet cooler flow rate for the 750W - 180°C case.

4.4 DYNASTY model comparison

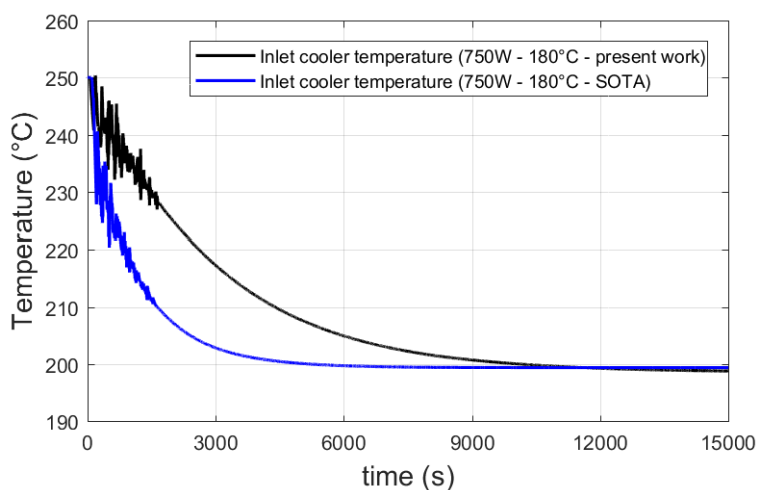


Figure 4.23. Inlet cooler temperature for the 750W - 180°C case.

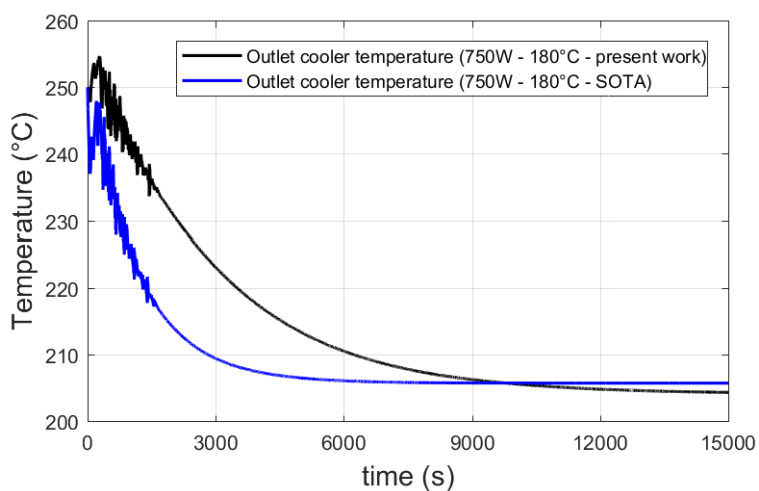


Figure 4.24. Outlet cooler temperature for the 750W - 180°C case.

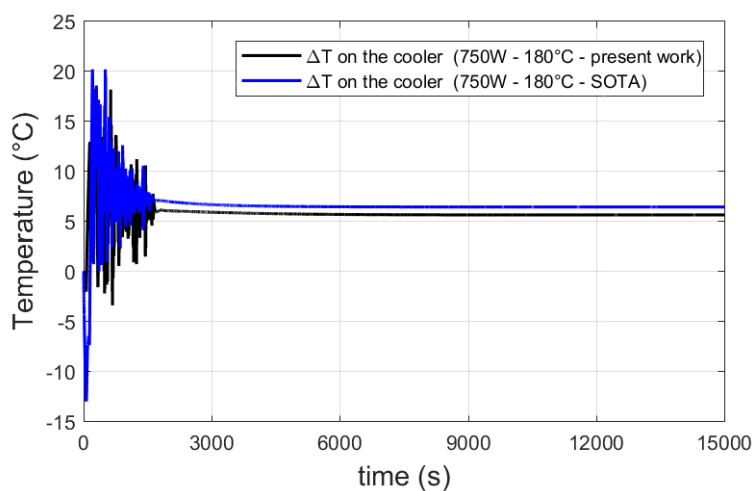


Figure 4.25. Temperature difference on the cooler for the 750W - 180°C case.

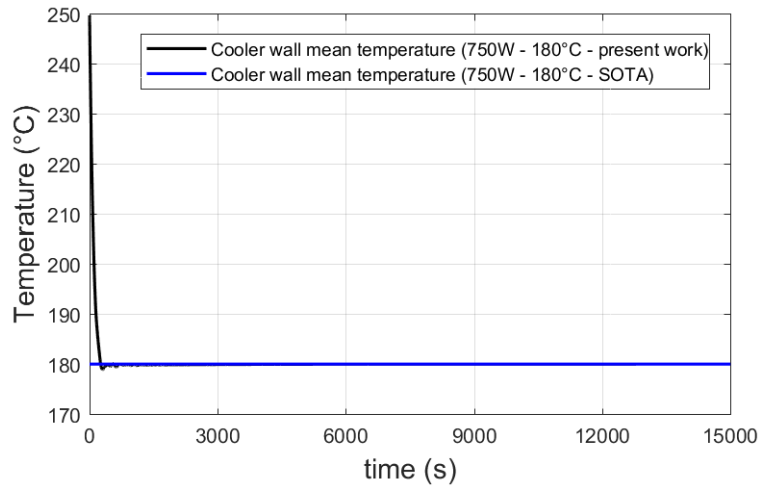


Figure 4.26. Cooler wall mean temperature for the 750W - 180°C case.

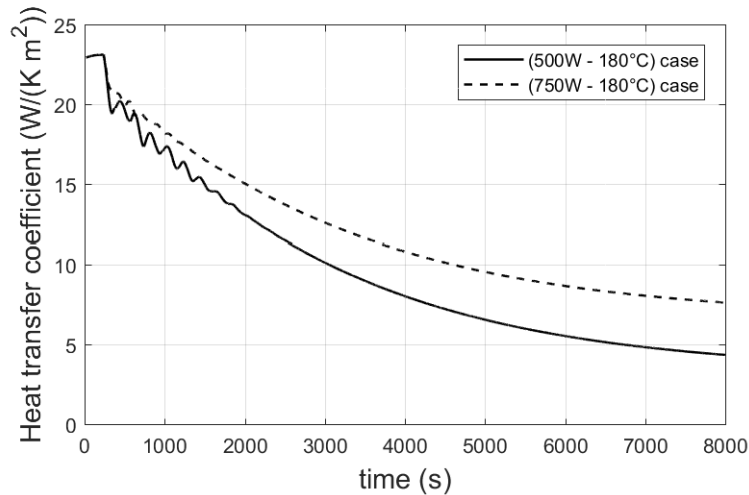


Figure 4.27. Cooler wall heat transfer coefficient comparison for the 500W-180°C and 750W-180°C.

External power: 750 W - Cooler wall temperature: 230°C

The features presented before once again show up here: the lower steady state values in the new set-up, the spikes in the mean temperature, the close steady state values (Figs. 4.28-4.32).

However, in this case, the final steady state values for the *old* and *new* setups are not as near as they were in the (750W – 180°C) case. Indeed, higher temperatures are reached by the fluid, and therefore by the metal and insulator; hence the increase (from 500W to 750W, at 230°C) in the heat exchange coefficient is not as high as it was for the case comparison at 180°C, resulting in final values that are not as adjacent as were the ones at (750W – 180°C).

4.4 DYNASTY model comparison

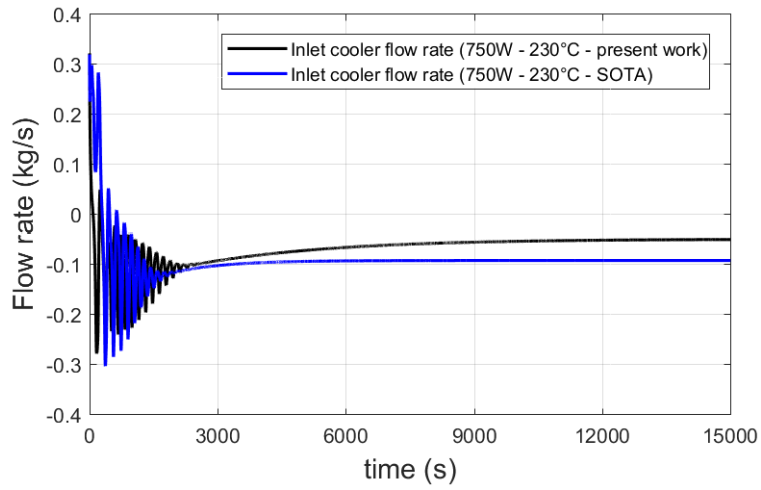


Figure 4.28. Inlet cooler flow rate for the 750W - 230°C case.

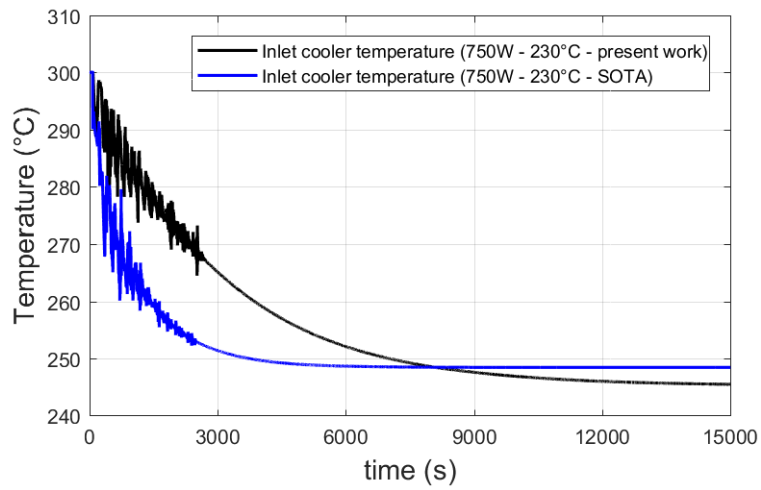


Figure 4.29. Inlet cooler temperature for the 750W - 230°C case.

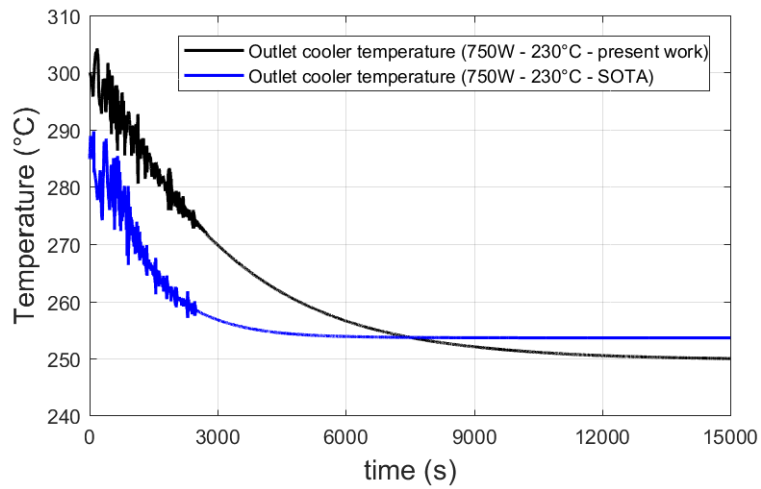


Figure 4.30. Outlet cooler temperature for the 750W - 230°C case.

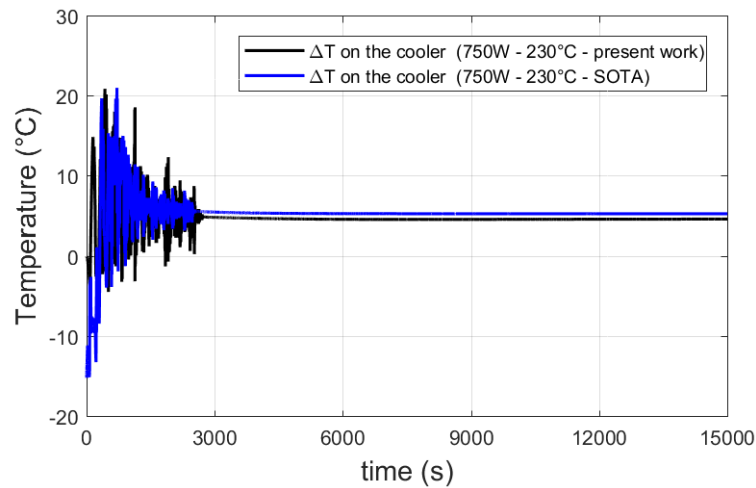


Figure 4.31. Temperature difference on the cooler for the 750W - 230°C case.

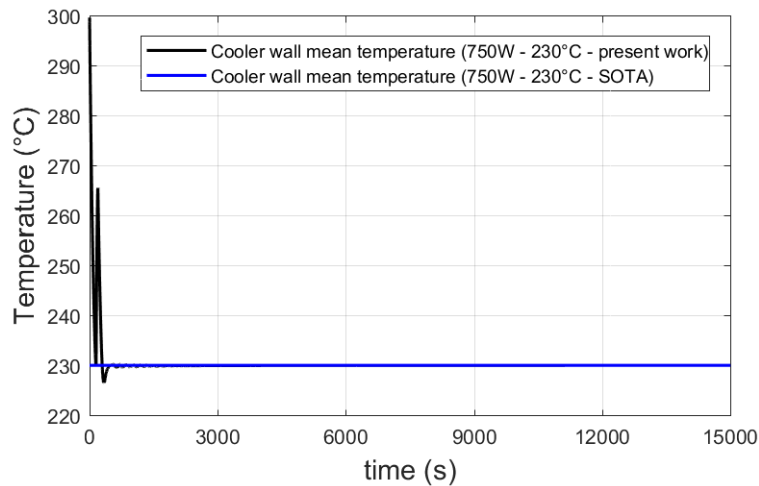


Figure 4.32. Cooler wall mean temperature for the 750W - 230°C case.

Overall both the set-ups show analogous trends in all the simulations and the steady state is eventually reached, confirming the initial hypotheses. The controller is able to bring the mean temperature back to the reference value in a sufficiently short time, making the two set-ups comparable; their comparability is indeed testified by the fact that in all cases a practically equal temperature difference on the cooler is obtained. On the other hand, the simulations performed with the new set-up model always reach a lower steady state value with respect to the old set-up ones.

From the gathered information, some considerations can be made.

It appears that the controller presence always plays a relevant role in determining differences between the old and new set-up in the transient part of the simulation; indeed, the desired cooler wall temperature cannot be instantly reached (as it is in the old set up) and this causes the fluid inside the pipe (for the new model) to be subject to different conditions than its SOTA counterpart. More in detail, the most reasonable explanation to the inequalities between the temperature trends is that in the first part of the transient (up to about 2000 seconds) the cooler wall temperature has excursions up to almost $\pm 5^\circ\text{C}$; in other terms, when the wall mean temperature shows oscillations of 0.5°C (Fig.

4.4 DYNASTY model comparison

4.33 for the 500W,180°C case) it may be that other nodes show oscillations of 3.5°C - 4°C with respect to the reference temperature.

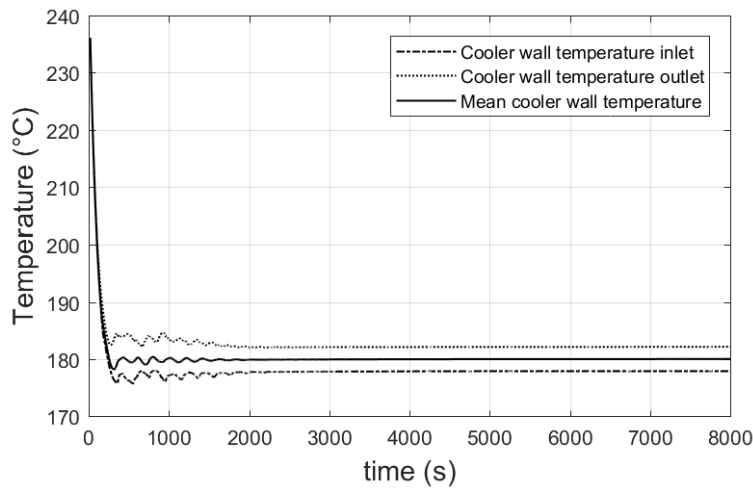


Figure 4.33. Cooler wall temperature at inlet and outlet of pipe, compared with the mean wall temperature.

The spatial temperature distribution for the cooler pipe wall at different time instants can be observed in Fig 4.34 for the 500W - 180°C case; on the steady state (it is already reached at about 8000 s), a $\pm 2^\circ\text{C}$ variation can be noticed with respect to the wanted reference temperature.

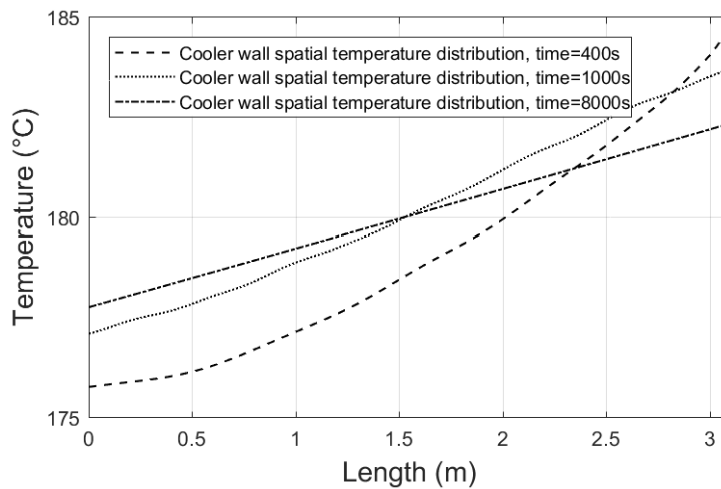


Figure 4.34. Cooler wall spatial temperature distribution for different time instants.

The cooler wall temperature spatial discrepancy in the interval 0-2000 s is reflected also in the longer flow rate oscillations; in all cases the flow rate value eventually settles to a lower level than the one found in the old set-up. The reduced flow rate value may explain why temperatures are higher for the new set up case in the 3000-6000 s interval.

From the analysis of the 750W external power, 180°C case it is possible to deduce that the controller action has also an influence in determining the steady state values of the analyzed quantities; in particular, this influence seems stronger as the given power increases and the cooler temperature remains low. Indeed, a higher external power, with a “low” cooler temperature, indirectly causes the fan to impose a higher flow rate, thus a higher heat exchange coefficient, making the old and new set ups more analogous. Conversely, this becomes less true with the increase of the reference cooler wall temperature or with the reduction of power (the required heat exchange coefficient is lower).

Understanding the contribution of the insulation and surface heat exchange on the pipe surface to the simulation output is not straightforward; indeed, a first thought would suggest that due to the non-adiabaticity of the tubes the fluid temperature should result lower in the new set-up cases. This is not happening in the first part of the transients since, as already explained, the controller is not perfectly guaranteeing uniform temperature in that interval; however, in the second part of every transient analyzed (from about 6000s and forth) it is possible to see that the assumed condition verifies and, in the end, both temperatures are lower in the new set up case. An analysis of Fig 4.35 for the 500W - 180°C case suggests that considering the insulation has a contribution in determining the found lower temperature values. The bottom horizontal pipe is considered for both old and new set up and the fluid temperatures are analyzed; for the old set-up case, as the steady state is reached no difference between the outlet and inlet temperatures can be appreciated while an approximate 2°C temperature discrepancy is seen between the new set up temperatures.

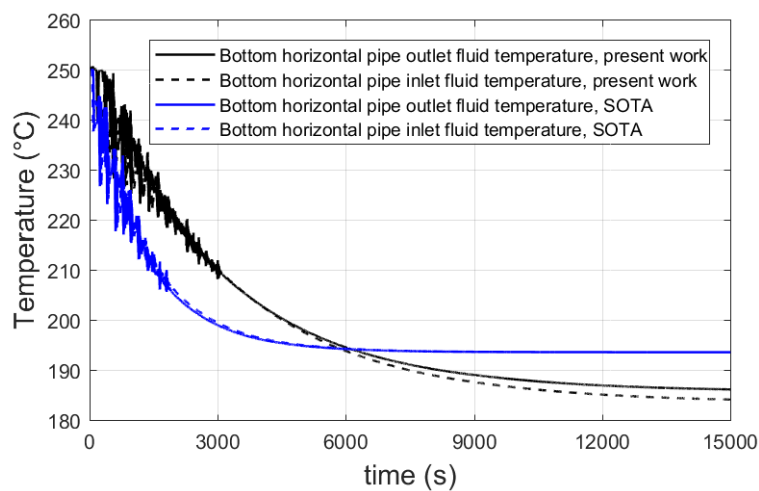


Figure 4.35. Inlet and outlet bottom pipe fluid temperature comparison for old and new set-ups.

This difference can only be due to the presence of the insulation: indeed, insulation must play a role in heat removal since lower temperatures are reached in spite of the lower flow rate.

This view is also confirmed by examining the inlet and outlet temperatures of the vertical heated pipe in Fig. 4.36: the temperature difference between inlet and outlet is higher in the new set-up due to the reduced flow rate, but the absolute value of the reached temperature is lower both because of the dispersions happening locally and both for the heat losses which occurred in the previous stages of the loop.

4.5 Concluding remarks

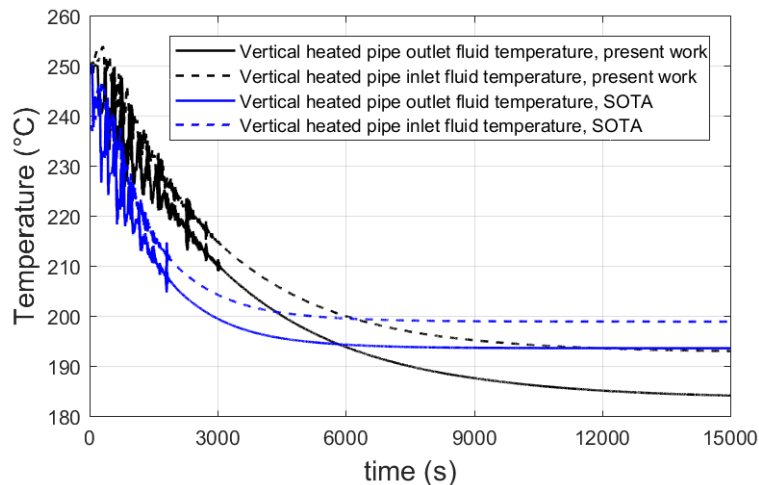


Figure 4.36. Inlet and outlet vertical heated pipe fluid temperature comparison for old and new set-ups.

4.5 Concluding remarks

A one-dimensional object-oriented approach has been used to investigate the finite time horizon behavior of the natural circulation flow in DYNASTY. The chapter focused on the development of new components that could better model some of DYNASTY peculiar features since this could not be achieved with the models already present in literature.

Indeed, the model components *PipeFEM_2* and *ThermostatedPipe_2* are characterized by some modeling assumptions which are incompatible with the operating conditions of the DYNASTY facility: in DYNASTY the pipes are not adiabatic, but subject to heat dispersion and the cooler is not kept at uniform constant temperature but heat is removed through the action of air cross flow. The adoption of these components to model DYNASTY clashes with physical reality in the moment that experimental validation is sought; the main obstacle would come from the apparent difficulty to recreate the thermal uniformity on the cooler pipe surface.

Moreover, it is also expected that heat losses to the exterior may modify the trend of the natural circulation flow. The components developed in this work try to overcome the aforementioned issues.

The *PipeFEM2WithLosses* serves the purpose of modeling the typical pipe of the DYNASTY loop considering also the rock wool layer and the metallic foil which cover it and implementing the heat exchange on the surface of the whole pipe through the means of empirical correlations.

The *VentilatedCooler* and *VentilatedCooler_controller* components have the function to model the behavior of the naturally circulating fluid inside a pipe which is cooled by the action of an air cross flow. In particular, the latter enables variation of the air velocity following the variation of the wall mean temperature, so to mimic (without obviously never reaching the condition) the uniform wall temperature requirement obtained in the previous model. This feature allows for comparison between previous and present work DYNASTY models. These comparisons were performed for a selected number of cases and the results highlighted the differences caused by the introduction of the new components.

Overall, for all the examined cases, the adoption of the new components to model DYNASTY allows a more comprehensive and detailed representation of the experimental reality. The differences which are found in the time trends of the analyzed quantities (temperature and mass flow rate) with respect to the previous set-up simulations are mostly due to the use of the controller and to the fact that it actually takes a certain time before both the wall mean temperature and all the pipe nodes are

actually close to the reference value. This brings changes in the flow rate and temperatures behaviors in the transient part of the simulations.

On the other hand, part of the differences that are seen in temperature when the steady state is reached are attributed to the presence of the insulation; indeed, at that point in time the controller has stabilized and reduced the temperature discrepancy on the cooler wall.

Generally, the introduction of the new components did not compromise the trends of the flow quantities, which remained very similar; for all the simulations and for both the set-ups the steady state was eventually reached. Therefore, it seems that the use of the new components, and therefore the removal of some simplifying assumptions, does not modify the attainment of the stationarity on the finite time horizon even in spite of the two models not being completely analogous. It is also to expect that even the analysis of different external power - cooler wall reference temperature cases characterized by an oscillating behavior would not change this evaluation since, as it has been noted, the presence of the cooler enlarges the oscillation duration and eventually introduces further instability; indeed, the fluid flow rate inversions cause quick changes of the air velocity implying further non-uniformity of the cooler wall temperature. However, confirming this last consideration would require more simulations to be executed.

4.5 Concluding remarks

5 Conclusions and further developments

Natural circulation dynamics in presence of distributed heating in the DYNASTY facility constitutes the back-bone of this thesis, which is then focused on the analysis and improvements of models which aim to study the equilibrium of the natural circulation, on both a finite and infinite time horizon.

The study of natural circulation dynamics is accomplished resorting to two different tools, namely stability maps and 1D O-O models which concentrate respectively on the equilibrium behavior on the asymptotic and finite time frame. The use of both modeling approaches is necessary: not only they found on a similar background but their use is complementary, as stability maps constitute the starting point on which a later dynamic analysis is based on and considerations obtained for one type of models are very likely to be valid on the other too. Their adoption constitutes then the background to the thesis development.

In spite of being one of the most utilized instruments for describing the asymptotic behavior of NCLs, the stability map was never subjected to a sensitivity analysis; this work aimed, for the first time, to characterize the equilibrium state stability prediction with considerations on the variations caused by realistic alterations in the underlying assumptions and in the input reference parameter values.

The single-varied sensitivity study on the parameters inherent to the map construction revealed that for the DYNASTY facility operative range, the stability map for DYNASTY is strongly influenced by the way the flow regime transition is implemented and, in a more general way, by the type of correlation adopted for the friction factor. An increase in the Reynolds number at which the laminar-to-turbulent transition is supposed to happen in the flow entails an enlargement in the number of unstable states on the map, strongly impacting the prediction on the asymptotic equilibrium of a state. Among the other parameters analyzed, such as the facility size and the temperature depending properties, none has an impact as relevant as the major pressure losses definition.

It is of interest to notice how variations in the pipe thermal inertia, one of the features which if not considered causes strong variations in the map shape, has negligible worth in the map maximum figure of merit variation (more than the 97% of this value change is due to the friction factor definition). All these observations may be useful for 1D O-O models too since most of the modeling choices employed in stability maps are found there too; the main advance lies in the fact that performing a sensitivity study for stability maps is less demanding than it is for dynamic models.

Moreover, the knowledge of the parameter impact on the equilibrium behavior will surely come at hand during experimental assessment of the models.

As far as the study of the equilibrium of a state on a finite time horizon is concerned, 1D O-O models, based on the Modelica language, were adopted to tackle the problem in this work.

The models already present in literature were not capable of describing DYNASTY at best and this led to development of new components able to catch the missing features.

The realization of new components allowed to take care of the heat losses from pipes and of the presence of the controlled air flow rate which removes heat from the cooler pipe.

The set of simulations performed on the “new” model of DYNASTY allowed to discover that, when analogous conditions are imposed, minor differences exist in the predicted dynamics of the system with respect to the SOTA model; in particular, the fan action seems to have the strongest impact in the simulation output, modifying the temperature and flow rate absolute values but not their general trends. Overall, for the analyzed cases, the improved model results do not show differences with the SOTA model ones in the prediction of the stationarity of the flow quantities and this actually serves as verification of the new models with the old ones. In addition to confirming the correct behavior of the new models, the new modeling capabilities introduced by them were also highlighted, opening to the possibility of modeling experimental cases which were not accessible before (i.e., heat removed from the loop with a varying controlled flow rate, heat removed by the cooler with natural circulation, etc.).

For what concerns future developments, a multi-varied sensitivity analysis could be performed starting from the results obtained from the single-varied study developed in this work, so to highlight the possible presence of second order correlations between variables.

On the finite time horizon side, the said components can be used for a benchmark with models already available in other environments. Beside the benchmark, the main interest resides in the validation of the new components developed in Modelica; the experimental activity will finally offer insight on the dynamics of natural circulation in presence of distributed heating and there is the need of models capable of representing its behavior. The newly realized components may also be used in the future for modeling the pipes of natural circulation coupled loops, since another experimental facility is going to be operative at PoliMi for the purpose. The latter will be an important step in supplying considerations for the design of the passive emergency coolant system for the decay heat removal in the Molten Salt Fast Reactor.

References

- Astrom, K. J. (2010). *Feedback Systems. An introduction for scientist and engineers*. Princeton University Press.
- Bergman, T. L., Lavine, A. S., Incropera, F. P., DeWitt, D. P., (2011). *Fundamentals of Heat and Mass Transfer*. John Wiley & Sons, Inc., Hoboken, NJ, United States.
- Boerema, N., Morrison, G., Taylor, R., Rosengarten, G., (2012). *Liquid sodium versus Hitec as heat transfer fluid in solar thermal central receiver*. Solar energy 86, 2293-2305.
- Cammi, A., Cauzzi, M., Luzzi, L., Pini, A., (2016). *DYNASTY: AN EXPERIMENTAL LOOP FOR THE STUDY OF NATURAL CIRCULATION WITH INTERNALLY HEATED FLUIDS*. 12th International Conference on Heat Transfer, Fluid Mechanics and Thermodynamics.
- Casella, F., Leva L. (2006). *Modelling of thermo-hydraulic power generation processes using Modelica*. Mathematical and Computer Modelling of Dynamical Systems 12, 19-33.
- Chen, K. (1985). *On the instability of closed-loop thermosiphons*. Journal of Heat Transfer 107,826-832.
- Churchill, S. (1975). Int. J. Heat Mass Transfer, 18, 1049.
- Coastal Chemical Co., (2016). *HITEC Heat Transfer Salt*.
- Creveling, H., De Paz, J., Balaldi, J., Schoenhals, R., (1975). *Stability characteristics of a single-phase free convection loop*. J. Fluid Mech. 67, 65-84.
- De Nevers, N. (1970). *Fluid Mechanics*. Addison-Wesley, Reading, MA.
- DYMOLA. (2018). Dassault-Systèmes. France.
- Norma EN ISO 1127 "Acciai inossidabili".
- Fritzson, P. (2011). *A cyber-physical modeling language and the OpenModelica environment*. Istanbul, Turkey, July 4-8, 2011: 7th International Wireless Communications and Mobile Computing Conference, (IWCMC).
- Fritzson, P. (2015). *Introduction to Modeling and Simulation of Technical and Physical Systems*. Wiley-IEEE Press.
- Gorman, M., Widmann, P., Robbins, K., (1987). *Nonlinear dynamics of a convection loop: a quantitative comparison of experiment with theory*. Physics of Nonlinear Phenomena 19, 255-267.
- Hallican, K.P., Viskanta, R., (1986). *Heat transfer from a rod bundle under natural circulation conditions*. Division of Accidental Evaluation, Office of Nuclear Regulatory Research, U.S. Nuclear Regulatory Commission.
<http://samofar.eu/>. (n.d.).
- <https://www.gen-4.org/>. (2017). Generation IV International Forum.
- Hydraulic Institute. (1979). *Engineering Data Book*. Cleveland, Ohio: Hydraulic Institute.
- Jérôme Serp et al. (2014). *The molten salt reactor (MSR) in generation IV: Overview and perspectives*. Progress in Nuclear Energy 77, 308-319.

- Jiang, Y. Y., Shiji, M., (2002). *Flow instability in a natural circulation loop: influences of wall thermal conductivity*. Nuclear Engineering and Design 222, 16-28.
- Keller, J. B. (1966). *Periodic oscillations in a model of thermal convection*. Journal of Fluid Mechanics 1 (26), 599-606.
- Luzzi, L., Misale, M., Devia, F., Pini, A., Cauzzi, M., Fanale, F., Cammi, A., (2017). *Assessment of analytical and numerical models on experimental data for the study of single-phase natural circulation dynamics in a vertical loop*. Chemical Engineering and Science 162, 262-283.
- Lyapunov, A. (1892). *The general problem of the stability of motion*. Kharkov Mathematical Society, Collected Works II, 7.
- M. Brovchenko et al. (2012). *Preliminary safety calculations to improve the design of Molten Salt Fast Reactor*. PHYSOR 2012 Advances in Reactor Physics Linking Research, Industry, and Education.
- MATLAB. (2017). <https://it.mathworks.com>.
- Misale, M. (2014). *Overview on single-phase natural circulation loops*. Proceedings of the Int. Conf. on Advances in Mechanical And Automation Engineering (MAE), Rome, Italy, June, 7-8.
- Misale, M., Devia, F., Garibaldi, P., (2005). *Some considerations on the interaction between the fluid and the wall tube during experiments in a single-phase natural circulation loop*. Proceedings of the 3rd IASME/WSEAS Int. Conf. on Heat Transfer, Thermal Engineering and Environment, Corfu, Greece, August 20-22.
- Misale, M., Ruffino, P., Frogheri, M., (2000). *The influence of the wall thermal capacity and axial conduction over a single-phase natural circulation loop: 2-D numerical study*. Heat and Mass Transfer 36, 533-539.
- Padovani, E. (2017). *Modeling of the DYNASTY facility and development of its data acquisition and control system*.
- Perry, R. (2008). *Perry's Chemical Engineers' Handbook, eighth ed.* McGraw-Hill, New York.
- Pini, A. (2017). *Analytical and numerical investigation of single-phase natural circulation dynamics in presence of distributed heat sources*. PhD. Thesis.
- Rao, N. M., Pawar, K., Kshiragar, P., (2012). *The influence of the core capacitance on the dynamic performance of a single-phase natural circulation loop with end heat exchangers*. Heat Transfer Engineering 34, 323-337.
- Roland Kossel et al. (2006). *Simulation of complex systems using Modelica and tool coupling*. The Modelica Association, Modelica 2006, September 4-5.
- Ruiz, D., Cammi, A., Luzzi, L., (2015). *Dynamic stability of natural circulation loops for single-phase fluids with internal heat generation*. Chemical Engineering Science 126, 573-583.
- Serrano R, Fradera J, Cuesta S. (2013). *Molten salts database for energy applications*. Chemical Engineering & Processing: Process Intensification 2013, pp. 87-2012.
- Swapnalee, B. T., Vijayan, P. K., (2011). *A generalized flow equation for single phase natural circulation loops obeying multiple friction laws*. International Journal of Heat and Mass Transfer 54, 2618-2629.

- ThermoPower. (2016). <http://thermopower.sourceforge.net>.
- Vijayan, P. K., Austregesilo, H., Teschendorff, V., (1995). *Simulation of the unstable oscillatory behaviour of single phase natural circulation with repetitive flow reversals in a rectangular loop using the computer code ATHLET*. Nuclear Engineering and Design 155, 614-623.
- Vijayan, P., Bhojwani, V., Bade, M., Sharma, M., Nayak, A., Saha, D., Sinha, R., (2001). *Investigations on the effect of heater and cooler orientation on the steady-state transient and stability behaviour of single-phase natural circulation in a rectangular loop*. Tech.rep., Bhabha Atomic Research Centre.
- Vijayan, P. K. (2002). *Experimental observations on the general trends of the steady state and stability behaviour of single-phase natural circulation loops*. Nuclear Engineering and Design 215, 139-152.
- Vijayan, P. K., Sharma, A. K., Saha, D., (2007). *Steady state and stability characteristics of single-phase natural circulation in a rectangular loop with different heater and cooler orientations*. Experimental Thermal and Fluid Science 31, 925-945.
- Welander, P. (1967). *On the oscillatory instability of a differentially heated fluid loop*. Journal of Fluid Mechanics 29, 17-30.